

# On the association between core-collapse supernovae and H II regions

Paul A. Crowther <sup>\*</sup>

*Dept of Physics & Astronomy, University of Sheffield, Hicks Building, Hounsfield Rd, Sheffield, S3 7RH, United Kingdom*

10 October 2018

## ABSTRACT

Previous studies of the location of core-collapse supernovae (ccSNe) in their host galaxies have variously claimed an association with H II regions; no association; or an association only with hydrogen-deficient ccSNe. Here, we examine the immediate environments of 39 ccSNe whose positions are well known in nearby ( $\leq 15$  Mpc), low inclination ( $\leq 65^\circ$ ) hosts using mostly archival, continuum-subtracted H $\alpha$  ground-based imaging. We find that 11 out of 29 hydrogen-rich ccSNe are spatially associated with H II regions ( $38 \pm 11\%$ ), versus 7 out of 10 hydrogen-poor ccSNe ( $70 \pm 26\%$ ). Similar results from Anderson et al. led to an interpretation that the progenitors of type Ib/c ccSNe are more massive than those of type II ccSNe. Here, we quantify the luminosities of H II region either coincident with, or nearby to the ccSNe. Characteristic nebulae are long-lived ( $\sim 20$  Myr) giant H II regions rather than short-lived ( $\sim 4$  Myr) isolated, compact H II regions. Therefore, the absence of a H II region from most type II ccSNe merely reflects the longer lifetime of stars with  $\lesssim 12 M_\odot$  than giant H II regions. Conversely, the association of a H II region with most type Ib/c ccSNe is due to the shorter lifetime of stars with  $> 12 M_\odot$  stars than the duty cycle of giant H II regions. Therefore, we conclude that the observed association between certain ccSNe and H II provides only weak constraints upon their progenitor masses. Nevertheless, we do favour lower mass progenitors for two type Ib/c ccSNe that lack associated nebular emission, a host cluster or a nearby giant H II region. Finally, we also reconsider the association between long Gamma Ray Bursts and the peak continuum light from their (mostly) dwarf hosts, and conclude that this is suggestive of very high mass progenitors, in common with previous studies.

**Key words:** stars: early-type – stars: supernovae: general – ISM: H II regions – galaxies: star clusters, galaxies: ISM

## 1 INTRODUCTION

The past decade has seen major advances in establishing the progenitors of core-collapse supernovae (ccSNe, Smartt 2009). Three discrete sub-populations of hydrogen-rich ccSNe are known, exhibiting plateau’s (II-P), slow declines (II-L) and rapid declines (IIb) in their light curves (Arcavi et al. 2012), representing progressively lower hydrogen envelope masses. It has been empirically established that the most common of these (II-P) are the direct progeny of red supergiants (Smartt et al. 2009). Some of the rarer subtypes (II-L and IIb) have been proposed to originate from yellow supergiants, hydrogen-rich Wolf-Rayet stars or interacting binaries, while hydrogen-rich ccSNe with narrow components in their spectra (IIc) seem to involve interactions with dense circumstellar material (Kiewe et al. 2012).

No progenitors of hydrogen-deficient (Ib/c) ccSNe have yet been detected (Crockett et al. 2007; Yoon et al. 2012) which are

believed to either arise from massive Wolf-Rayet stars that have stripped their hydrogen from powerful stellar winds (e.g. Conti 1976; Crowther 2007), or lower mass stars in close binary systems (Podsiadlowski et al. 1992; Nomoto et al. 1995; Fryer et al. 2007), or some combination thereof (Smith et al. 2011; Langer 2012). It is likely that helium-strong IIb and Ib ccSNe possess similar progenitor channels (Arcavi et al. 2012), while helium-weak Ic ccSNe may arise from disparate progenitors (e.g. Dessart et al. 2012). In particular, broad-lined type Ic ccSNe are notable in several ways; they represent the majority of hydrogen-deficient ccSNe in dwarf hosts (Arcavi et al. 2010), there is a broad-lined Ic-Gamma Ray Burst (GRB) connection (Woosley & Bloom 2006), while long GRBs prefer metal-poor hosts (Levesque et al. 2010).

In view of the scarcity of nearby ccSNe amenable to the direct detection of the progenitor star, studies have turned to the host environment. For example, the population of hydrogen-deficient ccSNe are dominated by Ic ccSNe in large galaxies, versus Ib and broad-lined Ic ccSNe in dwarf galaxies (Arcavi et al. 2010), although the

\* Paul.Crowther@sheffield.ac.uk

**Table 1.** Examples of nearby H II regions, spanning a range of luminosities, for an assumed O7V Lyman continuum ionizing flux of  $10^{49}$  (ph s $^{-1}$ ), adapted from Kennicutt (1984, 1998).

Region	Type	galaxy	Distance (kpc)	Diameter (pc)	L(H $\alpha$ ) (erg s $^{-1}$ )	N(O7V)
Orion (M 42)	Classical	Milky Way	0.5	5	$1 \times 10^{37}$	<1
Rosette (NGC 2244)	Classical	Milky Way	1.5	50	$9 \times 10^{37}$	7
N66	Giant	SMC	60	220:	$6 \times 10^{38}$	50
Carina (NGC 3372)	Giant	Milky Way	2.3	300:	$1.5 \times 10^{39}$	120
NGC 604	Giant	M 33	800	400	$4.5 \times 10^{39}$	320
30 Doradus	Supergiant	LMC	50	370	$1.5 \times 10^{40}$	1100
NGC 5461	Supergiant	M 101	6400	1000:	$7 \times 10^{40}$	5000

overall statistics of Ib/c versus II ccSNe are relatively insensitive to host galaxy.

In addition, the immediate environment from which the ccSNe originated has also been examined. The first serious attempt to assess their association with H II regions was by van Dyk (1992). From a sample of 38 core-collapse SNe of all subtypes, he concluded that approximately 50% were associated with a H II region, with no statistically significant difference between type II and Ib/c SNe, albeit hampered by poor positional accuracy (up to  $\pm 10''$ ). Bartunov et al. (1994), also concluded that both H-rich and H-deficient core-collapse SNe were concentrated towards H II regions, implying similar ages/masses. Improved statistics (49 ccSNe) enabled van Dyk et al (1996) to confirm earlier results, concluding that the (massive) Wolf-Rayet scenario could be excluded for most type Ib/c ccSNe, albeit once again subject to poor positional accuracy for many targets.

More recently, James & Anderson (2006), Anderson & James (2008) and Anderson et al. (2012) have taken a statistical approach to the environment of ccSNe, involving its position with respect to the cumulative distribution of H $\alpha$  emission in the host galaxy, whose recession velocities extended up to  $cz = 10,000$  km s $^{-1}$ . Anderson & James (2008) found a low fraction of type II SNe to be associated with H II regions, concluding that the “*type II progenitor population does not trace the underlying star formation.*” In contrast, they noted that type Ib, and especially Ic ccSNe are spatially coincident with H II regions, suggesting a progenitor mass sequence from II  $\rightarrow$  Ib  $\rightarrow$  Ic. Anderson et al. (2012) include additional statistics for hydrogen-rich ccSNe from which they claim a mass sequence II $n$   $\rightarrow$  II-P  $\rightarrow$  II-L  $\rightarrow$  IIb. The latter naturally connects IIb and Ib ccSNe, but the low progenitor masses inferred for II $n$  ccSNe does not readily match expectations that these arise from massive Luminous Blue Variables (Smith 2008).

To add to the puzzle, Smartt (2009) argued against a monotonic mass sequence for progenitors of II  $\rightarrow$  Ib  $\rightarrow$  Ic on the basis of the rate of Ib/c ccSNe, the lack of direct detections of Ib/c progenitors (e.g. Crockett 2009) and inferred low Ib/c ccSNe ejecta masses. From a qualitative study of the environment of the volume- and epoch- limited sample of ccSNe of Smartt et al. (2009), 0 from 17 type II SN observed at high spatial resolution are located in bright H II regions (Smartt, priv. comm.). Meanwhile, only 1 case from 9 Ib/c ccSNe from Crockett (2009) for which high spatial resolution imaging was available, is located in a large star forming region, albeit spatially offset from H II emission (Smartt, priv. comm.). Therefore, high resolution imaging does not appear to support any significant association between ccSNe and H II regions.

In addition to the association of ccSNe with H II regions, or lack thereof, studies of the location of ccSNe with respect to the

host galaxy light have also been performed. Kelly et al. (2008) found that type Ic ccSNe are located in the brightest regions of their host galaxies, type II ccSNe are randomly distributed, with intermediate properties for type Ib ccSNe. Long duration GRBs, in common with type Ic ccSNe, are also strongly biased towards the brightest regions of their hosts (Fruchter et al. 2006), adding to the GRB-Ic SN link.

In the present study we re-assess the the degree of association of nearby ccSNe with H II regions in their hosts, in an attempt to reconcile the recent Smartt (2009) and Anderson et al. (2012) studies. Section 2 provides a background to H II regions, star clusters and massive stars. Section 3 assesses the association of nearby core-collapse SN with H $\alpha$  emission, while Section 4 looks into how/whether these results contribute to the question of progenitor masses for different flavours of ccSNe. In Section 5 we briefly re-assess the significance that certain ccSNe and long-duration GRBs are located in the brightest regions of their host galaxies, while brief conclusions are drawn in Section 6.

## 2 H II REGIONS AND MASSIVE STARS

In this section we provide a brief background to the expected connections between massive stars and H II regions, of relevance to our empirical study set out in Section 3.

### 2.1 Clusters and massive stars

It is widely accepted that the majority of stars form within star clusters (Lada & Lada 2003), although recent evidence suggests star formation occurs across a broad continuum of stellar densities (e.g. Evans et al. 2009) from dense star clusters to diffuse OB associations (Gieles & Portegies Zwart 2011). Nevertheless, given their short-lifetimes (2.5–50 Myr) only a few percent of massive stars ( $\geq 8M_{\odot}$ ) appear genuinely ‘isolated’ (de Wit et al. 2005) such that they either tend to be associated with their natal cluster or are potential runaways from it<sup>1</sup>.

According to Weidner & Kroupa (2006), there is a tight relation between cluster mass, and the most massive star formed within the cluster, although this remains controversial (Calzetti et al. 2010, Eldridge 2012). If this is so, the galaxy-wide stellar initial mass function (IMF) will also depend upon the cluster mass function and the mass range spanned by star clusters (Pflamm-Altenburg

<sup>1</sup> Runaways may be ejected from their cluster either dynamically during the formation process or at a later stage after receiving a kick following a supernova explosion in a close binary system.

et al. 2007). By way of example, a cluster with a mass of  $\sim 10^2 M_\odot$ , similar to the  $\rho$  Oph star forming region (Wilking et al. 1989), will barely produce any massive stars. In contrast, a cluster with a stellar mass of  $10^4 M_\odot$  such as NGC 3603 (Harayama et al. 2008), would be expected to form  $\sim 100$  massive stars, with the most massive examples exceeding  $100 M_\odot$  (Schnurr et al. 2008; Crowther et al. 2010). Massive stars, therefore, tend to be intimately connected with the youngest, brightest star clusters.

## 2.2 H II regions: from classical to supergiant

In view of the Salpeter IMF slope for high mass stars (Bastian et al. 2010), 8–20  $M_\odot$  early B-type stars form  $\sim 75\%$  of their overall statistics. However, the most frequently used indicator of active star formation is nebular hydrogen emission (e.g. H $\alpha$ ) from gas ionized by young, massive stars. The Lyman continuum ionizing output from such stars is a very sensitive function of temperature (stellar mass), such that one O3 dwarf ( $\sim 75 M_\odot$ ) will emit more ionizing photons than 25,000 B2 dwarfs ( $\sim 9 M_\odot$ , Conti et al. 2008). Therefore, H II regions are biased towards the  $\sim 25\%$  of high mass stars exceeding  $20 M_\odot$ , namely O-type stars (B stars will produce extremely faint H II regions).

Beyond several Mpc, current sensitivities limit the detection of H II regions to relatively bright examples, involving several ionizing early O-type stars (Pflamm-Altenburg et al. 2007). Still, the H $\alpha$  luminosity of bright H II regions can be converted into the corresponding number of Lyman continuum ionizing photons, for which the number of equivalent O7 dwarf stars, N(O7V), serves as a useful reference (Vacca & Conti 1992). Table 1 lists examples of nearby H II regions (adapted from Kennicutt 1984, 1998) which range from classical H II regions powered typically by one or a few stars (e.g. M 42), through giant, extended H II regions powered by tens of O stars (Carina Nebula) to exceptionally bright ‘supergiant’ regions powered by hundreds of O stars (30 Doradus). We will follow these template H II regions when we investigate the nebular environment of ccSNe in Section 3. Although there is a spread in H II region size at a particular H $\alpha$  luminosity (e.g. Lopez et al. 2011, their figure 1), faint regions are typically small ( $\leq 10$  pc), giant regions are extended ( $\sim 100$  pc) and supergiant regions tend to be very extended (several hundred pc).

Kennicutt et al. (1989) have studied the behaviour of the H II region luminosity function in nearby spirals and irregular galaxies. Early-type (Sa-Sb) spirals possess a steep luminosity function, with the bulk of massive star formation occurring in small regions ionized by one of a few O stars (M 42-like), plus a low cut-off to the luminosity function. Late-type spirals and irregulars possess a shallower luminosity function, in which most of the massive stars form within (30 Dor-like) large H II regions/OB complexes. For example, although the LMC contains considerably fewer H II regions than M 31 (SAB), it contains ten H II regions more luminous than any counterpart in M 31 (Kennicutt et al. 1989).

## 2.3 Lifetime of H II regions

Before turning to our survey of nearby ccSNe, let us first assess the empirically determined duration of the H II region phase, for which both a plentiful supply of ionizing photons (from O stars) and neutral gas (left over from the star formation process) are required. The former is limited to  $\sim 10$  Myr according to the latest evolutionary model predictions for  $20 M_\odot$  stars (Ekström et al. 2012), and is often merely adopted as the H II lifetime, while the latter depends

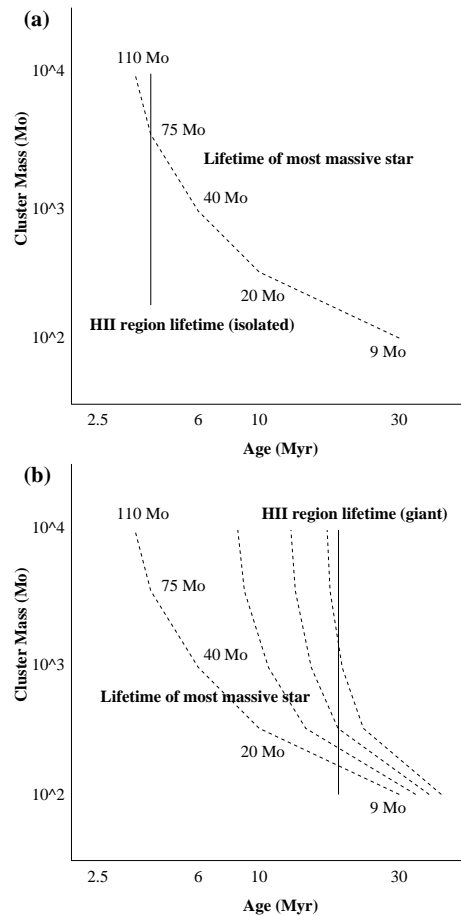


**Figure 1.** (a) Schematic comparing the lifetime of the most massive star in a cluster (dotted line, according to Pflamm-Altenburg et al. 2007) and isolated H II regions (vertical solid line, adapted from Walborn 2010). Core-collapse SNe should only be associated with isolated H II regions for very massive progenitors; (b) as (a) except for (super)giant H II regions, comprising 4 distinct star forming episodes separated by 5 Myr, with the age referring to the first stellar generation. For a total duty cycle of 20 Myr, an association between ccSNe and giant H II regions would be expected except for progenitors with masses below  $\sim 12 M_\odot$  or more massive progenitors from subsequent stellar generations as indicated.

sensitively upon its environment. Walborn (2010) studied the properties of young, intermediate mass star clusters within the Local Group which indicate that the H II region phase is present for only the first  $\sim 3$ –4 Myr. The gas is swept up and expelled via radiative and mechanical feedback from stars, and subsequently supernovae (e.g. Dale et al. 2012).

Gas has already been removed from relatively high mass, isolated clusters such as Westerlund 1 after 5 Myr ( $\sim 10^5 M_\odot$ , Clark et al. 2005). Therefore, one would *not* expect ccSNe to be spatially coincident with *isolated* H II regions unless the mass of the progenitor was sufficiently high ( $> 75 M_\odot$ ) for its lifetime to be comparable to the gas dispersion timescale.

This is illustrated in Figure 1(a) where we compare the lifetime of the most massive stars in clusters<sup>2</sup> (according to Eqn. 10 from Pflamm-Altenburg et al. 2007), with an estimate of the dura-

<sup>2</sup> Stellar lifetimes are adopted from rotating, solar metallicity models of Ekström et al. (2012)

tion of isolated H II regions (adapted from Walborn 2010). Solely very massive ( $> 75M_{\odot}$ ) stars would end their life before the gas in the associated H II region had dispersed.

Of course, not all massive star formation occurs within isolated, compact star clusters. Giant and supergiant H II regions extend to several hundred parsec in size (Table 1), are ionized by successive generations of star clusters, with a total duty cycle of  $\sim 20$  Myr. Therefore, older (lower mass) populations will appear co-located with younger (higher mass) stars in external (super)giant H II regions. Indeed, 30 Doradus would only subtend  $\sim 1$  arcsec at a distance of 50 Mpc.

For giant H II regions such as the Carina Nebula, several clusters exist with distinct ages, ranging from 1–2 Myr (Trumpler 14, e.g. Vazquez et al. 1996) to 5–10 Myr (Trumpler 15, e.g. Wang et al. 2011). Indeed, the proximity of the supergiant H II region 30 Doradus enables individual stars to be studied in detail (e.g. Evans et al. 2011). Walborn & Blades (1997) identified five distinct spatial structures within 30 Dor, (i) the central 1–2 Myr cluster R136; (ii) a surrounding triggered generation embedded in dense knots ( $< 1$  Myr); (iii) a OB supergiants spread throughout the region (4–6 Myr); (iv) an OB association to the southeast surrounding R143 ( $\sim 5$  Myr); (v) an older (20–25 Myr) cluster to the northwest (Hodge 301, Grebel & Chu 2000).

Therefore, a massive star from the first stellar generation exploding within such an environment as a SN after 5–10+ Myr would still be associated with a bright H II region, even if its natal star cluster had cleared the gas from its immediate vicinity, as illustrated in Fig. 1(b). A total duty cycle of 20 Myr for giant H II regions sets a lower threshold of  $12 M_{\odot}$  to the progenitor mass (from the initial stellar generation) for possible association with the giant H II region. Progressively higher mass progenitors from subsequent generations (for illustration, four generations separated by 5 Myr are shown in Fig. 1b) would be required. For example, a star formed 10 Myr after the initial burst would only be associated with the giant H II region if its initial mass exceeded  $20 M_{\odot}$ .

Finally, (nuclear) starburst regions of galaxies, in which gas is continuously accreted, may have still longer duty cycles of  $\sim 100$  Myr, preventing any constraints upon progenitor masses.

In summary we set out five scenarios, depending on whether or not the ccSNe are spatially coincident with H II regions, as follows:

- **Class 1:** The ccSNe progenitor is coincident with an isolated, young, bright star cluster from which the gas has been expelled, so a H II region is *absent*. At optical wavelengths, a star cluster rapidly fades (by 1 mag) at early times between 5–10 Myr, with a slower decline of 0.5 mag between 10–30 Myr (e.g. Bik et al. 2003), so a high mass progenitor ( $\geq 20 M_{\odot}$ ) might be anticipated;

- **Class 2:** Either the ccSNe progenitor is coincident with an isolated, faint star cluster, or is not coincident with any detectable star cluster. In this case the cluster may have already dissolved and an H II region again *absent*. This scenario would favour an older ( $\gg 10$  Myr) cluster, and correspondingly lower mass progenitor ( $< 20 M_{\odot}$ );

- **Class 3:** The ccSNe progenitor was formed in a star cluster, but was subsequently ejected via either dynamical interactions or after receiving a kick from the supernova of a close companion, so it is not directly associated with a H II region, although a bright H II region is *nearby*. For a dynamical interaction origin, if a massive star has a space velocity of  $50 \text{ km s}^{-1}$  with respect to its natal cluster, typical of a runaway, its projected distance would be up to 150 pc after 3 Myr, or 1.5 kpc after 30 Myr. According to Fujii & Portegies Zwart (2011) the fraction of dynamical runaways is

low ( $< 0.1\%$ ) for high mass ( $10^5 M_{\odot}$ ) star clusters, but increasing to 1–10% for high mass stars in less massive ( $10^4 M_{\odot}$ ) clusters. Therefore, one would anticipate a nearby (few hundred pc), high mass, dense star cluster, given the short lifetime of high mass ( $\geq 25 M_{\odot}$ ) stars, which would most likely lie within a giant H II region (e.g. Carina Nebula, 30 Doradus).

- **Class 4:** A H II region is *present* at the ccSNe position, albeit with a low luminosity. This favours a very high mass progenitor ( $> 75 M_{\odot}$ ) if the star forming region is compact/isolated, or a significantly lower mass ( $\leq 20 M_{\odot}$ ?) if it is merely an older, extended star forming region;

- **Class 5:** A H II region is again *present* at the ccSNe position, albeit spatially extended, with a high luminosity. The progenitor was formed in a cluster within a large star forming complex in which ongoing star formation is maintaining the Lyman continuum radiation. The natal cluster may be detected, it could have already dissolved, or the star could be a runaway from a nearby high mass cluster. For a giant H II region duty cycle of 20 Myr, a lower limit of  $12 M_{\odot}$  can be assigned for a progenitor formed in the first generation of stars, with an increasing mass limit for subsequent generations (recall Fig. 1b). If the ccSNe is associated with a very long-lived starburst region, no robust limit to the progenitor mass can be assigned.

### 3 ARE CCSNE ASSOCIATED WITH H II REGIONS?

In this section we discuss the supernova sample investigated, together with methods used and re-assess whether nearby ccSNe are associated with H II regions in their host galaxy.

#### 3.1 Supernova sample

Here, we examine the association of ccSNe with H II regions in their host galaxies. We follow an approach broadly similar to van Dyk (1992) and van Dyk et al. (1996). This technique in complementary to qualitative approaches (Crockett 2009; Smartt, priv. comm.) and the cumulative distribution technique of James & Anderson (2006), Anderson & James (2008) and Anderson et al. (2012).

We limit our sample to local, historical, non-type Ia SNe from the Asiago Catalogue<sup>3</sup> with a cutoff date of 31 Mar 2012. Ground-based images used in this study have a spatial resolution of 0.6–4 arcsec, aside from the LMC, so we set an upper limit of 15 Mpc for ccSNe host galaxies, at which the typical image quality (FWHM  $\sim 1''.5$ ) corresponds to the radius of a giant H II region ( $\sim 100$  pc). Distances are uniformly obtained from the Extragalactic Distance Database (EDD, Tully et al. 2009). For reference, Tables B1-B2 in Appendix B lists a ccSNe host galaxies for which EDD distances lie in the 15–20 Mpc range.

In total 88 ccSNe within 15 Mpc are listed in the Asiago Catalogue, from which 11 were removed on the basis that they are believed to be SN imposters or LBV eruptions<sup>4</sup>. We also omit 21 ccSNe for which merely offsets relative to the centre of host galaxy are known, although we retain historical SNe whose positions are known to a precision of  $\sim 1$  arcsec.

Finally, we exclude 15 additional SNe whose host galaxies are

<sup>3</sup> <http://graspa.oapd.inaf.it>

<sup>4</sup> SN 1954J, 1961V, 1978K, 1997bs, 1999bw, 2000ch, 2002kg, 2002bu, 2008S, 2010da and 2010dn

**Table 2.** Properties of type Ib/c ccSNe used in the present study, including spectral types (col 2), host galaxies (col 3), distance (col 4), positions (col 5–6, from Asiago Catalogue except where noted), deprojected galactocentric distances (col 7,  $R_{\text{SN}}$ ), source of H $\alpha$  imaging (col 8, key in Table 5), whether the SN is associated with a cluster (col 9), or nebular emission (col 10), including results from HST imaging in parentheses. Col 11 provides information on the closest H II region, including its offset and deprojected distance from the SN and whether it is spatially extended (ext.) or compact (comp.). Cols 12–14 present the flux ( $F$ ,  $\leq \pm 0.1$  dex), radius ( $r$ ,  $\pm 0''.5$ ) and H $\alpha$  luminosity ( $L$ , factor of two) of the H II region, while Col 15 shows the class of environment.

SN	SN type	Host	$d$ Mpc	SN (J2000) $\alpha, \delta$	$R_{\text{SN}}$ $R_{25}$	Tel ID	Cl? H $\alpha$ ? (HST)	Comment	$F(\text{H}\alpha + [\text{N II}])$ erg s $^{-1}$ cm $^{-2}$	$r(\text{H II})$ arcsec	$L(\text{H}\alpha)$ 10 $^{37}$ erg s $^{-1}$	Class
1983N <sup>1</sup>	Ib	M 83	4.92	13 36 51.28 −29 54 02.8	0.48	j1	✗ ✓ (✗) (✗?)	Ext. H II reg. 1''/25 pc E Twin GH II reg. 8''/180 pc SE	$6 \times 10^{-15}$ $1.4 \times 10^{-13}$	1.5 5	3 80	4
1985F	Ib/c	NGC 4618	9.2	12 41 33.01 +41 09 05.9	0.10	i	✓ ✓ (✓) (✓?)	Coincident w GH II reg.	$5 \times 10^{-14}$	2.5	46	5
1994I	Ic	M 51a	8.39	13 29 54.07 +47 11 30.5	0.06	h	✗ ✓ (✗) (✓)	Ext. GH II reg. 2''/80 pc W Ext. GH II reg. 9''/0.38 kpc SW	$1.0 \times 10^{-14}$ $2 \times 10^{-14}$	2 2	13 30	5
1997X	Ib	NGC 4691	12.0	12 48 14.28 −03 19 58.5	0.14	11	✗ ✗	H II reg. 1''.5/100 pc SW (Giant?) H II reg. 6''/0.4 kpc SSW	– –	1 3	– –	3
2002ap	Ic	M 74	9.0	01 36 23.85 +15 45 13.2	0.89	e1,n	✗ ✗ (✗) (✗)	Ext. H II 10''/400 pc SE	$2 \times 10^{-15}$	4	2	2
2003jg	Ib/c	NGC 2997	11.7	09 45 37.91 −31 11 21.0	0.07	f	✗ ✗ (✗)	Ext H II reg. 2''/140 pc E Nuclear starburst 12''/650 pc E	$1.2 \times 10^{-15}$ $7 \times 10^{-13}$	1.5 10	4 2200	2
2005at	Ic	NGC 6744	11.6	19 09 53.57 −63 49 22.8	0.30	j1	✓ ✓	Coincident with ext. H II reg.	$2 \times 10^{-15}$	1.5	7	4
2005kl	Ic	NGC 4369	11.2	12 24 35.68 +39 23 03.5	0.17	m	✗ ✓	(Giant?) H II reg. 1''.5/80 pc SE	–	2	–	5
2007gr	Ic	NGC 1058	9.86	02 43 27.98 +37 20 44.7	0.45	i	✓ ✓ (✓) (✓?)	Ext. H II reg. 1''.5/75 pc NE Ext. GH II reg. 2''/100 pc W	$1.1 \times 10^{-14}$ $4 \times 10^{-14}$	2 2.5	16 60	5
2008eh	Ib/c?	NGC 2997	11.3	09 45 48.16 −31 10 44.9	0.50	f	✗ ✓	Edge of GH II reg. Ext. GH II reg. 4''.5/250 pc S	$1.2 \times 10^{-14}$ $2 \times 10^{-14}$	2 2.5	40 70	5

1: SN 1983N coordinates from Sramek et al. (1984)

observed at high inclination ( $\geq 65^\circ$ ) owing to the potential for confusion with unrelated line-of-sight H II regions. Inclinations were obtained from HyperLeda<sup>5</sup>, such that 41 ccSNe meet our criteria. Basic properties of these ccSNe are listed in Tables 2 and 3 for type Ib/c and type II ccSNe, respectively, with positions adopted from Asiago except where noted.

Uncalibrated H $\alpha$  images were available for NGC 4369 and NGC 4691, while no H $\alpha$  observations of either NGC 2082 or UGC 12160 were available. Therefore, the final sample comprises 39 SNe, subdivided into 29 type II and 10 type Ib/c ccSNe. Basic properties of the SN host galaxies are presented in Table 4, which include high inclination galaxies (shown in bold) plus hosts lacking accurate ccSNe coordinates (shown in italics).

### 3.2 H $\alpha$ datasets of ccSNe host galaxies

We have examined the immediate environment of these 41 ccSNe in their 30 host galaxies using (primarily) archival, continuum subtracted H $\alpha$  (+[N II]) imaging. Calibrated images are available for 37 ccSNe, uncalibrated images are available for SN 1997X (NGC 4691) and SN 2005kl (NGC 4369) from the 2.0m Liverpool Telescope and 2.5m Isaac Newton Telescope, respectively. We exclude SN 1992ba (NGC 2082) and SN 1995X (UGC 12160) from our global statistics since no H $\alpha$  images of their host galaxies are publicly available, although we discuss literature descriptions for these cases. Therefore in 39 cases we have examined the association between ccSNe with H II regions, and in 37 cases measured nebular fluxes and converted these into H $\alpha$  luminosities. In view of the possibility that the SN progenitor may have been ejected from its birth

cluster, we examine the environment to typical projected distances of 0.5 kpc.

Table 5 indicates the source of the continuum subtracted H $\alpha$  images used in our study. The majority of archival images were provided in flux calibrated format, for which the 11Mpc H $\alpha$  and UV Survey (11HUGS, Kennicutt et al. 2008) and SINGS (Kennicutt et al. 2009)<sup>6</sup> alone enabled the nebular environment of 40% of the ccSNe to be assessed. The majority of the remaining host galaxies were included in other H $\alpha$  surveys of nearby galaxies, namely H $\alpha$ GS (James et al. 2004), SINGG (Meurer et al. 2006) and those by Hoopes et al. (2001) and Knapen et al. (2004). For M 101, we used the low-resolution, flux calibrated 0.6m KPNO Schmidt imaging by Hoopes et al. (2001) together with higher spatial resolution, uncalibrated 2.5m INT/Wide Field Camera imaging obtained from the ING archive<sup>7</sup>, which was also used in several other cases (e.g. NGC 7292). We have also inspected Hubble Space Telescope (HST) WFPC2, ACS and WFC3 imaging from the ESA Hubble Science Archive<sup>8</sup>, which is available for a subset of the ccSNe. The Hubble Heritage Team ACS/WFC mosaic of M 51a was obtained from a dedicated website<sup>9</sup>. Narrow-band H $\alpha$  imaging is only available for 8 ccSNe from our sample, while broad band images have been obtained in 22 cases, the latter relevant for the potential association with compact star clusters.

NGC 2997, NGC 1559 and the LMC host the remaining four ccSNe omitted from these H $\alpha$  surveys. For the LMC we employ continuum subtracted H $\alpha$  imaging obtained with a Nikon survey

<sup>5</sup> <http://leda.univ-lyon1.fr>

<sup>6</sup> Available from Local Volume Legacy Survey (LVLS) at <http://www.ast.cam.ac.uk/research/lvls>

<sup>7</sup> <http://casu.ast.cam.ac.uk/casuadc/archives/ingarch>

<sup>8</sup> <http://archives.esac.esa.int/hst/>

<sup>9</sup> <http://archive.stsci.edu/prepds/m51/>

**Table 3.** Properties of type II ccSNe used in the present study. Column headings are as in Table 2.

SN	SN type	Host	$d$ Mpc	SN (J2000) $\alpha, \delta$		$R_{SN}$ $R_{25}$	Tel ID	CI? (HST)	H $\alpha$ ? (HST)	Comment	$F(\text{H}\alpha + [\text{N II}])$ $\text{erg s}^{-1} \text{cm}^{-2}$	$r(\text{H II})$ arcsec	$L(\text{H}\alpha)$ $10^{37} \text{erg s}^{-1}$	Class
1923A	II-P:	M 83	4.92	13 37 09.2	-29 51 04	0.33	j1	$\times$ ( $\times$ )	$\checkmark$ ? ( $\checkmark$ )	Ext. GH II reg. $\sim 4''/100$ pc N	$3 \times 10^{-14}$	4	78	5
1964H <sup>5</sup>	II	NGC 7292	12.9	22 28 24.06	+30 17 23.3	0.51	d2,l2	$\times$ ( $\times$ )	$\times$ ( $\times$ )	H II reg. $5''/0.35$ kpc NW GH II reg $7''/0.5$ kpc W	$1.4 \times 10^{-15}$ $4 \times 10^{-15}$	2	4 13	2
1968D	II	NGC 6946	7.0	20 34 58.32	+60 09 34.5	0.14	k	$\times$ ( $\times$ )	$\times$ ( $\times$ )	H II reg. $4''.3/150$ pc SSE Ext. H II reg. $12''/400$ pc NNE	$5 \times 10^{-15}$ $1.1 \times 10^{-14}$	2	3 7	2
1968L	II-P	M 83	4.92	13 37 00.51	-29 51 59.0	0.02	j1	$\times$ ( $\times$ )	$\checkmark$ ( $\checkmark$ )	GH II reg. $1''/25$ pc E Double GH II reg. $3''/75$ pc N	$3 \times 10^{-13}$ $2 \times 10^{-12}$	1	150 1200	5
1970G <sup>5</sup>	II-L	M 101	6.96	14 03 00.76	+54 14 33.2	0.46	b,l2	$\checkmark$ ( $\times$ )	$\checkmark$ ( $\times$ ?)	Edge of GH II reg.	$2 \times 10^{-12}$	20	2070	5
1980K	II-L	NGC 6946	7.0	20 35 30.07	+60 06 23.7	0.99	h	$\times$ ( $\times$ )	$\times$ ( $\times$ ?)	H II reg. $60''/2.1$ kpc WNW	$6 \times 10^{-15}$	2	4	2
1986L <sup>5</sup>	II-L	NGC 1559	12.6	04 17 29.4	-62 47 01	0.55	j2	$\times$ ( $\times$ )	$\times$ ( $\times$ )	H II reg. $2''/150$ pc N GH II reg. $3''/230$ pc SW	$2 \times 10^{-15}$ $3 \times 10^{-14}$	1	8 95	3
1987A	IIpec	LMC	0.05	05 35 28.01	-69 16 11.6	-	a1,a2	$\times$ <sup>1</sup> ( $\times$ )	$\checkmark$ ( $\times$ ?)	H II complex $2.75''/40$ pc NW GH II reg. $20.5''/300$ pc NE	$1.3 \times 10^{-10}$ $1.4 \times 10^{-8}$	2'	7 735	4
1992ba	II	NGC 2082	13.1	05 41 47.1	-64 18 00.9	0.55			2					
1993J	IIb	M 81	3.6	09 55 24.95	+69 01 13.4	0.32	h	$\times$ ( $\times$ )	SNR? (SNR)	Coincident with faint emission Ext. H II reg. $21''/580$ pc NE	$1.1 \times 10^{-15}$ $1.1 \times 10^{-14}$	2	0.1 1.3	2
1995V	II-P	NGC 1087	14.4	02 46 26.77	-00 29 55.6	0.36	d2	$\times$ ( $\times$ )	$\times$ ? ( $\times$ ?)	GH II reg. $5''/0.6$ kpc SW	$5 \times 10^{-15}$	3.5	18	2
1995X	II	UGC 12160	14.4	22 40 51.30	+75 10 11.5	0.42			3					
1996cr	IIn:	Circinus	4.21	14 13 10.01	-65 20 44.4	0.18	c	$\times$ ( $\times$ )	$\checkmark$ ( $\checkmark$ )	GH II reg. $3''/100$ pc SE Ext. GH II reg. $15''/0.5$ kpc NNW	$3 \times 10^{-14}$ $7 \times 10^{-14}$	4	31 67	5
1998dn	II	NGC 337A	11.4	01 01 27.08	-07 36 36.7	1.21	d1	$\times$ ( $\times$ )	$\times$ ( $\times$ )	Bright H II reg. $5''.5/500$ pc NW	$5 \times 10^{-14}$	2.5	14	3
1999em <sup>5</sup>	II-P	NGC 1637	9.77	04 41 27.05	-02 51 45.8	0.22	e1	$\times$ ( $\times$ )	$\times$ ( $\times$ )	H II reg. $6''/300$ pc SE H II reg. $9''.5/0.5$ kpc SE	$7 \times 10^{-16}$ $7 \times 10^{-15}$	2	1.6 15	2
1999eu	II-P	NGC 1097	14.2	02 46 20.79	-30 19 06.1	0.83	e2	$\times$ ( $\times$ )	$\times$ ( $\times$ )	H II reg. $3''.75/375$ pc W	$8 \times 10^{-16}$	2	8	2
1999gi	II-P	NGC 3184	13.0	10 18 16.66	+41 26 28.2	0.28	h	$\times$ ( $\times$ )	$\checkmark$ ( $\times$ ?)	Ext. H II reg. $2''/125$ pc SW Ext. H II reg. $2''/125$ pc NE	$3 \times 10^{-15}$ $9 \times 10^{-15}$	2	8 22	5
2001X <sup>5</sup>	II-P	NGC 5921	14.0	15 21 55.46	+05 03 43.1	0.34	d2	$\times$ ( $\times$ )	$\times$ ( $\times$ )	Diffuse H II reg. $3''/0.3$ kpc SE Ext. H II reg. $4''/0.4$ kpc N	$3 \times 10^{-15}$ $9 \times 10^{-15}$	2	12 36	3
2001ig	IIb	NGC 7424	7.94	22 57 30.69	-41 02 25.9	1.02	e1	$\times$ ( $\times$ )	$\checkmark$ ( $\times$ )	Edge of ext. H II reg.	$1.5 \times 10^{-15}$	2.5	2	4
2002hh <sup>5</sup>	II-P	NGC 6946	7.0	20 34 44.25	+60 07 19.4	0.38	k	$\times$ ( $\times$ )	$\checkmark$ ( $\times$ )	Ext. GH II reg. $2''.5/85$ pc NW	$4 \times 10^{-14}$	4	26	5
2003B	II-P	NGC 1097	14.2	02 46 13.78	-30 13 45.1	1.04	e2	$\times$ ( $\times$ )	$\checkmark$ ( $\times$ )	Edge of ext. GH II reg.	$6 \times 10^{-15}$	3	58	5
2003gd	II-P	M 74	9.0	01 36 42.65	+15 44 19.9	0.51	j1	$\times$ ( $\times$ )	$\times$ ( $\times$ )	H II reg. $7''/300$ pc SW Ext. GH II reg. $12''/500$ pc SW	$2 \times 10^{-15}$ $2 \times 10^{-14}$	1.5	2 20	2
2004dj	II-P	NGC 2403	3.16	07 37 17.02	+65 35 57.8	0.34	h <sup>4</sup>	$\checkmark$ ( $\times$ )	$\times$ ( $\times$ ?)	Ext. H II reg. $21''/450$ pc NW Ext. GH II reg. $21''/450$ pc SE	$4 \times 10^{-14}$ $5 \times 10^{-13}$	2.5	6 73	1
2004et	II-P	NGC 6946	7.0	20 35 25.33	+60 07 17.7	0.82	h	$\times$ ( $\times$ )	$\times$ ( $\times$ ?)	Ext. H II reg. $9''/300$ pc N	$3 \times 10^{-15}$	2	2	2
2005cs	II-P	M 51a	8.39	13 29 52.85	+47 10 36.3	0.30	h	$\checkmark$ ? ( $\times$ )	$\checkmark$ ( $\times$ )	Ext. H II reg. $1''/40$ pc E Ext. GH II reg. $13''/0.55$ kpc E	$1.4 \times 10^{-15}$ $1.0 \times 10^{-14}$	1.5	2 13	4
2008bk	II-P	NGC 7793	3.61	23 57 50.42	-32 33 21.5	0.75	e2	$\times$ ( $\times$ )	$\times$ ( $\times$ )	H II reg. $7''/200$ pc SW	$1.8 \times 10^{-14}$	3	5	2
2009N	II-P	NGC 4487	11.0	12 31 09.46	-08 02 56.3	0.77	d1	$\times$ ( $\times$ )	$\times$ ( $\times$ )	Comp. H II reg. $3''/200$ pc NW Ext. H II reg. $3''/200$ pc NE	$8 \times 10^{-16}$ $3 \times 10^{-15}$	1.5	2 2.5	2
2009ib	II-P	NGC 1559	12.6	04 17 39.92	-62 46 38.7	0.67	j2	$\times$ ( $\checkmark$ )	$\times$ ( $\times$ ?)	Ext. H II reg. $1''.5/170$ kpc SE Ext. GH II reg. $6''/0.7$ kpc SW	$3 \times 10^{-15}$ $1.3 \times 10^{-14}$	1	9 40	2
2011dh	IIb	M 51a	8.39	13 30 05.12	+47 10 11.3	0.50	h	$\times$ ( $\times$ )	$\times$ ( $\times$ )	Bright H II $8''/0.35$ kpc SE Ext. GH II reg. $11''/0.5$ kpc NE	$5 \times 10^{-15}$ $1.0 \times 10^{-14}$	2	7 14	2
2012A	II-P	NGC 3239	10.0	10 25 07.39	+17 09 14.6	0.42	g	$\times$ ( $\times$ )	$\checkmark$ ( $\times$ )	Edge of H II reg. Ext. GH II reg. $10''/0.6$ kpc NE	$6 \times 10^{-15}$ $4 \times 10^{-13}$	2	9 525	4
2012aw	II-P	M 95	10.0	10 43 53.76	+11 40 17.9	0.62	h	$\times$ ( $\times$ )	$\times$ ( $\times$ )	H II reg. $5''/260$ pc NNE H II reg. $10''/525$ pc SW	$4 \times 10^{-16}$ $1.2 \times 10^{-15}$	2	0.6 2	2

1: SN 1987A is associated with a faint cluster (Panagia et al. 2000) that would be not detected at the typical distance of the other ccSNe.

2: SN 1992ba is located within or close to a bright H II region according to Schmidt et al. (1994)

3: SN 1995X is located close to the maximum H $\alpha$  brightness of UGC 12160 according to Anderson et al. (2012)4: KPNO 2.1m H $\alpha$  imaging of Kennicutt et al. (2003) is supplemented by continuum subtracted NOT/ALFOSC H $\alpha$  imaging from Larsen & Richtler (1999)

5: Coordinates: SN 1964H (Porter 1993); SN 1970G (Allen et al. 1976); SN 1986L (McNaught &amp; Waldron 1986); SN 1999em (Jha et al. 1999); SN 2001X (Li et al. 2001); SN 2002hh (Stockdale et al. 2002)

**Table 4.** Basic properties of host galaxies of ccSNe used in the present study (within 15 Mpc), drawn from RC3 or HyperLeda. Hosts viewed at unfavourable high inclinations ( $\geq 65^\circ$ ) were excluded from the study, but are listed (in bold) separately, as are hosts of ccSNe excluded owing to imprecise SN positions (in italics).

PGC	M	NGC	UGC	Type	$cz$ km s <sup>-1</sup>	$i$	PA	$d$ Mpc	Ref mag	$m_{B_T}$ mag	$A_B$ mag	$M_{B_T}$	ccSNe
03671		337A		SAB(s)dm	1074	56.1	8	11.4 ± 2.1	1	12.70	0.35	-17.94	1998dn
05974	74	628	01149	SA(s)c	657	6.5 <sup>o</sup>	25 <sup>o</sup>	9.0	1	9.95	0.25	-20.07	2002ap, 2003gd
10314		1058	02193	SA(rs)c	518	58.5	90.4	9.86 ± 0.61	1	11.82	0.22	-18.37	1969L, 2007gr
10488		1097		SB(s)b	1271	55.0	138.2	14.2 ± 2.6	1	10.23	0.10	-20.63	1992bd, 1999eu, 2003B
10496		1087	02245	SAB(rs)c	1517	54.2	12	14.4 ± 1.8	1	11.46	0.12	-19.46	1995V
14814		1559		SB(s)cd	1304	60.2	62.8	12.6 ± 2.5	1	11.00	0.11	-19.61	1984J, 1986L, 2009ib
15821		1637		SAB(rs)c	717	31.1	16.3	9.77 ± 1.82	1	11.47	0.15	-18.63	1999em
17223	—	LMC	—	SB(s)m	278	35.3	170	0.050 ± 0.002	m	0.91	0.27	-17.86	1987A
17609		2082		SB(r)b	1184	26.2	—	13.1 ± 1.8	1	12.62	0.21	-18.18	1992ba
21396		2403	03918	SAB(s)cd	131	61.3	126	3.16 ± 0.16	c,d,k,l	8.93	0.14	-18.74	2004dj
27978		2997		SA(s)c	1088	54.3	96.6	11.3 ± 0.8	1	10.06	0.39	-20.59	2003jg, 2008eh
28630	81	3031	05318	SA(s)ab	-34	62.7	157	3.65 ± 0.18	a,d,e,k,l	7.89	0.29	-20.18	1993J
30087		3184	05557	SAB(rs)cd	592	14.4	135	13.0	1	10.36	0.06	-20.27	1921B, 1937F, 1999gi
30560		3239	05637	IB(s)m pec	753	46.8	—	10.0	1	11.73	0.12	-18.39	2012A
32007	95	3351	05850	SB(r)b	778	54.6	9.9	10.0 ± 1.0	c,d,h,l	10.53	0.10	-19.76	2012aw
40396		4369	07489	(R)SA(rs)a	1045	18.9	—	11.2 ± 1.1	1	12.33	0.09	-18.01	2005kl
41399		4487		SAB(rs)cd	1034	58.2	74.2	11.0 ± 0.8	1	11.69	0.08	-18.59	2009N
42575		4618	07853	SB(rs)m	544	57.6	40.2	9.20 ± 0.57	1	11.22	0.08	-18.67	1985F
43238		4691		(R)SB0/a(s) pec	1110	38.8	28.0	12	1	11.66	0.10	-18.84	1997X
47404	51a	5194	08493	SA(s)bc pec	463	32.6	163.0	8.39 ± 0.84	b,l	8.96	0.13	-20.79	1994I, 2005cs, 2011dh
48082	83	5236		SAB(s)c	513	14.1	45 <sup>p</sup>	4.92 ± 0.25	g,l	8.20	0.24	-20.29	1923A, 1968L, 1983N
50063	101	5457	08981	SAB(rc)cd	241	16	—	6.96 ± 0.35	b,d,h,l	8.31	0.03	-20.99	1909A, 1951H, 1970G
50779	—	Circinus	—	SA(s)b?	434	64.3	36.1	4.21 ± 0.78	1	12.10	2.00	-18.02	1996cr
54849		5921	09824	SB(r)bc	1480	49.5	140.0	14.0 ± 3.2	1	11.49	0.15	-19.39	2001X
62836		6744		SAB(r)bc	841	53.5	15.4	11.6 ± 0.9	1	9.61	0.16	-21.34	2005at
65001		6946	11597	SAB(rs)cd	40	18.3	—	7.0	1	9.61	1.24	-20.86	1917A 1948B, 1968D 1980K, 2002hh, 2004et
68941		7292	12048	IBm	986	54.5	101.0	12.9 ± 1.0	1	13.03	0.23	-17.75	1964H
69470			12160	Scd?	1555	38.1	14.8	14.4 ± 3.0	1	14.85	2.04	-17.98	1995X
70096		7424		SAB(rs)cd	939	59	—	7.94 ± 0.77	1	10.96	0.04	-18.56	2001ig
73049		7793		SA(s)d	227	53.7 <sup>n</sup>	99.3 <sup>n</sup>	3.61 ± 0.18	1	9.63	0.07	-18.42	2008bk
02052		150		SB(rs)b?	1584	<b>66.9</b>	—	14.9 ± 2.2	1	12.00	0.05	-18.92	1990K
09031		891	01831	SA(s)b? edge	528	<b>90</b>	—	9.91 ± 0.5	c,e,l	10.81	0.24	-19.47	1986J
10329		1073	02210	SB(rs)c	1208	52.3	—	12.3 ± 1.7	1	11.47	0.14	-19.12	1962L
12286		1313		SB(s)d	470	34.8	—	4.25 ± 0.21	f,l	9.20	0.40	-19.25	1962M
22338	—	ESO 209-G009	—	SB(s)cd? edge	1119	<b>90</b>	—	13.4 ± 1.0	1	12.68	0.94	-18.89	2005ae
26512		2841	04966	SA(r)b?	638	<b>65.2</b>	—	14.1 ± 1.4	1	10.09	0.06	-20.71	1972R
28655	82	3034	05322	I0 edge	203	<b>76.9</b>	—	3.52 ± 0.18	k,l	9.30	0.58	-18.91	2004am, 2008iz
30197		3198	05572	SB(rs)c	663	<b>77.8</b>	—	13.8 ± 1.4	1	10.87	0.05	-19.87	1966J
33408		3510	06126	SB(s)m edge	713	<b>78.1</b>	—	14.7 ± 1.7	1	14.30	0.11	-16.65	1996cb
34030	108	3556	06225	SB(s)cd edge	699	<b>67.5</b>	—	9.55 ± 1.26	1	10.69	0.06	-19.27	1969B
34695	66	3627	06346	SAB(s)b	727	<b>67.5</b>	—	8.28 ± 0.41	c,d,l	9.65	0.12	-20.48	1973R, 2009hd
39225		4214	07278	IAB(s)m	291	43.7	—	2.87 ± 0.14	k,l	10.24	0.08	-17.25	1954A
39600	106	4258	07353	SAB(s)bc	448	<b>68.3</b>	—	7.61 ± 0.38	c,e,i,j,l	9.10	0.06	-20.28	1981K
41333		4490	07651	SB(s)d pec	565	<b>79</b>	—	9.20 ± 0.57	1	10.22	0.08	-19.68	1982F, 2008ax
42002		4559	07766	SAB(rc)cd	807	64.8	—	8.67 ± 0.57	1	10.46	0.06	-19.29	1941A
43451		4725	07989	SAB(r)sb pec	1206	45.4	—	12.4 ± 1.2	1	10.11	0.04	-20.40	1940B
45279		4945		SB(s)cd? edge	563	<b>90</b>	—	3.36 ± 0.17	1	9.30	0.64	-19.25	2005af, 2011ja
51106		5530		SA(rs)bc	1194	<b>66.5</b>	—	11.8 ± 2.2	1	11.78	0.42	-19.00	2007it
67671			11861	SABdm	1481	<b>75</b>	—	14.4 ± 3.0	1	14.20	2.19	-18.78	1995ag, 1997db
68618	—	IC 5201	—	SB(rs)cd	915	<b>66.7</b>	—	9.20 ± 1.71	1	11.30	0.04	-18.56	1978G
69327		7331	12113	SA(s)b	816	<b>70</b>	—	14.7 ± 1.5	1	10.35	0.33	-20.82	1959D
71866		7713		SB(r)d?	692	<b>65.9</b>	—	9.95 ± 2.07	1	11.51	0.06	-18.54	1982L

a: Ciardullo et al. (1993); b: Feidmeier et al. (1997); c: Ciardullo et al. (2002); d: Freedman et al. (2001); e: Tonry et al. (2001); f: Méndez et al. (2002); g: Thim et al. (2003); h: Sakai et al. (2004); i: Macri et al. (2006); j: Mager et al. (2008); k: Dalcanton et al. (2009); l: Tully et al. (2009); m: Schaefer (2008); n: Carignan & Puche (1990); o: Kamphuis & Briggs (1992) p: Danver (1942)

**Table 5.** Source of ground-based H $\alpha$  and continuum imaging used in this study.

Tel ID	Telescope	Instrument	CCD scale arcsec/pix	FWHM arcsec	— H $\alpha$ —		Continuum	Reference
					$\lambda_c$ (Å)	FWHM (Å)		
a1	Nikon Survey Camera	2K CCD	12.0	30	6570	15	HaC (6676, 55)	Murphy & Bessell (2000)
a2	Parking Lot Camera	800×800	36.9	80	6571	14	R	Kennicutt et al. (1995)
b	KPNO 0.6m Schmidt	Tek 2K CCD	2.03	4.4	6573	67	R	Hoopes et al. (2001)
c	CTIO 0.9m	Tek 2K CCD	0.792	~3.0	6563	75	R	Kennicutt et al. (2008)
d1	JKT 1.0m	CCD	0.241	1.5–2	6594	44	R	Knapen et al. (2004)
d2			0.331	1.5–3	6594	44	R	James et al. (2004)
e1	CTIO 1.5m	CCD	0.434	1.0	6568	30	R	Meurer et al. (2006)
e2				1.2	6568	20	R	Kennicutt et al. (2003)
f	Danish 1.54m	DFOSC	0.400	1.8	6565	114	R	Larsen & Richtler (1999)
g	VATT 1.8m	CCD	0.400	~1.8	6580	69	R	Kennicutt et al. (2008)
h	KPNO 2.1m	CFIM	0.305	1.0	6573	67	R	Kennicutt et al. (2003)
i	Bok 2.3m	CCD21	0.432	~1.5	6575	69	R	Kennicutt et al. (2008)
j1 <sup>1</sup>	VLT 8.0m	FORS1+2	0.126	0.8	6563	61	HaC (6665, 65)	Hadfield et al. (2005)
j2 <sup>2</sup>			0.200	0.8	6563	61	V	
k <sup>3</sup>	Gemini-N 8.1m	GMOS	0.145	0.6	6560	70	HaC (6620, 60)	
l1	INT 2.5m	WFC	0.333	1.8	6568	95	R	Anderson & James (2008)
l2				1–2	6568	95	HaC (6657, 79), r	
m	LT 2.0m	RATCam	0.278	1.2	6557	100	r'	Anderson & James (2008)
n	CFHT 3.6m	CFH12K	0.206	0.9	6584	96	R	Crockett et al. (2007)

1: 067.D-0006(A), 069.B-0125(A), 380.D-0282(A), 081.B-0289(C); 2: 075.D-0213(A); 3: GN-2009B-Q-4

camera plus 2K CCD (M.S. Bessell, priv. comm.), lower resolution Parking Lot Camera (PLC) H $\alpha$  and R-band images from Bothun & Thompson (1988) and Kennicutt et al. 1995), plus higher resolution MCELS imaging of 30 Doradus obtained using the CTIO Curtis Schmidt telescope (Smith et al. 2000). For NGC 2997 we have resorted to the Danish 1.5m observations of Larsen & Richtler (1999). For NGC 1559, we have used high spatial resolution archival VLT/FORS1 imaging (from 075.D-0213(A), PI D. Baade). In addition, high spatial resolution H $\alpha$  imaging of several ccSNe host galaxies has been included in our extragalactic Wolf-Rayet surveys. These comprise VLT/FORS2 imaging of M 83 (Hadfield et al. 2003) plus unpublished VLT/FORS1 imaging of M 74 (from 380.D-0282(A), PI P. Crowther and NGC 6744 (081.B-0289(C), PI P. Crowther) and unpublished Gemini-N GMOS H $\alpha$  imaging of NGC 6946 (GN-2009B-Q-4, PI J. Bibby). The relatively small field of view of these instruments excluded the investigation of some ccSNe environments in these galaxies from out VLT or Gemini imaging, although (non-calibrated) archival VLT/FORS1 imaging is available for the SN 2008bk in NGC 7793 (067.D-0006(A), PI W. Gieren).

Flux calibration was necessary in these cases. The LMC Nikon survey camera image was calibrated against Parking Lot Camera datasets for 30 Doradus (Kennicutt et al. 1995). The Danish 1.54m datasets of Larsen & Richtler (1999) were calibrated with respect to 5 galaxies in common with 11HUGS (NGC 300, NGC 1313, M 83, NGC 6946, NGC 7793). VLT/FORS1+2 and Gemini-G GMOS images were calibrated against imaging of spectrophotometric standard stars (LTT 4816, LTT 1020, BD+28 4211).

Finally, where necessary (e.g. H $\alpha$ GS), astrometric calibration was performed using the Starlink *gai*a package<sup>10</sup> using the USNO-A2 catalogue, with typical RMS of <1 pix, corresponding to <0.5 arcsec in the majority of instances.

For the present sample, 8 (19%) of the ccSNe originate

from early-type spirals (S0/a/b), 31 (76%) from late-type spirals (Sc/d/m) and 2 (5%) from irregulars (Im). 25 (61%) ccSNe are from high luminosity ( $M_B < -19$  mag) hosts, with 16 (39%) from low luminosity galaxies, with a similar fraction of type II and type Ib/c ccSNe from dwarf hosts.

Table 6 presents star formation rates and star formation intensities for all host galaxies, excluding those lacking calibrated H $\alpha$  imaging (NGC 2082, 4369, 4691, UGC 12160). H $\alpha$  fluxes are adjusted for the contribution of [N II]  $\lambda\lambda 6548-6583$  preferentially from integrated spectrophotometry (e.g. Moustakas & Kennicutt 2006) or the Lee et al. (2009b)  $M_B$ -calibration. Similarly, extinction corrections,  $A_{H\alpha}$ , are preferentially obtained from measured integrated nebular H $\alpha$ /H $\beta$  ratios (e.g. Moustakas & Kennicutt 2006, via eqn. 4 from Lee et al. 2009b), or are the sum of (measured) foreground and (estimated) internal extinctions. Foreground extinctions are from Schlafly & Finkbeiner (2011, recalibration of Schlegel et al. 1998), for which we assume  $A_{H\alpha} = 0.62 A_B$ , while internal extinctions are estimated from a scaling relation between extinction and  $M_B$  (Lee et al. 2009b). In the case of Circinus, an extinction of  $A_B = 2.0$  mag was adopted (Freeman et al. 1977) owing to its low galactic latitude.

Integrated fluxes largely confirm previous results (e.g. Lee et al. 2009b), aside from differences in distances and the source of fluxes. One notable exception is NGC 6744, for which the newly calibrated Larsen & Richtler (1999) datasets reveal a lower limit of  $4.7 \times 10^{-12}$  erg s $^{-1}$  cm $^{-2}$  (6.4' radius) to the H $\alpha$ + [N II] flux, significantly higher than  $2.0 \times 10^{-12}$  erg s $^{-1}$  cm $^{-2}$  from Ryder & Dopita (1993), as reported in Kennicutt et al. (2008). A net flux of  $1.2 \times 10^{-12}$  erg s $^{-1}$  cm $^{-2}$  within the central region (3.5' radius) from Larsen & Richtler (1999) matches that from the calibrated VLT/FORS1 dataset to within 2%. Uncertainties for hosts in which fluxes, [N II]/H $\alpha$  and reddenings have been measured, such as M 74, are typically  $\pm 20\%$ , whereas cases for which calibrations have been adopted for [N II]/H $\alpha$  (factor of two) and  $A_{H\alpha}$  ( $\pm 50\%$ ), such as NGC 337A, are typically  $\pm 40\%$ .

Star formation intensities are uniformly based upon  $R_{25}$ , al-

<sup>10</sup> <http://star-www.dur.ac.uk/pdraper/gaia/gaia.html>



**Table 6.** Integrated  $H\alpha$  + [N II] fluxes ( $H\alpha$  in italics) of host galaxies of ccSNe used in the present study, from which star formation rates (SFR) and star formation intensities ( $\Sigma$ ) are obtained. Galaxy radii are from RC3 or HyperLeda ( $R_{25}$ ), or Bothun & Thompson (1998,  $R_D$ ). Uncertainties, where known, are indicated, while the [N II]/ $H\alpha$  calibration from Lee et al. (2009b) is reliable to a factor of two, and the  $A_{H\alpha}$  calibration is robust to  $\pm 50\%$ , such that global  $H\alpha$  luminosities (SFR and  $\Sigma$ ) should be reliable to between  $\pm 20\%$  (direct measurements of [N II]/ $H\alpha$  and  $A_{H\alpha}$ ) and  $\pm 40\%$  (calibrations).

PGC	Alias	$d$ Mpc	$\log F(H\alpha + [N II])$ erg s <sup>-1</sup> cm <sup>-2</sup>	Ref	[N II]/ $H\alpha$	$A_{H\alpha}$ mag	Ref	L( $H\alpha$ ) erg s <sup>-1</sup>	SFR $M_{\odot}$ yr <sup>-1</sup>	$R_{25}$ ( $R_D$ ) arcmin	$R_{25}$ ( $R_D$ ) kpc	$\Sigma_{R_{25}}$ ( $\Sigma_{R_D}$ ) $M_{\odot}$ yr <sup>-1</sup> kpc <sup>-2</sup>
03671	NGC 337A	11.4	-11.73 ± 0.10	6, 9 (d1)	0.16	0.71	9( $M_B$ )	$4.8 \times 10^{40}$	0.38	2.9	9.7	$1.3 \times 10^{-3}$
05974	M 74	9.0	-10.84 ± 0.04	1	0.35 ± 0.05	0.30 ± 0.18	3	$1.4 \times 10^{41}$	1.1	5.2	13.7	$1.8 \times 10^{-3}$
10314	NGC 1058	9.86	-10.63 ± 0.05	1	0.48 ± 0.05	0.69 ± 0.22	5	$3.5 \times 10^{40}$	0.27	1.5	4.3	$4.7 \times 10^{-3}$
10488	NGC 1097	14.2	-10.95	3	0.46	1.50 ± 0.08	9( $M_B$ ),3	$7.3 \times 10^{41}$	5.8	4.7	19.2	$5.0 \times 10^{-3}$
10496	NGC 1087	14.4	-11.30 ± 0.04	2	0.40 ± 0.03	0.75 ± 0.20	5	$1.8 \times 10^{41}$	1.4	1.9	7.8	$7.4 \times 10^{-3}$
14814	NGC 1559	12.6	-10.81 ± 0.10	9 (j2)	0.31	0.86	9( $M_B$ )	$4.9 \times 10^{41}$	3.9	1.7	6.3	$3.1 \times 10^{-2}$
15821	NGC 1637	9.77	-11.59 ± 0.07	4, 9 (e1)	0.85	0.69	8, 9( $M_B$ )	$3.0 \times 10^{40}$	0.24	2.0	5.6	$2.4 \times 10^{-3}$
17223	LMC	0.05	-6.96 ± 0.05	1	0.15	0.64	9( $M_B$ )	$5.0 \times 10^{40}$	0.40	323 (103)	4.7 (1.5)	$5.8 \times 10^{-3}$ ( $5.6 \times 10^{-2}$ )
21396	NGC 2403	3.16	-10.25 ± 0.04	1	0.22 ± 0.04	0.45 ± 0.20	3	$8.5 \times 10^{40}$	0.67	10.9	10.1	$2.1 \times 10^{-3}$
27978	NGC 2997	11.3	-10.80 ± 0.10	7, 9 (f)	0.46	1.25	9( $M_B$ )	$5.1 \times 10^{41}$	4.1	4.5	14.6	$6.1 \times 10^{-3}$
28630	M 81	3.65	-10.31 ± 0.02	1	0.55 ± 0.08	0.15 <sup>+0.30</sup> <sub>-0.15</sub>	3	$5.8 \times 10^{40}$	0.46	13.5	14.2	$7.1 \times 10^{-4}$
30087	NGC 3184	13.0	-11.12 ± 0.05	3	0.52 ± 0.05	0.63 ± 0.18	3	$1.8 \times 10^{41}$	1.4	3.7	14.0	$3.1 \times 10^{-3}$
30560	NGC 3239	10.0	-11.32 ± 0.03	1	0.09 ± 0.01	0.30 ± 0.21	5	$6.9 \times 10^{40}$	0.55	2.5	7.3	$3.3 \times 10^{-3}$
32007	M 95	10.0	-11.24 ± 0.08	1	0.66 ± 0.03	0.73 ± 0.17	3	$8.1 \times 10^{40}$	0.64	3.7	10.7	$1.8 \times 10^{-3}$
41399	NGC 4487	11.0	-11.93 ± 0.10	6, 9 (d1)	0.21	0.65	9( $M_B$ )	$2.9 \times 10^{40}$	0.23	2.1	6.7	$1.7 \times 10^{-3}$
42575	NGC 4618	9.2	-11.36 ± 0.04	1	0.28 ± 0.03	0.13 <sup>+0.21</sup> <sub>-0.13</sub>	5	$3.9 \times 10^{40}$	0.31	2.1	5.6	$3.2 \times 10^{-3}$
47404	M 51a	8.39	-10.42 ± 0.08	1	0.59 ± 0.01	1.05 ± 0.21	5	$5.3 \times 10^{41}$	4.2	5.6	13.6	$7.1 \times 10^{-3}$
48082	M 83	4.92	-10.00 ± 0.04	1	0.40	1.08	9( $M_B$ )	$5.6 \times 10^{41}$	4.4	6.4	9.2	$1.7 \times 10^{-2}$
50063	M 101	6.96	-10.22 ± 0.13	1	0.54	1.10	9( $M_B$ )	$6.3 \times 10^{41}$	5.0	14.4	29.1	$1.9 \times 10^{-3}$
50779	Circinus	4.21	-11.19 ± 0.06	1	0.16	1.74	9( $M_B$ )	$5.8 \times 10^{40}$	0.46	3.5	4.2	$8.2 \times 10^{-3}$
54849	NGC 5921	14.0	-11.63 ± 0.05	2	0.28	0.83	9( $M_B$ )	$9.3 \times 10^{40}$	0.73	2.5	9.9	$2.4 \times 10^{-3}$
62836	NGC 6744	11.6	-11.33 <sup>†</sup>	7, 9 (f)	0.61	1.28	9( $M_B$ )	$1.5 \times 10^{42}$ <sup>†</sup>	12.0 <sup>†</sup>	10.0	33.6	$3.4 \times 10^{-3}$ <sup>†</sup>
65001	NGC 6946	7.0	-10.42 ± 0.06	3	0.45 ± 0.09	0.45 ± 0.30	3	$2.3 \times 10^{41}$	1.8	5.7	11.7	$4.3 \times 10^{-3}$
68941	NGC 7292	12.9	-11.78 ± 0.04	2	0.15	0.60	9 ( $M_B$ )	$5.0 \times 10^{40}$	0.39	1.1	4.0	$7.8 \times 10^{-3}$
70096	NGC 7424	7.94	-11.28 ± 0.07	4, 9 (e1)	0.20	0.62	9( $M_B$ )	$5.7 \times 10^{40}$	0.45	4.8	11.0	$1.2 \times 10^{-3}$
73049	NGC 7793	3.61	-10.60 ± 0.08	3	0.31 ± 0.07	0.67 ± 0.16	3	$5.5 \times 10^{40}$	0.44	4.7	4.9	$5.8 \times 10^{-3}$

1: Kennicutt et al. (2008); 2: James et al. (2004); 3: Kennicutt et al. (2009); 4: Meurer et al. (2006); 5: Moustakas & Kennicutt (2006); 6: Knapen et al. (2004); 7: Larsen & Richtler (1999); 8: Kennicutt & Kent (1983); 9: this work (note)

†: Lower limit using aperture of radius  $6'.4$  ( $0.64 R_{25}$ )

though the intensity is also calculated for the LMC from its V-band scale length,  $R_D$  (Hunter & Elmegreen 2004) following Bothun & Thompson (1988).

### 3.3 Calculation of $H\alpha$ luminosities

We have calculated  $H\alpha$  luminosities of H II regions in close proximity to the ccSNe location in the following way. Fluxes were measured using apertures no smaller than the image FWHM. Aside from the LMC Nikon Survey Camera and CTIO 1.5m/CFCCD imaging,  $H\alpha$  filters include the contribution of [N II]  $\lambda 6548$ –84. To adjust for this contribution, we either selected the [N II]/ $H\alpha$  ratio measured from spectrophotometry of their host galaxies, or estimated the ratio from an empirical scaling relation between [N II]/ $H\alpha$  and the absolute B-band magnitude  $M_B$  (Kennicutt et al. 2008), as above for global star formation rates. Of course, this adds an additional uncertainty, namely the radial metallicity gradient. By way of example, Bresolin et al. (2004) measured  $0.31 \leq [N II]/H\alpha \leq 0.64$  for 10 H II regions spanning the full radial extent of the disk of M 51a. Here, we adopt  $[N II]/H\alpha = 0.59$  (Moustakas & Kennicutt 2006), such that  $H\alpha$  luminosities should be underestimated by, at most,  $\sim 20\%$  in the outer disk where metallicities are lower than average. However, no correction is attempted due to the azimuthal

variation in metallicity, as shown from integral field spectroscopy of M 74 by Sánchez et al. (2011, their fig. 17).

Corrected  $H\alpha$  fluxes were converted into intensities, using the method set out above for global star formation rates. Once again, we neglect spatial variations of internal extinctions. For example, a global average of  $A_{H\alpha} = 1.05$  mag is adopted for M 51a (Moustakas & Kennicutt 2006), whereas Bresolin et al. (2004) obtained  $0.09 \leq A_{H\alpha} \leq 1.05$  mag for 10 H II regions distributed throughout its disk<sup>11</sup>. For M 51a, the luminosity of individual H II regions may be overestimated by up to a factor of 2.5. Once again, no radial correction is attempted owing to the clumpy nature of dust attenuation, as shown in integral field spectroscopy of M 74 by Sánchez et al. (2011, their fig. 11).

Overall, our adoption of global [N II]/ $H\alpha$  and  $A_{H\alpha}$  values should have a negligible effect for the majority of sources, such that the 20–40% uncertainties quoted above will apply to individual H II regions. However,  $H\alpha$  luminosities of regions far from large H II complexes – typically those at large galactocentric radii – may be overestimated by up to a factor of two ([N II]/ $H\alpha$  and  $A_{H\alpha}$  corrections act in opposite senses). The average galactocentric distance is

<sup>11</sup> We have converted the  $c(H\beta)$  values from Bresolin et al. (2004) to  $A_{H\alpha}$  via  $E(B-V) \sim 0.7 c(H\beta)$  and  $A_{H\alpha} \sim 2.5 E(B-V)$

**Table 7.** Summary of the present work and related studies, indicating sample size,  $N_{\text{SNe}}$ , mean distances,  $\bar{d}$ , the number of ccSNe associated with H II regions,  $N_{\text{HII}}$  or the normalized cumulative rank (NCR) pixel (see James & Anderson 2006). Distances are obtained from individual SN hosts, drawn preferentially from the Extragalactic Distance Database ( $\leq 3000 \text{ km s}^{-1}$ , Tully et al. 2009) or otherwise NASA Extragalactic Database.

SN type	van Dyk et al. (1996)			Anderson et al. (2012)			Smartt (priv. comm.)			This work		
	$N_{\text{SNe}}$	$\bar{d}$ (Mpc)	$N_{\text{HII}}/N_{\text{SNe}}$	$N_{\text{SNe}}$	$\bar{d}$ (Mpc)	$\overline{\text{NCR}}^{\text{a}}$	$N_{\text{SNe}}$	$\bar{d}$ (Mpc)	$N_{\text{HII}}$	$N_{\text{SNe}}$	$\bar{d}$ (Mpc)	$N_{\text{HII}}/n_{\text{SNe}}$
II	32	16.2	72±10%	163.5	32	0.25±0.02	17	14.6	0	29	8.7	38±11%
Ib	17	17.7	68±12%	39.5	40	0.32±0.04	9	19.3	1	10	9.9	70±26%
Ic				52	42	0.47±0.04						

(a)  $\text{NCR} = 0$  if the ccSN site is not associated with any  $\text{H}\alpha$  emission and  $\text{NCR} = 1$  if it is associated with the brightest  $\text{H}\alpha$  emission in its host.

$R_{\text{SN}}/R_{25} = 0.47$  ( $\sigma=0.30$ ), although  $\text{H}\alpha$  luminosities of nebulae located in the extreme outer disks of their hosts may be overestimated (e.g. SN 1980K, SN 2001ig, SN 2002ap, SN 2004et). Nevertheless, such adjustments would not affect our main conclusions.

### 3.4 Results

Following van Dyk (1992), a ccSNe is considered to be associated with a H II region if it is offset by an amount less than or equal to the radius of the H II region. For example, SN 1923A lies 4'' from a H II region whose radius is  $\sim 4''$ , while SN 1964H lies 5'' from a H II region, whose radius is 2''. Therefore the former is considered to be associated with a H II region while the latter is not. More details notes relating to individual ccSNe are provided in Appendix A.

Tables 2-3 present basic properties of individual type Ib/c and type II ccSNe, respectively, including the radius and  $\text{H}\alpha$  flux/luminosity of the nearest H II region. Overall, approximately half (18 of the 39) of our sample of ccSNe are associated with H II regions. Of these, the mean  $\text{H}\alpha$  luminosity is  $3 \times 10^{38} \text{ erg s}^{-1}$ , excluding SN 1970G which lies at the periphery of the supergiant H II region NGC 5455 within M 101. If we now separate these ccSNe into their main types, a much higher fraction of type Ib/c ccSNe (7 out of 10), namely  $70 \pm 26\%$ , are associated with nebular emission than type II ccSNe (11 out of 29), for which the fraction is  $38 \pm 11\%$ . This is qualitatively in agreement with the ground-based studies of Anderson & James (2008) and Anderson et al. (2012).

However, recall the lack of an association between H II regions and nearby ( $cz < 2000 \text{ km s}^{-1}$ ) ccSNe (Smartt et al. 2009) discovered between 1998–2008.5 observed at high spatial resolution (Crockett 2009; Smartt, priv. comm.). Only 4 type II ccSNe are in common between the present study and the subset of ccSNe from Smartt et al. (2009) that have been observed with HST. Of these, the ground-based study reveals consistent results, except for SN 2005cs (II-P). Fig. 2 shows that SN 2005cs appears to be associated with nebular emission from ground-based KPNO 2.1m imaging, yet HST ACS/WFC imaging reveals that it is offset by  $\sim 1''$  (40 pc at 8.4 Mpc), as discussed by Li et al. (2006).

Turning to Ib/c ccSNe, only 3 are in common between the present study and Crockett (2009). Broadly consistent results are obtained, although SN 2007gr (Ic) merits discussion, since it is the only Ib/c associated with a star forming region at the spatial resolution of HST. SN 2007gr is formally associated with  $\text{H}\alpha$  emission on the basis of our ground-based imaging (Fig. A32), whereas Crockett et al. (2008) indicate a small offset from  $\text{H}\alpha$  emission (from INT/WFC). More recent HST WFC2/F675W and WFC3/F625W suggest faint nebulosity is spatially coincident with the SN position.

In Table 7 we provide a summary of the present results, to-

gether with previous related studies. Despite the low number statistics, our results have the advantage over previous ground-based studies owing to smaller positional uncertainties with respect to van Dyk et al. (1996) and significantly smaller average distances than Anderson et al. (2012). For a nominal ground-based imaging quality of  $\text{FWHM} \sim 1.5\text{\AA}$ , the typical spatial resolution achieved is 125 pc (van Dyk et al. 1996), 260 pc (Anderson et al. 2012) and 70 pc in the present work. A characteristic scale of  $\sim 10$  pc – an order of magnitude higher – is achieved from the HST-selected sample of Smartt et al. (2009) and Crockett (2009). This is likely the origin of the very different statistics with respect to the ground-based studies. We shall return to the issue of spatial resolution in Sect. 5.

## 4 IMPLICATIONS FOR PROGENITOR MASSES OF CCSNE

### 4.1 Core-collapse SN environments

We now attempt to combine our results with the earlier discussion to place constraints upon ccSNe progenitors, recognising that this approach is inferior to than methods involving photometric detection of immediate ccSNe progenitors (e.g. Smartt et al. 2009).

We have examined the environment of each ccSNe and assign each case to one of the five classes set out in Sect. 2. For our previous examples, SN 1923A narrowly lies within the radius of a luminous H II region (Fig. A1) so it is assigned to class 5, whereas SN 1964H lies far from nebular emission (Fig. A2), so it is assigned to **Class 2** since it is not coincident with a bright star cluster.

Unsurprisingly, owing to the poor spatial resolution and sensitivity of the ground-based imaging, only one of the ccSNe, SN 2004dj (II-P), was assigned to Class 1, i.e. nebular emission absent but (young) cluster detected, as shown in Fig. A27. A massive progenitor ( $>20 M_{\odot}$ ) might be expected for SN 2004dj, although detailed studies of the cluster indicate a lower progenitor mass  $<20 M_{\odot}$  (Vinkó et al. (2006, 2009). As discussed above for the case of SN 2005cs (Fig. 2), more ccSNe from our sample would have been included in this category on the basis of HST imaging (e.g. SN 2009ib).

Half of type II ccSNe (15 from 29) were assigned to class 2, i.e. ccSNe lacking nebular emission, an associated (bright) cluster or a nearby giant H II region. The progenitor masses of such are expected to be  $< 20 M_{\odot}$ , in accord with Smartt et al. (2009) since the majority of these H-rich ccSNe either have unknown subclass or are type II-P – exceptions are type IIb ccSNe SN 1993J (Fig. A11) and SN 2011dh (Fig. A37).

Two H-deficient ccSNe also fall in this category (SN 2002ap, SN 2003jg), of which SN 2002ap represents an archetypal case

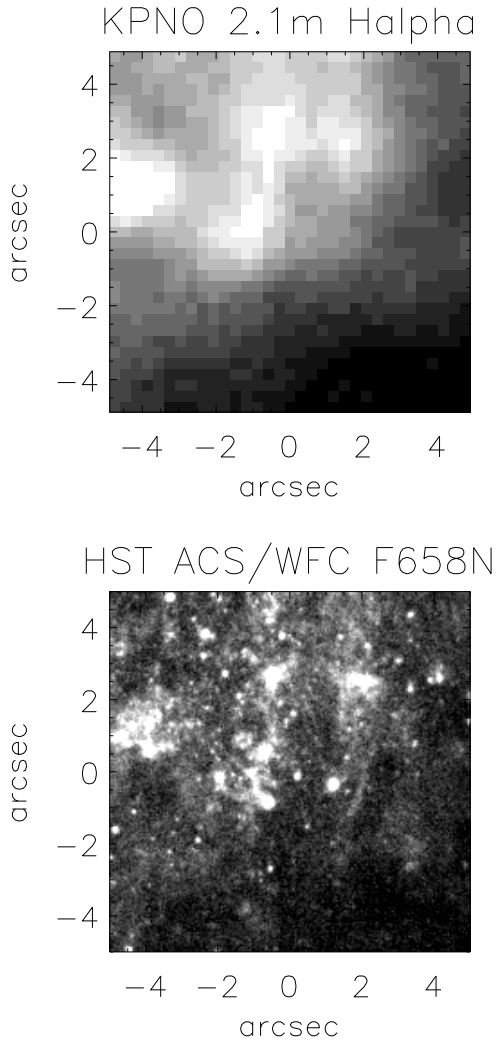


**Figure 2.** (top)  $10 \times 10$  arcsec<sup>2</sup> KPNO 2.1m H $\alpha$  image (from Kennicutt et al. 2003) showing the environment of SN 2005cs in M 51a, corresponding to  $400 \times 400$  pc at a distance of 8.39 Mpc; (bottom) MultiDrizzled HST ACS/WFC F658N image from GO 10452 (PI S. Beckwith, see discussion in Li et al. 2006). North is up and east is to the left.

(Fig. A22). The inclusion of type Ic ccSNe in this category favour an interacting binary scenario over a single star progenitor for these cases, as discussed by Crockett et al. (2007) for SN 2002ap. Indeed, Mazzali et al. (2002, 2007) proposed a binary scenario for SN 2002ap involving a progenitor with  $15\text{--}25 M_{\odot}$ . The case of SN 2003jg is marginal since it lies  $2''$  away ( $140$  pc deprojected) from a H II region, whose radius is  $1''.5$  on the basis of ground-based Danish 1.5m imaging (Fig. A26) such that it narrowly fails to meet our threshold for association.

From our sample we identify 3 potential runaways from nearby giant H II regions (Class 3), namely SN 1986L (II-L), SN 1997X (Ib) and SN 2001X (II-P), of which the former serves as a useful example (Fig. A9). Here we consider possible runaways if they lie at deprojected distances of up to  $0.4$  kpc from luminous H II regions ( $L(H\alpha) \geq 10^{38}$  erg s<sup>-1</sup>). If this were so, we are unable to assign progenitor masses, although high runaway masses are believed to be favoured (Fujii & Portegies Zwart 2011). Of course, the presence of a nearby giant H II region does not require a high mass

cluster that is sufficiently dense for runaways via dynamical interactions during the cluster formation. In addition, the close proximity of a giant H II region to the ccSNe does not necessarily imply the progenitor originated from this region (Class 2 is also likely).

Turning to ccSNe which are associated with H II regions, we find six cases matching Class 4, involving a relatively faint H II region in close proximity to the ccSN. Of these, every H II region is spatially extended, namely: SN 1983N (Ib), SN 1987A (IIpec), SN 2001ig (IIb), SN 2005at (Ic), SN 2005cs (II-P) and SN 2012A (II-P), indicating a lower limit to the progenitor mass of  $12$  ( $20$ )  $M_{\odot}$  for a duty cycle of  $20$  ( $10$ ) Myr. We cannot exclude the possibility of higher mass progenitors since the H II regions identified as extended from ground-based imaging may involve multiple compact H II regions in some instances. Still, close binary (accretion or merger) predictions favour a mass of  $\sim 15 M_{\odot}$  for the progenitor of SN 1987A (Podsiadlowski 1992). Panagia et al. (2000) discuss a loose  $12 \pm 2$  Myr cluster likely to be associated with the progenitor of SN 1987A, although this would not be detected in ground-based imaging at the typical distance of other ccSNe in our sample.

The spatial resolution of ground-based observations certainly limits the potential association with H II regions (recall Table 7). Fig. 2 contrasts (non-Adaptive Optics) ground-based and space-based H $\alpha$  imaging of the immediate environment of SN 2005cs. HST imaging reveals several compact H II regions that are in close proximity to the ccSNe, albeit none spatially coincident with it, although in addition, bright H II regions are often in close proximity to the SN site, such that a runaway status cannot be excluded either (e.g. SN 1983N, Fig. A7).

Finally, 12 of the 39 ccSNe are associated with giant H II regions (Class 5), comprising  $50 \pm 22\%$  ( $5/10$ ) of the type Ib/c SNe, though only  $24 \pm 9\%$  ( $7/29$ ) of the type II ccSNe sample. Solely SN 1985F (Ib/c) is spatially coincident with a bright cluster (Fig. A8), while some others are found in complexes (e.g. SN 2007gr, Fig. A32). Age estimates for individual stellar populations within each region are not available, so we consider a characteristic duty cycle of (super)giant H II regions of  $20$  ( $10$ ) Myr, from which lower progenitor mass limits of  $12$  ( $20$ )  $M_{\odot}$  are implied for the initial stellar generation, with higher limits for subsequent episodes of star formation. Unfortunately, no limit to the progenitor mass of SN 1968L (II-P) can be assigned since it lies within the nuclear starburst of M 83 (Fig. A4).

Detailed studies based either on either pre-supernova imaging (e.g. Aldering et al. 1994) or post-supernova light curves (e.g. Chugai & Utrobin 2000) have been carried out in some cases. For example, the former technique was used by Leonard et al. (2002) to obtain an upper limit of  $15^{+5}_{-3} M_{\odot}$  for the progenitor mass of SN 1999gi (II-P, see also Hendry 2006) while the latter approach enabled Iwamoto et al. (1994) to estimate a progenitor mass of  $\sim 15 M_{\odot}$  for SN 1994I (Ic). Therefore a giant H II region duty cycle of  $20$  Myr is the most realistic case (recall also Sect. 2.3), which naturally provides only weak limits upon progenitor masses for these II-P, IIn and Ib/c types of ccSNe (e.g. Smartt 2009).

#### 4.2 Previous ccSNe environmental studies in context

We have attempted to constrain progenitor masses from the association between ccSNe and H II regions, or lack thereof. Overall, establishing progenitor masses in either case is challenging, given the *short* duration of the H II region phases for isolated, compact clusters and the *long* duration of the giant H II region phase for extended, star forming complexes, which form the majority of the sample. SN 2004dj (II-P) ought to provide the strongest indirect

**Table 8.** Summary of expected association between H II regions and ccSNe (+ long GRBs) in host galaxies of differing star formation intensities ( $\Sigma_R$ ), following Kennicutt et al. (1989) and Gieles (2009). Star formation intensities are obtained from  $R_{25}$  (spirals) or  $R_D$  (irregulars). A 20 Myr duty cycle is adopted for giant H II regions, versus  $\sim 4$  Myr for isolated H II regions.

Host	Star Formation Intensity	$\Sigma_{R_{25}}$ ( $\Sigma_{R_D}$ ) ( $M_\odot \text{ yr}^{-1} \text{ kpc}^{-2}$ )	Cluster range ( $M_\odot$ )	Characteristic H II region	SN/GRB-H II association?	Example
Sab	Low	$4 \times 10^{-5}$	$10^{2-4}$	Isolated	$\times$ (all types)	M 31
Scd	High	$2 \times 10^{-3}$	$10^{2-6}$	Giant; Isolated	$\times$ ( $\leq 12 M_\odot$ ), ? (12–85 $M_\odot$ ), $\checkmark$ ( $\geq 85 M_\odot$ )	M 101
Irr	Low	( $5 \times 10^{-3}$ )	$10^{2-4}$	Isolated	$\times$ (all types)	SMC
Irr	High	(1.5)	$10^{2-6}$	Giant; Isolated	$\times$ ( $\leq 12 M_\odot$ ), ? (12–85 $M_\odot$ ), $\checkmark$ ( $\geq 85 M_\odot$ )	NGC 1569

Star formation intensities: M 31 (Lee et al. 2009b); M 101: This work; SMC: Massey et al. (2007); NGC 1569: Kennicutt et al. (2008).

(young) age constraint, since this is spatially coincident with a star cluster though not a H II region. However, direct analysis of its light curve suggests an old age/low mass (Vinkó et al. 2006, 2009). Therefore, ccSNe progenitor inferences from H II regions should be treated with caution, especially for high inclination hosts and/or low spatial resolution observations.

How, then, should one interpret previous interpretations of the association between H II regions and ccSNe, or lack thereof? According to Anderson & James (2008), a progenitor mass sequence II  $\rightarrow$  Ib  $\rightarrow$  Ic was proposed, with H-rich ccSNe further subdivided into II<sub>n</sub>  $\rightarrow$  II-P  $\rightarrow$  II-L  $\rightarrow$  IIb by Anderson et al. (2012).

We concur with Anderson et al. that the higher frequency of type Ib/c with H II regions than type II ccSNe arises from the relative lifetimes of their progenitors with respect to H II regions. However, we disagree with their implications since the H II regions detected at distances typical of their sample ( $\bar{d} = 35$  Mpc, Table 7) are extended, giant, multi-generation H II regions. Let us assume that type II ccSNe result from progenitors with 8–20  $M_\odot$  (Smartt 2009) from the first stellar population. A duty cycle of  $\sim 20$  Myr would imply that 40% of type II progenitors with 12–20  $M_\odot$  are associated with H II regions, while 60% of progenitors with 8–12  $M_\odot$  are not, based upon a standard Salpeter IMF slope for massive stars. Although approximate, such expectations agree well with the  $34 \pm 11\%$  of type II ccSNe that are associated with H II regions in our study.

To illustrate the restricted progenitor mass limits that can be achieved from this approach, the only case of a type II<sub>n</sub> supernova in our present study is SN 1996cr. It has been proposed that these arise from massive Luminous Blue Variables (Smith 2008), yet Anderson et al. (2012) claim type II<sub>n</sub> SN possess the lowest mass progenitors of all massive stars. SN 1996cr is associated with a giant H II region, although is not coincident with a bright cluster, so one can merely set a lower mass limit of 12  $M_\odot$  to the progenitor, with no robust upper limit, so one cannot argue against a high mass progenitor on the basis of its immediate environment.

Of course, a higher fraction ( $70 \pm 26\%$ ) of type Ib/c ccSNe are associated with H II regions. This suffers from small number statistics, but likely reflects the shorter lifetime of stars with  $\geq 12 M_\odot$ , the majority of which will be associated with a  $\sim 20$  Myr duty cycle of giant H II regions. In general, this fails to discriminate between most single star (Crowther 2007; Georgy et al. 2012), and close binary progenitor scenarios (Podsiadlowski et al. 1992; Yoon et al. 2010), aside from a higher mass threshold ( $\geq 12 M_\odot$ ?) for Ib/c than type II ccSNe ( $\geq 8 M_\odot$ ). Still, for the two cases lacking any associated H II region or nearby giant H II region, SN 2002ap (Ic), SN 2003jg (Ib/c), a close binary scenario is favoured.

## 5 DISCUSSION

### 5.1 Can local H II regions constrain ccSNe progenitor masses?

We have assessed the immediate nebular environment of ccSNe in nearby star forming galaxies, and confirm the results from Anderson & James (2008) and Anderson et al. (2012) that type Ib/c ccSNe are more likely to be associated with a H II region than type II ccSNe. However, the typical H II regions identified in H $\alpha$  imaging from ground based telescopes are extended, giant H II regions with long duty cycles. Indeed, the issue of differing duty cycles for compact, isolated H II regions versus extended, H II complexes is particularly relevant for late-type spirals and irregulars. Such hosts dominate the statistics of Anderson et al. (2012), for which large star forming complexes – ionized by multiple generations of star clusters – are common (Kennicutt et al. 1989).

Nevertheless, firm limits upon the lifetime ( $\leq 4$  Myr) and mass ( $\geq 85 M_\odot$ ) of ccSNe progenitors would be possible if examples of isolated, classical H II regions could be identified. Resolving the specific location of the ccSNe within such a region is only realistic at much higher spatial resolution than typically achieved here, whether from space with HST or using Adaptive Optics with large ground-based telescopes (recall Fig. 2). From Table 7, ccSNe are rarely associated with compact H II regions, although this is unsurprising in view of the small numbers of very high mass stars within nearby star-forming galaxies.

Overall, we confirm previous findings by Anderson & James (2008) and Anderson et al. (2012) that the association between different SNe flavours and H II regions does vary between H-rich and H-poor ccSNe. Unfortunately, minimal implications for progenitor masses can be drawn which prevents discrimination between the single versus close binary progenitor scenarios proposed for Ib/c (and IIb) ccSNe (Anderson & James 2008). Our findings fail to support claims that the progenitors of II<sub>n</sub> ccSNe possess relatively low masses (Anderson et al. 2012). In only a few cases does the lack of nebular emission provide limits upon progenitor masses, i.e. favouring the close binary scenario for 2 type Ib/c ccSNe.

### 5.2 Core-collapse SNe beyond the local universe

Mindful of the spatial resolution issue, let us re-assess the Kelly et al. (2008) study of SNe locations, with respect to the continuum ( $g'$ -band) light of their low redshift ( $z < 0.06$ ) host galaxies. Kelly et al. revealed that Ic SNe are much more likely to be found in the brightest regions of their hosts than type II SNe, with intermediate properties for type Ib SNe. Kelly et al. (2008) argued that if the brightest locations correspond to the largest star-forming regions,

type Ic SNe are restricted to the most massive stars, while type Ib and especially type II-P SNe are drawn from stars with more moderate masses.

The SN host sample of Kelly et al. (2008) is not expected to be significantly different from our present sample. From Table 6, star formation intensities from the present (spiral) hosts are uniformly high, with an average value of  $\Sigma_{R_{25}} = 5 \times 10^{-3} M_{\odot} \text{ yr}^{-1} \text{ kpc}^{-2}$ . This is more representative of 'typical' late-type (Scd) spirals, even for Sab hosts ( $\Sigma_{R_{25}} \sim 8 \times 10^{-3} M_{\odot} \text{ yr}^{-1} \text{ kpc}^{-2}$  for Circinus). For the irregular galaxies, comparisons with the reference galaxies are more difficult due to the lack of V-band scale lengths for NGC 3239 and NGC 7292. If intensities are typically an order of magnitude higher (on the basis of the LMC), these are intermediate between the extremes of the SMC and NGC 1569.

Therefore, how should the difference between type Ib/c and type II ccSNe identified by Kelly et al. (2008) be explained? In the  $g'$ -band, a star cluster will fade by 1 mag at young ages (5 to 10 Myr), with a further 1 mag dimming at intermediate ages (10 to  $\sim 60$  Myr), as shown in fig. 5 from Bik et al. (2003). Still, individual star clusters are not spatially resolved in ground-based imaging so it is more likely that the difference relates to the different frequencies of type Ib/c and type II ccSNe in large star forming complexes, as discussed above for our local sample.

Very high mass ( $\sim 50 M_{\odot}$ ) stars are anticipated to be limited to massive (bright) clusters, whereas lower mass ccSNe progenitors ( $\sim 10 M_{\odot}$ ) will be found in clusters spanning a broad range of masses. The former are typically found in large (bright) star forming complexes (e.g. Carina Nebula, 30 Doradus). Therefore the higher frequency for H-deficient ccSNe in bright regions of their hosts with respect to H-rich ccSNe does suggest that a non-negligible fraction of type Ib and especially Ic ccSNe originate from higher mass stars than type II ccSNe. In reality, a mixture of close binaries and higher mass single stars are likely to be responsible for type Ib/c ccSNe (Bissaldi et al. 2007; Smith et al. 2011).

### 5.3 Long Gamma Ray Bursts

From an analysis of high redshift galaxies, Fruchter et al. (2006) revealed that long GRBs ( $\langle z \rangle = 1.25$ ) were also strongly biased towards the brightest part of their hosts, in contrast to core-collapse SNe ( $\langle z \rangle = 0.63$ , most presumably type II-P) which merely traced the light from their hosts.

One significant difference between the low-redshift Kelly et al. (2008) SN study and the high-redshift GRB study of Fruchter et al. (2006) is that hosts of the former are relatively high mass, metal-rich spirals, while those of the latter are low mass, metal-poor dwarfs. In normal star-forming galaxies the cluster mass distribution follows a power law with index  $-2$ , albeit truncated at high mass depending upon the star formation intensity ( $\Sigma_R$ , Gieles 2009). Consequently, similar absolute numbers of stars are formed in low mass ( $M_{\text{cl}} \sim 10^2 M_{\odot}$ ), intermediate mass ( $\sim 10^3 M_{\odot}$ ) and high mass ( $\sim 10^4 M_{\odot}$ ) clusters, albeit with the former deficient in stars at the extreme upper end of the IMF.

This star cluster mass function is repeated in nearby dwarf galaxies (Cook et al. 2012), but galaxy-wide triggers may induce intense, concentrated bursts of star formation (e.g. NGC 1569, Hunter et al. 2000), leading to disproportionately numerous massive star clusters (Billett et al. 2002; Portegies Zwart et al. 2010)<sup>12</sup>.

We have attempted to set out the potential association between H II regions, ccSNe (and long GRBs) for star forming spirals and irregulars in Table 8. Here, the full spectrum of galaxy types has been distilled down to two dominant types for both spirals and irregulars, depending upon the rate of star formation, or more strictly the star formation intensity. For spiral galaxies we quote intensities with respect to  $R_{25}$ , while the V-band scale length  $R_D$  (Hunter & Elmegreen 2004) is used for irregulars. Of course, intensities depend upon the diagnostic used to calculate star formation rates (Calzetti et al. 2007; Lee et al. 2009b; Botticella et al. 2012), and very different intensities would follow from the use of alternative radii (e.g. Kennicutt et al. 2005).

From Table 8 one would not expect ccSNe to usually be associated with bright regions in low intensity environments, such as typical early-type spirals (e.g. M 31) or dwarf irregulars (e.g. SMC), owing to the scarcity of giant H II regions in such hosts. Indeed, isolated H II regions in such galaxies would rarely produce high mass stars (recall Fig. 1a). Exceptions do exist of course, including early-type spiral galaxies that possess high star formation intensities (e.g. M 81), plus abnormal regions within non-starburst irregulars such as NGC 346 in the SMC.

In contrast, the high star formation intensity of late-type spirals (e.g. M 101) and starburst irregulars (e.g. NGC 1569) will produce many large, star-forming complexes. Consequently, ccSNe will frequently be associated with bright star forming regions within their host galaxies. Of the present ccSNe sample, whose hosts are typical of high intensity late-type spirals, 18/37 ccSNe lie within  $\sim 300$  pc of a bright ( $L(\text{H}\alpha) > 10^{38} \text{ erg s}^{-1}$ ) star forming region. Our sample includes only two irregular galaxies, so we are unable to assess the situation for starburst versus non-starburst dwarf galaxies.

Nevertheless, we can re-assess the likelihood that long GRBs arise from moderate ( $\sim 15 M_{\odot}$ ) or high ( $\sim 50 M_{\odot}$ ) mass stars if the local volume is fairly representative of metal-poor star formation (Lee et al. 2009a). In the former case, long GRBs would be dominated by quiescent star formation from non-starburst dwarfs, whose H II regions would be isolated (and faint) since they would lack the high mass clusters necessary for very massive stars, and their corresponding bright H II regions). In the latter case, long GRBs would be associated with stars formed in very massive clusters, since where localised activity takes place in dwarf galaxies, it can be very intense (Billett et al. 2002).

The tight correlation between long GRBs and the brightest regions of their hosts (Fruchter et al. 2006), does not *prove* a link between high mass stars and long GRBs but it is certainly highly *suggestive*. Recall the preference for broad-lined type Ic ccSNe towards dwarf galaxies (Arcavi et al. 2010), the broad lined Ic-GRB connection (Woolley & Bloom 2006) plus the preference of long GRBs for metal-poor hosts (Levesque et al. 2010).

Of course, the formation of dense star clusters will lead to a significant number of high mass runaway stars, either dynamically ejected during the formation process or at later stages after receiving a kick following a supernova explosion within a close binary system (e.g. Fujii & Portegies Zwart et al. 2011). Still, the majority of high mass runaways will remain relatively close to their birth cluster in view of their short lifetimes and typical ejection velocities of  $\sim 100 \text{ km s}^{-1}$ .

For example, the progenitor of the nearby GRB 980425/SN

<sup>12</sup> Of course, not all dwarf galaxies are starbursting. Within the local vol-

ume ( $< 11$  Mpc) only a quarter of the star formation from dwarf galaxies is formed during starbursts (Lee et al. 2009a)

1998bw was located close to another bright H II region in its (late-type) host galaxy, albeit offset by 0.8 kpc from a 30 Dor-like giant H II region (Hammer et al. 2006). Either the SN/GRB progenitor was dynamically ejected from the H II region at relatively high velocities, or it was formed in situ in a more modest star forming region, which is comparable to the Rosette Nebula (Table 1). Evans et al. (2010) have identified VFTS #016 as a high mass runaway from R136 in the 30 Doradus, having traversed 0.12 kpc in the 1–2 Myr since the formation of the cluster.

Therefore, from environmental considerations one can understand the preference for certain flavours of ccSNe towards the brightest regions of their host galaxies. Still, there is little predictive power regarding progenitor masses, other than potentially a high likelihood for very massive stars to produce long GRBs/broad-lined Ic ccSNe.

## 6 CONCLUSIONS

We have reexamined the immediate H II environment of ccSNe from nearby ( $\leq 15$  Mpc) low inclination ( $\leq 65^\circ$ ), host galaxies. A total of 41 ccSNe have good position accuracy, of which ground-based H $\alpha$  imaging is available in 39 cases. Our findings can be summarised as follows:

(i) Overall, half of the ccSNe are associated with nebular emission, in close agreement with van Dyk (1992). Separating these into type II and type Ib/c ccSNe, 11 of the 29 hydrogen-rich ccSNe are associated with nebular emission ( $38 \pm 11\%$ ), versus 7 of the 10 hydrogen-poor ccSNe ( $70 \pm 26\%$ ), supporting previous studies of Anderson & James (2008) and Anderson et al. (2012).

(ii) Of the 18 ccSNe associated with star forming regions, 12 are associated with giant H II regions, with the remaining 6 associated with low luminosity, extended H II regions. Overall, the mean H $\alpha$  luminosity of star forming regions associated with ccSNe is typical of a modest giant H II region,  $3 \times 10^{38}$  erg s $^{-1}$ , if we were to exclude SN 1970G which lies at the periphery of the supergiant H II region NGC 5455 within M 101. Both categories have multiple sites of star formation, and so long duty cycles ( $\sim 20$  Myr), implying only weak limits upon progenitor masses ( $\geq 12 M_\odot$ ).

(iii) Of the 21 ccSNe not associated with star forming regions, only one case is coincident with a bright cluster (SN 2004dj), from which a massive progenitor ( $> 20 M_\odot$ ) would be expected. More detailed studies of the cluster indicate a lower progenitor mass  $< 20 M_\odot$  (Vinkó et al. 2006, 2009) in common with most of the other ccSNe that are not associated with a star forming region. In a few instances, nearby giant H II regions indicate the possibility that the progenitor was a (high-mass) runaway from a putative dense star cluster.

(iv) Our primary result is that the different frequency of association with H II regions for hydrogen-rich (mostly II-P) and hydrogen-poor (Ib/c) ccSNe is attributed simply to different minimum progenitor mass thresholds,  $\sim 8 M_\odot$  and  $\sim 12 M_\odot$ , respectively, since they correspond to upper age limits of  $\sim 50$  Myr and  $\sim 20$  Myr. Among the type Ib/c ccSNe, only two cases lacked both nebular emission and a nearby giant H II region (SN 2002ap, SN 2003jg), favouring the interacting binary channel ( $< 20 M_\odot$ ).

(v) For the present sample, 8 of the ccSNe originate from early-type spirals (S0/a/b), 31 from late-type spirals (Sc/d/m) and 2 from irregulars (Im), with the majority (61%) arising from high luminosity ( $M_B < -19$  mag) hosts. Giant H II regions are common in these hosts because star formation intensities are uniformly high,

whereas isolated, compact H II regions would be expected to dominate in low star formation intensity hosts. Core-collapse SNe from isolated, classical H II regions would provide firm limits upon the lifetime ( $\leq 3\text{--}5$  Myr) and mass ( $\geq 50\text{--}100 M_\odot$ ) of the progenitor owing to the brief lifetime of such H II regions, although this would require higher spatial resolution (HST or ground-based Adaptive Optics). An association between a ccSN and compact H II region has not been observed with HST to date (Table 7).

(vi) We have also qualitatively reassessed the preference for type Ib/c towards the brightest regions of their host galaxies (Kelly et al. 2008). This is suggestive that a fraction of H-poor ccSNe originate from significantly higher mass stars than type II ccSNe, since high mass stars are more likely to be associated with high mass clusters within large (bright) star forming complexes. The preference for long GRBs towards the brightest regions of their metal-poor hosts (Fruchter et al. 2006) is also suggestive of very high mass progenitors. This is because low intensity star forming dwarfs do not form very high mass stars, yet dominate the overall metal-poor star formation in the local volume (Lee et al. 2009a).

## ACKNOWLEDGEMENTS

I wish to thank the referee for suggestions which helped to clarify some aspects of this work. In addition, I am especially grateful to John Eldridge for alerting me to this issue, and to Mark Gieles and Rob Kennicutt for useful discussions. Janice Lee and Johan Knapen kindly provided me with electronic access to archival imaging, while Maryam Modjaz kindly provided updated SN spectral types prior to publication.

This study was based in part on observations made with (a) ESO Telescopes at the La Silla Paranal Observatory under programme IDs 067.D-0006(A), 069.B-0125(A), 069.D-0453(A), 075.D-0213(A), 380.D-0282(A) and 081.B-0289(C); (b) Gemini Observatory under programme GN-2009B-Q-4, which is operated by the Association of Universities for Research in Astronomy, Inc., under a cooperative agreement with the NSF on behalf of the Gemini partnership: the National Science Foundation (United States), the Science and Technology Facilities Council (United Kingdom), the National Research Council (Canada), CONICYT (Chile), the Australian Research Council (Australia), Ministério da Ciência, Tecnologia e Inovação (Brazil) and Ministerio de Ciencia, Tecnología e Innovación Productiva (Argentina); (c) NASA/ESA Hubble Space Telescope, obtained from the data archive at the Space Telescope Institute. STScI is operated by the association of Universities for Research in Astronomy, Inc. under the NASA contract NAS 5-26555. This research has also used the facilities of the CADM operated by the National Research Council of Canada with the support of the Canadian Space Agency; (d) Isaac Newton Group Archive which is maintained as part of the CASU Astronomical Data Centre at the Institute of Astronomy, Cambridge; (e) Liverpool Telescope Data Archive, provided by the Astrophysics Research Institute at Liverpool John Moores University.

This research has made extensive use of the NASA/IPAC Extragalactic Database (NED) which is operated by the Jet Propulsion Laboratory, California Institute of Technology, under contract with the National Aeronautics and Space Administration. We also acknowledge the usage of the HyperLeda database (<http://leda.univ-lyon1.fr>).

## REFERENCES

- Aldering, G., Humphreys, R.M., Richmond, M. 1994, *AJ* 107, 662
- Allen, R.J., Goss, W.M., Ekers, R.D., de Bruyn, A.G. 1976, *A&A* 48, 253
- Anderson, J.P., James, P.A. 2008, *MNRAS*, 390, 1527
- Anderson, J.P., Haberman, S.M., James, P.A., Hamuy, M., 2012, *MNRAS* 424, 1372
- Arcavi, I., et al. 2010, *ApJ* 721, 777
- Arcavi, I., et al. 2012, *ApJ* 756, L30
- Bartunov, O.S., Tsvetkov, D. Y., Filimonova, I.V., 1994, *PASP*, 106, 1276
- Bastian, N., Covey, K.R., Meyer, M.R. 2010, *ARA&A* 48, 339
- Bik, A., Lamers, H.J.G.J.L.M., Bastian, N., Panagia, N., Romaniello, M. 2003, *A&A* 397, 473
- Billett, O.H., Hunter, D.A., Elmegreen B.G., 2002, *AJ* 123, 1454
- Bissaldi, E., Calura, F., Matteucci F., Longo, F., Barbiellini, G. 2007, *A&A*, 471, 585
- Bothun, G.D., Thompson, I.B. 1988, *AJ* 96, 877
- Botticella, M.T., Smartt, S.J., Kennicutt, R.C.Jr., Cappellaro, E., Sereno, M., Jee, J.C. 2012, *A&A*, 537, A132
- Bresolin, F., Garnett, D.R., Kennicutt, R.C.Jr. 2004, *ApJ* 615, 228
- Calzetti, D., Kennicutt, R.C., Engelbracht C.W. et al. 2007, *ApJ*, 666, 870
- Calzetti, D., Chandar, R., Lee, J.C., Elmegreen, B.G., Kennicutt, R.C., Whitmore, B. 2010, *ApJ*, 719, L158
- Carignan, C., Puche, D. 1990, *AJ* 100, 394
- Chugai, N.N., Utrobin, V.P., 2000, *A&A* 354, 557
- Ciardullo, R., Jacoby, G.H., Tonry, J.L., 1993, *ApJ* 419, 479
- Ciardullo, R., Feldmeier, J.J., Jacoby, G.H., Kuzio de Naray, R., Laychak, M.b., Durrell, P.R., 2002 *ApJ* 577, 31
- Clark, J.S., Negueruela, I., Crowther, P.A., Goodwin, S.P. 2005, *A&A*, 434, 949
- Conti, P.S., 1976, *Proc. 20th Colloq. Int. Ap. Liege*, p. 193
- Conti, P.S., Crowther, P.A., Leitherer, C., 2008, *From Luminous Hot Stars to Starburst Galaxies* (Cambridge: CUP)
- Cook, D.O., Seth, A.C., Dale, D.A. et al. 2012, *ApJ*, 751, 100
- Crockett, R.M., 2009, PhD Thesis, Queen's University Belfast
- Crockett, R.M. et al. 2007, *MNRAS* 381, 835
- Crockett, R.M. et al. 2008, *ApJ* 672, L99
- Crowther, P.A., 2007, *ARA&A*, 45, 177
- Crowther, P.A., Schnurr, O., Hirschi R., Yusof, N., Parker, R.J., Goodwin, S.P., Kassim, H.A. 2010, *MNRAS*, 408, 731
- Dale, J.E., Ercolano, B., Bonnell, I.A. 2012, *MNRAS* 424, 377
- Dalcanton J.J., et al., 2009, *ApJS* 183, 67
- Danver, C.G. 1942, *Ann. Obs. Lund* 10, 1
- de Wit, W.J., Testi, L., Palla, F., Zinnecker, H. 2005, *A&A*, 437, 247
- Dessart, L., Hillier, D.J., Li, C., Woosley, S. 2012, *MNRAS* 424, 2139
- Ekström, S. et al. 2012, *A&A*, 537, A146
- Eldridge, J.J., 2012, *MNRAS*, 422, 794
- Evans, N.J. II, Dunham, M.M. Jørgensen, J.K., 2009, *ApJS*, 181, 321
- Evans, C.J. et al. 2010, *ApJ*, 715, L74
- Evans C.J. et al. 2011, *A&A*, 530, A108
- Feldmeier J.J., Ciardullo, R., Jacoby, G.H., 1997, *ApJ* 479, 231
- Freedman W.F. et al., *ApJ* 553, 47
- Freeman, K.C., Karlsson, B., Lynga, G., Burrell, J.F., van Woerden, H., Goss, W.M., Mebold, U., *A&A* 55, 445
- Fruchter, A.S. et al. 2006, *Nat.*, 441, 463
- Fryer, C.L. et al. 2007, *PASP*, 119, 861
- Fujii, M.S., Portegies Zwart, S.F., 2011, *Sci* 334, 1380
- Georgy, C. et al. 2012, *A&A* 542, A29
- Gieles, M. 2009, *MNRAS*, 394, 2113
- Gieles, M., Portegies Zwart, S.F., 2011, *MNRAS*, 410, L6
- Grebel, E.K., Chu, Y.-H., 2000, *AJ* 119, 787
- Hadfield, L.J., Crowther, P.A., Schild, H., Schmutz, W. 2005, *A&A* 439, 265
- Hammer, F., Flores, H., Schaerer, D., Dessauges-Zavadsky, M., Le Flocc'h, E., Puech, M., 2006, *A&A*, 454, 103
- Harayama, Y., Eisenhauer, F., Martins, F., 2008, *ApJ*, 675, 1319
- Hendry, M.A., 2006, PhD thesis, University of Cambridge
- Hoopes, C.G., Walterbos, R.A.M., Bothun, G.D. 2001, *ApJ*, 559, 878
- Hunter, D.A., Elmegreen, B.G., 2004, *AJ*, 128, 2170
- Hunter, D.A., O'Connell, R.W., Gallagher, J.S., Smecker-Hane, T.A., 2000, *AJ* 120, 2383
- Iwamoto, K., Nomoto, K., Höflich, P., Yamaoka, H., Kumagai, S., shigeyama, T. 1994, *ApJ* 437, L115
- James, P.A. et al. 2004, *A&A*, 414, 23
- James, P.A., Anderson, J.P. 2006, *A&A* 453, 57
- Jha, S., Challis, P., Garnavich, P. Kirshner, R., Calkins, M., Stanek, K. 1999, *IAU Circ* 7296
- Kamphuis, J., Briggs, F. 1992, *A&A* 253, 335
- Kelly, P.L., Kirschner, R.P., Pahre, M., 2008, *ApJ*, 687, 1201
- Kennicutt, R.C., 1984, *ApJ*, 287, 116
- Kennicutt, R.C. 1998, *ARA&A*, 36, 189
- Kennicutt, R.C., Kent, S.M. 1983, *AJ*, 88, 1094
- Kennicutt, R.C., Edgar, B.K., Hodge, P.W., 1989, *ApJ*, 337, 761
- Kennicutt, R.C. Bresolin, F., Bomans, D.J., Bothun, G.D., Thompson, I.B. 1995, *AJ*, 109, 594
- Kennicutt, R.C. et al. 2003, *PASP*, 115, 928
- Kennicutt, Jr, R. C., Lee, J. C., Funes, J. G., Sakai, S., & Akiyama, S. 2005, in *ASSL*, Vol. 329, Starbursts: From 30 Doradus to Lyman Break Galaxies, ed. R. de Grijs & R. M. González Delgado, 187
- Kennicutt R.C., Lee, J.C., Funes, S.J., José, G., Sakai, S., Akiyama, S. 2008, *ApJS* 178, 247
- Kennicutt R.C. et al. 2009, *ApJ*, 703, 1672
- Kiewe, M. et al. 2012, *ApJ* 744, 10
- Knapen, J.H. et al. 2004 *A&A* 426, 1135
- Lada, C.J., Lada, E.A., 2003, *ARA&A*, 41, 57
- Langer, N., 2012, *ARA&A* 50, 107
- Larsen, S.S., Richtler T. 1999, *A&A*, 345, 59
- Lee J.C., Kennicutt, R.C. Jr, Funes, J.G., José, G., Sakai, S., Akiyama, S. 2009a, *ApJ*, 692, 1305
- Lee J.C. et al. 2009b, *ApJ*, 706, 599
- Leonard, D.C. et al. 2002, *AJ* 124, 2490
- Levesque, E., M., Kewley, L.J., Berger, E., Zahid, H.J. 2010, *AJ* 140, 1557
- Li, W., Fan, Y., Qiu, Y.L., Hu, J.Y. 2001, *IAU Circ* 7591
- Li, W., van Dyk, S.D., Filippenko, A.V., Cuillandre, J.-C., Jha, S., Bloom, J.S., Riess, A.G., Livio, M. 2006, *ApJ* 641, 1060
- Lopez, L.A., Krumholz, M.R., Bolatto, A.D., Prochaska, J.X., Ramirez-Ruiz, E. 2011, *ApJ* 731, 91
- Macri L.M., Stanek, K.Z., Bersier, D., Greenhill, L.J., Reid, M.J., 2006, *ApJ*, 652, 1133
- Mager V.A., Madore, B.F., Freedman, W.L., 2008, *ApJ*, 689, 721
- Massey, P., Olsen, K.A.G., Hodge, P.W., Jacoby, G.H., McNeill, R.T., Smith, R.C., Strong, S.B., 2007, *AJ*, 133, 2393
- Mazzali, P.A. et al. 2002, *ApJ* 572, L61
- Mazzali, P.A. et al. 2007, *ApJ* 670, 592
- McNaught, R.H., Waldron, D. 1986, *IAU Circ* 4261
- Méndez B., Davis, M., Moustakas, J., Newman, J., Madore, B.F., Freedman, W.L., 2002, *AJ*, 124, 213
- Meurer, G.R. et al. 2006, *ApJSS* 165, 307
- Moustakas, J., Kennicutt, R.C., Jr 2006, *ApJS* 164, 81
- Murphy, M.T., Bessell, M.S., 2000 *MNRAS*, 311, 741
- Nomoto, K., Iwamoto, K., Suzuki, T., 1995, *PhR* 256, 173
- Panagia, N., Romaniello, M., Scuderi, S., Kirschner, R.P. 2000, *ApJ* 539, 197
- Pennington, R.L., Talbot, R.J.Jr, Dufour, R.J. 1982, *AJ* 87, 1538
- Pflamm-Altenburg, J., Weidner, C., Kroupa, P., 2007, *ApJ*, 671, 1550
- Podsiadlowski, P. 1992, *PASP* 104, 717
- Podsiadlowski, P., Joss, P.C., Hsu, J.J.L. 1992, *ApJ* 391, 246
- Portegies Zwart, S.F., McMillan, S.L.W., Gieles, M. 2010, *ARA&A*, 48, 431
- Porter, A.C. 1993, *PASP* 105, 1250
- Rumstay, K.S., Kaufman, M., 1983, *ApJ*, 274, 611
- Ryder, S.D., Dopita, M.A. 1993, *ApJS* 88, 415
- Sakai S., Ferrarese, L., Kennicutt, R.C. Jr, Saha, A., 2004, *ApJ* 608, 42
- Sánchez, S.F., Rosales-Ortega, F.F., Kennicutt, R.C., Johnson, B.D., Diaz, A.I., Pasquali, A., Hao, C.N. 2011, *MNRAS* 410, 313
- Schaefer, B.E. 2008, *AJ* 135, 112
- Schlafly, E.F., Finkbeiner, D.P. 2011, *ApJ* 737, 103
- Schlegel, D.J., Finkbeiner, D.P., Davis, M. 1998, *ApJ* 500, 525

- Schmidt, B.P., Kirschner, R.P., Eastman, R.G., Phillips, M.M., Suntzeff, N.B., Hamuy, M., Maza, J., Aviles, R. 1994, *ApJ* 432, 42
- Schnurr, O., Casoli, J., Chené, A.-N., Moffat, A.F.J., St Louis, N., 2008, *MNRAS* 389, L38
- Smartt, S.J. 2009, *ARA&A*, 47, 63
- Smartt, S.J., Eldridge, J.J., Crockett, R.M., Maund, J.R., 2009, *MNRAS*, 395, 1409
- Smith N., 2008, in: F. Bresolin, P.A. Crowther, J. Puls (eds.) *IAU Symposium 250: Massive Stars as Cosmic Engines* (San Francisco: ASP), p.193
- Smith, M.C., Leiton, R., Pizarro, S. 2000 in: D. Allion, K. Olsen & G. Galaz (eds.), *Stars, Gas and Dust in Galaxies: Exploring the Links* (San Francisco: ASP), ASP Conf. Ser 221, p. 83
- Smith, N., Li, W., Filippenko, A.V., Chornock, R., 2011, *MNRAS*, 412, 1522
- Sramek, R.A., Panagia, N., Weiler, K.W. 1984, *ApJ* 285, L59
- Stockdale, C.J., Sramek, R.A., Rupen, M. et al. 2002, *IAU Circ.* 8018
- Thim F., Tammann, G.A., Saha, A., Dolphin, A., Sandage, A., Tolstoy, E., Labhardt, L. 2003, *ApJ* 590, 256
- Tonry J.L., Dressler, A., Blakeslee, J.P., Ajhar, E.A., Fletcher, A.B., Lup-piao, G.A., Metzger, M.R., Moore, C.B. 2001, *ApJ* 546, 681
- Tully, R.B., Rizzi, L., Shaya, E.J., Courtois, H.M., Makarov, D.I., Jacobs, B.A. 2009, *AJ* 138, 323
- Vacca, W.D., Conti, P.S., 1992, *ApJ*, 401, 543
- van Dyk, S.D., 1992, *AJ*, 103, 1788
- van Dyk, S., Hamuy, M., Filippenko, A.V. 1996, *AJ* 111, 2017
- Vazquez, R.A., Baume, G., Feinstein, A., Prado, P. 1996, *A&AS* 116, 75
- Vinkó, J., Takáts, K., Sárneczky, K. et al. 2006, *MNRAS* 369, 1780
- Vinkó, J., Sárneczky, K., Balog, Z. et al. 2009, *ApJ* 695, 619
- Walborn N.R., 2010, in: C. Leitherer, P.D. Bennett, P.W. Morris & J. Th. van Loon (eds.), *Hot and Cool: Bridging Gaps in Massive-Star Evolution* (San Francisco: ASP), ASP Conf. Ser 425, p. 45
- Walborn N.R., Blades J.C., 1997, *ApJS*, 112, 457
- Wang, J., Feigelson, E.D. Townsley, L.K. et al. 2011, *ApJS* 194, 11
- Weidner, C. Kroupa, P., 2006, *MNRAS*, 365, 1333
- Wilking, B.A., Lada, C.J., Young, E.T., 1989, *ApJ*, 340, 823
- Woosley, S.E., Bloom, J.S. 2006, *ARA&A* 44, 507
- Yoon, S.-C., Woosley, S.E., Langer, N. 2010, *ApJ*, 725, 940
- Yoon, S.-C., Gräfener, G., Vink, J.S., Kozyreva, A., Izzard, R.G. 2012, *A&A*, 544, L11



## APPENDIX A: DESCRIPTION OF INDIVIDUAL CCSNE ENVIRONMENTS

A brief description of the immediate environment of each ccSNe in its host galaxy is presented, together with ground-based net H $\alpha$  and continuum images on a (projected) scale of 1 $\times$ 1 kpc (2 $\times$ 2 kpc or 4 $\times$ 4 kpc in some cases). A brief description of the immediate environment of each ccSNe in its host galaxy is presented, together with ground-based net H $\alpha$  and continuum images on a (projected) scale of 1 $\times$ 1 kpc (2 $\times$ 2 kpc or 4 $\times$ 4 kpc in some cases). An illustrative case is included below, with discussions and figures for other ccSNe presented in the on-line only Appendix A.

### A1 SN 1923A in M 83

SN 1923A (II-P) was discovered in May 1923, 2.1' (0.33  $R_{25}$ ) NE from the centre of M 83 (NGC 5236, Pennington et al. 1982). The low inclination of M 83 implies negligible projection effects, so this corresponds to 3.0 kpc for the adopted 4.9 Mpc distance to M 83 (1'' closely approximates to 25 pc). As illustrated in Fig. A1, the SN position is immediately to the south of a bright, extended, star-forming region in our VLT/FORS2 imaging from June 2002, # 59 from the H II region catalogue of Rumstay & Kaufman (1983). A giant H II region within the complex lies 4'' (100 pc) to the N of the SN position, although extended emission extends significantly closer in our VLT/FORS2 imaging. The luminosity of the H II region is comparable to N66 (SMC), for which we measure  $1.7 \times 10^{38}$  ( $7.8 \times 10^{38}$ ) erg s $^{-1}$  using a 1'' (4'') radius aperture. HST WFC3 imaging (GO 11360, PI R.W. O'Connell) using the F657N filter provides a higher spatial view of the region, and reveals several point sources within the error circle of the SN position, plus a faint arc coincident with the SN that extends further to the SW. A more extended star forming region, #79 from Rumstay & Kaufman (1983), lies  $\sim$ 23'' (0.55 kpc) to the W, at the edge of Fig. A1.

### A2 SN 1964H in NGC 7292

This type II supernova occurred 29'' to the SW of the nucleus of NGC 7292 (Porter 1993), corresponding to a deprojected distance of 32'' (0.51  $R_{25}$ ) or 2.0 kpc for the adopted distance of 12.9 Mpc to NGC 7292. Calibrated JKT imaging of NGC 7292 from Jul 2000 (James et al. 2004) has been supplemented by INT/WFC imaging from Jul 1999. The latter are presented in Fig. A2, indicating that the SN location is devoid of nebular emission, with the closest Orion-like H II region to the SN offset 5'' to the NW, a deprojected distance of 350 pc away. Brighter, giant H II regions lie 7'' (0.5 kpc) to the W and 8'' (0.55 kpc) to the SW, with H $\alpha$ -derived luminosities of  $1.3 \times 10^{38}$  erg s $^{-1}$  and  $4.8 \times 10^{38}$  erg s $^{-1}$ , respectively. From inspection of HST WFPC2 imaging with the F300W filter (GO 8632, PI M.Giavalisco), no source is detected either at the position of the SN or the closest H II region.

### A3 SN 1968D in NGC 6946

SN 1968D (II) was discovered in Feb 1968, in a region of NGC 6946 lacking nebular emission, 0.8' (0.14  $R_{25}$ ) NE of its centre (van Dyk et al. 1994). The low inclination of NGC 6946 implies projection effects are negligible, so 1'' = 35 pc for the adopted distance of 7 Mpc. From our Gemini/GMOS imaging obtained in Aug 2009, the nearest major star forming region is located SSE of the SN position (van Dyk et al. 1996), Figure A3 shows that this comprises diffuse emission extending over 6'' (200 pc) plus two marginally

extended sources. Of these, the closest to the SN location lies 4''.5 (150 pc) away, and has a luminosity somewhat in excess of Orion, according to our Gemini GMOS imaging.

Additional isolated Orion-like H II regions are offset 6–7'' (200–230 pc) to the WNW and WSW, while brighter, extended H II regions lie 12'' (400 pc) to the NNE and 17'' (550 pc) to the NNW, with luminosities of  $7 \times 10^{37}$  erg s $^{-1}$  and  $1.4 \times 10^{38}$  erg s $^{-1}$ , respectively.

From inspection of HST/WFPC2 F547M and F656N imaging (GO 8591, PI Richstone) neither a star cluster nor nebular emission are identified at the SN position. Isolated, moderately extended sources are responsible for the nearby H $\alpha$  emission, while the brighter regions to the NNE and NNW are multiple.

### A4 SN 1968L in M 83

This type II-P supernova was discovered in July 1968, and occurred within the nuclear starburst of M 83 (van Dyk et al. 1996). As for SN 1923A, the low inclination of M 83 implies negligible projection effects, such that 1'' approximates to 25 pc at 4.9 Mpc. Figure A4 shows that nebular emission is extremely strong at the position of the SN, albeit offset from the peak H $\alpha$  emission, which lies to the N and E. At the spatial resolution (FWHM  $\sim$  0''.9 or 20 pc) of our VLT/FORS2 imaging from Jun 2002, the closest H II region is located 1'' (25 pc) to the E, and has a luminosity comparable to the Carina Nebula. Brighter giant H II regions lie 1''.5 (40 pc) to the SW and 2'' (50 pc) to the WNW, while a pair of exceptionally bright knots 4'' (100 pc) to the N, coincident with clusters #23, #24 and #27 from Harris et al. (2001), have a combined luminosity of  $1.2 \times 10^{40}$  erg s $^{-1}$  (similar to 30 Doradus).

From an inspection of the narrow-band continuum image, SN 1968L is not spatially coincident with a bright cluster. This is confirmed from inspection of HST WFPC2/F547M (GO 8234, PI D.Calzetti) and HST WFC3/F555W imaging (GO 11360, PI R.W. O'Connell), while WFC3/F657N imaging reveals solely diffuse emission at the SN position. The nebular emission to the E of SN 1968L is spatially extended, while a single compact source is responsible for the giant H II region to the NW. The nearest continuum sources to the SN location are clusters #13 and #15 from Harris et al. (2001) which are coincident with the giant H II region 1''.5 to the SW of the supernova position.

### A5 SN 1970G in M 101

SN 1970G (II-L) was discovered in Aug 1970, and occurred close to a very bright, spatially extended H II region NGC 5455 (Allen et al. 1976; Cowan et al. 1991), 6.6' (0.46  $R_{25}$ ) SW of the nucleus of M 101 (NGC 5457). Owing to the low inclination of M 101, there are no projection effects, so this corresponds to a distance of 13.5 kpc for the adopted 6.9 Mpc distance to M 101 (3'' corresponds to 100 pc). Due to the low resolution of the Hoopes et al. (2001) imaging, we employ higher spatial resolution INT/WFC imaging from Jun 2006 (FWHM  $\sim$  1''.1) to assess the detailed nebular morphology. From Fig. A5, the SN position is located at the periphery of NGC 5455, with the peak H $\alpha$  and continuum emission (# 416 from Hodge et al. 1990) located 5'' (170 pc) to the SE of the SN location. The H $\alpha$ -derived luminosity of this region is  $2 \times 10^{40}$  erg s $^{-1}$ , comparable to 30 Doradus, based on the Hoopes et al. (2001) imaging. The INT/WFC imaging reveals a faint continuum source within  $\sim$ 1'' of the position of SN 1970G (right panel of Fig. A5. Higher resolution HST WFPC2 imaging using the F606W

filter (GO 6713, PI W.B. Sparks) suggests that the SN is not coincident with nebular emission, with the nearest bright continuum source offset E by  $1''.6$ .

#### A6 SN 1980K in NGC 6946

This type II-L supernova, discovered in Oct 1980, occurred in the outer disk of NGC 6946,  $5'.45$  to the SE of the nucleus, which corresponds to a deprojected distance of  $5'.7$  ( $0.99 R_{25}$ ) or 11.5 kpc for the 7 Mpc distance to NGC 6946. Based on the radio SN position from Weiler et al. (1992), it fell beyond the field-of-view of our Gemini GMOS imaging, so instead we employ the KPNO 2.1m imaging from Mar 2001 (Kennicutt et al. 2003). Fig. A6 shows that there is no significant  $H\alpha$  emission close to the position of the SN. Extended  $H\text{II}$  regions lie  $50''$  (1.75 kpc) W,  $60''$  (2.1 kpc) WNW and  $55\text{--}65''$  (1.9–2.3 kpc) NE, with luminosities of  $2 \times 10^{37}$  erg  $s^{-1}$ ,  $4 \times 10^{37}$  erg  $s^{-1}$  and  $5 \times 10^{37}$  erg  $s^{-1}$ , respectively. SN 1980K is seen as a point source in HST/WFPC2 F606W imaging (GO 11229, PI M. Meixner), with a second, visually fainter point source  $0''.5$  (20 pc) to its E (Sugerman et al. 2012).

#### A7 SN 1983N in M 83

The type Ib SN 1983N was discovered in July 1983 (Wamsteker 1983), and occurred  $3'$  SW of the nucleus of M 83 (NGC 5236), corresponding to a deprojected distance of  $3'.1$  ( $0.48 R_{25}$ ) or 4.4 kpc for the adopted distance of 4.9 Mpc to M 83. Based upon the radio position of Sramek et al. (1983) this is close to a complex of star formation to the E, SW and very bright nebular emission to the SE. Clocchiatti et al. (1996) enable relative astrometry from our Jun 2002 VLT/FORS2 imaging. Figure A7 illustrates that an extended  $H\text{II}$  region, #222 from the catalogue of Rumstay & Kaufman (1983), lies  $1''$  (25 pc) to the east of the SN, which has a luminosity intermediate between the Orion and Rosette nebulae. An arc of nebular emission lies  $9''$  (220 pc) to the SW of SN 1983N, alias # 234 from Rumstay & Kaufman (1983). This has an integrated luminosity of  $1.6 \times 10^{38}$  erg  $s^{-1}$  ( $3''$  radius) while a giant  $H\text{II}$  region, #220 from Rumstay & Kaufman (1983), peaks  $9''$  (220 pc) to the SE and has a luminosity comparable to N66 (SMC). Broad band HST/STIS imaging (GO 9148, PI P. Garnavich) reveals several faint sources consistent with the SN error box, with brighter clusters coincident peak emission from the  $H\text{II}$  regions to the E, SW and SE.

#### A8 SN 1985F in NGC 4618

This type Ib/c supernova was discovered in Feb 1985 (Filippenko & Sargent 1985, 1986, Modjaz, priv. comm.), and is spatially coincident with a bright  $H\text{II}$  region and cluster,  $10''$  away from the centre of NGC 4618 (Filippenko et al. 1986), as shown in Fig. A8. Based upon the HyperLeda inclination and PA of the major axis of NGC 4618 this corresponds to a deprojected offset of  $12''$  ( $0.1 R_{25}$ ) or 0.5 kpc for the adopted distance of 9.2 Mpc to NGC 4618. Using the SN position of Filippenko & Sargent (1986), the 2.3m Bok imaging of NGC 4618 from Apr 2001 (Kennicutt et al. 2008) reveals that the  $H\alpha$ -derived luminosity of this (extended) region is N66-like, and is comparable to that of a neighbouring  $H\text{II}$  region,  $4''$  to the SW of SN 1985F, a deprojected distance of 220 pc away. HST/WFPC2 imaging using the F606W filter (GO 5446, PI Illingworth) confirms that the SN is coincident with an extended source,

while each of the ground-based continuum sources to the W and SW in spatially resolved into two primary extended clusters.

#### A9 SN 1986L in NGC 1559

SN 1986L (II-L) was discovered in NGC 1559 in Oct 1986 (Evans et al. 1986). Figure A9 presents net  $H\alpha$  VLT/FORS1 imaging obtained in Aug 2005 and reveals that the SN lies in an extended region of nebular emission, which extends north from a giant  $H\text{II}$  region several arcsec to the SW. This complex is  $45''$  west of the centre of NGC 1559, and corresponds to a deprojected offset of  $1'$  ( $0.55 R_{25}$ ) based on the HyperLeda inclination and major axis PA, equivalent to 3.5 kpc for the 12.6 Mpc distance to NGC 1559 (100 pc corresponds to  $1''.3$ ). The nebular flux at the SN position is relatively faint, based upon the astrometry of McNaught & Waldron (1986).  $H\text{II}$  regions are located  $2''$  (150 pc) to the NNE and  $3''$  (230 pc) to the NW with luminosities of  $8 \times 10^{37}$  erg  $s^{-1}$  and  $1.2 \times 10^{38}$  erg  $s^{-1}$ , respectively. In addition, a giant  $H\text{II}$  region  $\sim 3''$  (230 pc) to the SW of SN 1986L has a luminosity comparable to the Carina Nebula. Unfortunately, SN 1986L occurred outside the field of view of HST/WFPC2 imaging (GO 9042, PI S.J. Smartt).

#### A10 SN 1987A in LMC

SN 1987A, the best studied supernova of the modern era, lies in the periphery of the 30 Doradus (Tarantula Nebula) region of the LMC.  $H\alpha$  imaging from the Nikon Survey Camera (M.S. Bessell, priv. comm.) and MCELS (Smith et al. 2000) indicates faint nebular emission at the position of the SN. In Figure A10, we present the lower spatial resolution Parking Lot Camera images (Kennicutt et al. 1995),  $70''$  or 17 pc at the 50 kpc LMC distance. Nebular emission is present at the SN site, although it is relatively faint, and would not necessarily be detected in ground-based imaging of other ccSNe in our survey. Still, SN 1987A is in close proximity to a pair of bright knots of nebular emission  $2\text{--}3'$  ( $\sim 40$  pc) to the NW, with an integrated luminosity of  $6 \times 10^{37}$  erg  $s^{-1}$  ( $2'$  radius aperture), as measured from Nikon continuum-subtracted imaging, calibrated via Kennicutt et al. (1995). The centre of 30 Doradus lies  $20'$  (300 pc) to the NE, with an integrated luminosity of  $6 \times 10^{39}$  erg  $s^{-1}$  ( $10.5'$  radius aperture). Panagia et al. (2000) discuss the faint cluster coincident with SN 1987A, but again this would not be detected via ground-based imaging of SN beyond the Local Group.

#### A11 SN 1992ba in NGC 2082

This type II supernova was discovered by R. Evans in NGC 2082 in late Sep 1992 (Evans & Phillips 1992). SN 1992ba occurred  $26''$  to the W of the nucleus of NGC 2082, which deprojects to  $29''$  ( $0.5 R_{25}$ ) based on the low inclination from HyperLeda, plus an adopted PA=0. This corresponds to a galactocentric distance of 1.9 kpc for the 13.1 Mpc distance to NGC 2082. We do not have access to calibrated  $H\alpha$  imaging, so we have inspected archival R-band imaging from Oct 1992 (AAT Prime Focus) and Apr 2000 (3.5m NTT/EMMI). The latter are reveal continuum sources  $2''$  NW and  $2''.5$  SE, with a brighter source  $3''.5$  SE of SN 1992ba. Schmidt et al. (1994) note that this supernova occurred in, or near, a bright  $H\text{II}$  region.

**A12 SN 1993J in M 81**

This well-studied type IIb supernova was discovered in March 1993 (Ripero et al. 1993), and occurred  $2'.8$  SSW of the nucleus of M 81 (NGC 3031). The HyperLeda inclination of M 81 is high ( $62.7^\circ$ ) so this position corresponds to a deprojected offset of  $4'.4$  ( $0.32 R_{25}$ ), equivalent to a distance of 4.6 kpc for the 3.65 Mpc distance to M 81. From the KPNO 2.1m imaging from Mar 2001 (Kennicutt et al. 2003), shown in Fig. A11, SN 1993J is spatially coincident with a faint nebular emission, likely arising from the SNR itself. A brighter, Orion-like region lies  $21''$  to the NE, or a deprojected distance of 580 pc. An extended H II region, with a  $H\alpha + [N II]$  flux of  $4 \times 10^{-14}$  erg s $^{-1}$  cm $^{-2}$  lies  $38''$  (1.0 kpc deprojected) to the NW. The blue supergiant companion to the red supergiant progenitor is detected in late-time spectroscopy (Maund et al. 2004) and spectroscopy (Maund & Smartt 2009), the latter based upon extensive HST ACS and WFPC2 imaging.

**A13 SN 1994I in M 51a**

This type Ic supernova occurred close to the nucleus of M 51a in Apr 1994 (Puckett et al. 1994),  $18''$  to its SE. The low inclination of  $32.6^\circ$  for M 51a implies negligible projection effects, so this corresponds to a distance of 0.8 kpc ( $0.06 R_{25}$ ) for the adopted distance of 8.39 Mpc. Based on radio-derived coordinates from Rupen et al. (1994), Fig. A12 illustrates that SN 1994I lies within a large region of diffuse nebular emission. The closest identifiable source is a giant H II region  $2''$  (80 pc) to the W in the KPNO 2.1m imaging from Mar 2001 (Kennicutt et al. 2003). Brighter sources lie  $9''$  ( $0.38$  kpc) SW and  $13''$  ( $0.55$  kpc) W. SN 2004I does not appear to coincide with a bright star cluster in the KPNO 2.1m R-band imaging, although identification is severely hindered by diffuse emission and the moderate spatial resolution of the ground-based images. We have therefore inspected archival Hubble Space Telescope ACS/WFC (GO 10452, PIS. Beckwith) images obtained with the F555W and F658N ( $H\alpha + [N II]$ ) filters (e.g. Chandrar et al. 2011), which confirm no bright cluster is spatially coincident with SN 1994I.

**A14 SN 1995V in NGC 1087**

This type II-P supernova was discovered in Aug 1995 (Evans et al. 1995), and occurred  $24''$  E of the nucleus of NGC 1087 (Balam 1995). This corresponds to a deprojected offset of  $40''$  ( $0.36 R_{25}$ ) or 2.8 kpc for the adopted distance of 14.4 Mpc to NGC 1087. Fig. A13 shows JKT  $H\alpha$  imaging from Jan 2000 (James et al. 2004). Although seeing conditions were poor (FWHM $\sim 3''.5$ ), SN 1995V does not appear to be coincident with nebular emission, with the nearest identifiable H II region (and bright cluster) located  $5''$  ( $0.6$  kpc) to the SW.

**A15 SN 1995X in UGC 12160**

The type II supernova SN 1995X was discovered in UGC 12160 in Aug 1995 (Mueller et al. 1995). We do not have access to calibrated  $H\alpha$  imaging of UGC 12160, although Mueller et al. (1995) report narrow  $H\alpha$  emission from a H II region superimposed upon an early SN spectrum. The SN occurred  $22''$  NW of the centre of UGC 12160 (Sicoli et al. 1995), which corresponds to a deprojected distance of  $26''$  ( $0.42 R_{25}$ ) or 1.8 kpc for the adopted distance of 14.4 Mpc to UGC 12160. At this location, Anderson et al. (2012)

report a NCR pixel value of 0.903 from Liverpool Telescope RAT-Cam imaging, indicating it occurred close to the peak of  $H\alpha$  emission from the host.

**A16 SN 1996cr in Circinus**

This type II<sub>n</sub> supernova was discovered in Mar 1996, although was originally identified as an X-ray source (Bauer 2007). It occurred  $24''$  to the S of the nucleus of Circinus (ESO 097-G13), corresponding to a deprojected offset  $37''$  ( $0.18 R_{25}$ ) or 0.75 kpc for a 4.21 Mpc distance to Circinus. This galaxy suffers extensive foreground extinction ( $A_B \sim 2$  mag) due to its low galactic latitude ( $b = -3.8^\circ$ ).  $H\alpha$  imaging from Apr 2002 using the CTIO 0.9m (Kennicutt et al. 2008) is presented in Fig. A14. This reveals faint nebular emission at the position of SN 1996cr, as discussed by Bauer (2007), which connects to a bright H II region,  $3''$  to its SE, a deprojected distance of 100 pc away. A starburst ring of H II regions surrounds the (type 2 Seyfert) nucleus of Circinus (Marconi et al. 1994), the most southerly component of which lies  $15''$  ( $0.5$  kpc) NNW of SN 1996cr. No cluster is apparent at the location of the SN, although the CTIO imaging was obtained during poor seeing conditions (FWHM $\sim 3''.5$ ). We have therefore inspected HST WFPC2 F547M and F656N imaging (GO 7273) of Circinus (Wilson et al. 2000). No cluster is detected at the location of SN 1996cr, although compact  $H\alpha$  emission is confirmed, potentially resulting from the SN itself, in part.

**A17 SN 1997X in NGC 4691**

SN 1997X was discovered in Feb 1997, approximately  $9''$  E of the centre of NGC 4691 (Nakano et al. 1997). Using the inclination and major axis PA from HyperLeda this corresponds to a deprojected offset of  $11''$  ( $0.14 R_{25}$ ) or 0.7 kpc for a 12 Mpc distance to NGC 4691. Although we do not have access to calibrated  $H\alpha$  imaging of NGC 4691, Anderson & James (2008) discuss INT/WFC imaging, from which a normalized cumulative rank (NCR) pixel value of 0.323 is obtained for SN 1997X. Munari et al. (1998) report nebular  $H\alpha + [N II]$  emission from a H II region superimposed upon an early spectrum of this type Ib supernova (Modjaz et al., in prep.). Figure A15 presents the INT  $H\alpha$  imaging from Mar 2007, from which we note diffuse nebular emission centred upon the nucleus of NGC 4691, extending  $\pm 15''$  east-west. Superimposed upon the diffuse nebular emission are several spatially extended knots, the brightest of which lies  $6''$  ( $0.4$  kpc) WSW of the SN location.

**A18 SN 1998dn in NGC 337A**

SN 1998dn was discovered in Aug 1998 in NGC 337A,  $2.1'$  SW of its nucleus (Cao 1998), corresponding to a deprojected offset of  $3.5'$  ( $1.2 R_{25}$ ) or 11.6 kpc based on a 11.4 Mpc distance to NGC 337A. JHK  $H\alpha$  imaging from Apr 2002 (Knapen et al. 2004) is presented in Fig. A16 and shows that this type II SN lies in a region devoid of nebular emission, with the nearest bright H II region  $5''.5$  to the NW, which corresponds to a deprojected distance of 0.5 kpc for the HyperLeda inclination and PA.

**A19 SN 1999em in NGC 1637**

This type II-P supernova was discovered in Oct 1999,  $24''$  SW of the nucleus of NGC 1637 (Li 1999; Jha et al. 1999), corresponding to a deprojected offset of  $27''$  ( $0.22 R_{25}$ ) which is equivalent to a

galactocentric distance of 1.3 kpc for a 9.77 Mpc distance to NGC 1637. As shown in Fig. A17, SN 1999em was still very bright in Oct 2000 when the CTIO 1.5m H $\alpha$  imaging of Meurer et al. (2006) was obtained. We have therefore inspected pre-SN H $\alpha$  imaging from Ryder & Dopita (1993) obtained with the Siding Spring 40'' telescope which indicates negligible nebular emission at the SN site. The closest H II region to the SN location lies 6'' (0.3 kpc) SE and has a luminosity comparable to the Orion nebula. Other H II regions to the NW and SW each lie 7'' (375 pc) away, with H $\alpha$ + [N II] fluxes of  $1.7 \times 10^{-15}$  erg s $^{-1}$  cm $^{-2}$  and  $3.1 \times 10^{-15}$  erg s $^{-1}$  cm $^{-2}$ , respectively. A brighter source lies 9''.5 (0.5 kpc) to the SE, with a luminosity comparable to the Rosette nebula. Smartt et al. (2002) analysed Jan 1992 broad-band imaging from 3.6m CFHT in which the progenitor was undetected, i.e. there is no evidence for an host cluster. Note that the SN is detected in HST WFPC2 F555W imaging (GO 9155, PI D.C. Leonard) obtained in Sep 2001.

#### A20 SN 1999eu in NGC 1097

This type II-P supernova was discovered in Nov 1999 (Nakano et al. 1999a) within a spiral arm of NGC 1097, 2.6' to the SSE of its nucleus. This corresponding to a de-projected galactocentric distance of 3.9' (0.83  $R_{25}$ ) or 16 kpc for the HyperLeda inclination and major axis PA plus an EDD distance of 14.2 Mpc. Fig. A18 presents CTIO 1.5m H $\alpha$  imaging from Oct 2001 (Kennicutt et al. 2003), revealing no nebular emission at the position of SN 1999eu. The closest H II region lies 3''.75  $\pm$  to the W, at a deprojected distance of 375 pc, and is spatially extended EW, while a brighter complex with a H $\alpha$ + [N II] flux of  $2.5 \times 10^{-15}$  erg s $^{-1}$  cm $^{-2}$  (3 arcsec aperture radius) lies 13'' (1.3 kpc deprojected) to the E.

#### A21 SN 1999gi in NGC 3184

SN 1999gi was discovered in Dec 1999, 1' north of the nucleus of NGC 3184 (Nakano et al. 1999b), whose low inclination of 14 $^\circ$  implies negligible projection effects (0.28  $R_{25}$ ), such that the galactocentric distance is 3.9 kpc based on a 13 Mpc distance to NGC 3184. Fig. A19 shows KPNO 2.1m H $\alpha$  imaging from Apr 2002 (Kennicutt et al. 2003) which reveals diffuse emission at the position of the SN, intermediate between extended H II regions 2'' (125 pc) to the SW and NE. The former has a H $\alpha$  luminosity comparable to the Rosette nebula, while the latter is more extended and has a luminosity a factor of  $\sim 3$  times higher. Within the larger star forming complex, additional knots lie 6''.9 (430 pc) to the SW and 10'' (630 pc) to the NE, with H $\alpha$ + [N II] fluxes of  $4 \times 10^{-15}$  erg s $^{-1}$  cm $^{-2}$  and  $1 \times 10^{-14}$  erg s $^{-1}$  cm $^{-2}$ , respectively. Pre-SN WFPC2/WF images obtained with the F606W filter in Jun 1994 (GO 5446, PI G.D. Illingworth), identify nearby OB stars but not the progenitor of the type II-P supernova, while the SN is detected in WFPC2/PC F555W images (GO 8602, PI A.V. Filippenko) from Jan 2001 (Smartt et al. 2001; Leonard et al. 2002; Hendry 2006).

#### A22 SN 2001X in NGC 5921

This type II-P supernova was discovered in Feb 2001, 33'' SSW of the nucleus of NGC 5921 (Li et al. 2001). For the HyperLeda inclination and major axis PA, this deprojects to 49'' (0.34  $R_{25}$ ) or 3.4 kpc, with a scale of 1'' = 100 pc for the 14 Mpc distance to NGC 5921. From inspection of the net H $\alpha$  imaging from Apr 2001 (James et al. 2004), SN 2001X was exceptionally bright. Fig. A20 shows the JKT H $\alpha$  imaging from Mar 1999, plus R-band imaging

from Mar 2003 to assess the nebular environment. SN 2001X is coincident with faint nebulosity, while extended emission lies 3'' (0.3 kpc) SE of SN 2001X, comparable in luminosity to the Rosette nebula. A brighter compact source lies 4'' to the N (0.4 kpc), although SN 2001X is not strictly associated with either. Anderson et al. (2012) quote a NCR pixel value of 0.698 for SN 2001X based on Liverpool Telescope imaging from Apr 2009, obtained archival indicating a potential contribution from the SN remnant.

#### A23 SN 2001ig in NGC 7424

SN 2001ig (Iib) was discovered by R. Evans in Dec 2001, 2.95' NE of the nucleus of NGC 7424 (Evans et al. 2002). Based on the HyperLeda inclination of NGC 7424 and an adopted PA of the major axis of 0, the deprojected distance is 4'.9 (1.0  $R_{25}$ ) or 11.2 kpc for the adopted distance of 7.94 Mpc. Fig. A21 presents pre-explosion CTIO 1.5m H $\alpha$  imaging from Sep 2000 (Meurer et al. 2006). The figure shows that SN 2001ig occurred at the periphery of a modest luminosity (Orion-like), extended H II region. Faint diffuse emission is also detected 6–10'' to the S of the supernova, at a deprojected distance of 0.4–0.6 kpc. A brighter H II region, with  $F(\text{H}\alpha + [\text{N II}]) = 2.5 \times 10^{-15}$  erg s $^{-1}$  cm $^{-2}$  (2''.5 radius aperture), is located 17'' to the SW, corresponding to a deprojected distance of 1.1 kpc. Astrometry was verified from VLT/FORS2 R-band imaging of SN 2001ig obtained in Jun 2002 (069.D-0453, PI E.Cappellaro). High spatial resolution  $u'$ ,  $g'$ ,  $r'$  Gemini GMOS imaging from Sep 2004 is discussed by Ryder et al. (2006), who remark upon arcs of diffuse nebulosity from their deep  $u'$  imaging.

#### A24 SN 2002ap in M 74

This well studied type Ic supernova was discovered by Y. Hirose in Jan 2002 in the outer disk of M 74, 4.7' (0.89  $R_{25}$ ) SW of the nucleus (Nakano et al. 2002). The low inclination of M 74 (Kamphuis & Briggs 1992) implies that deprojection effects are negligible, such that the galactocentric distance is 12.2 kpc for a 9 Mpc distance to M 74. Its location was beyond the field-of-view of VLT/FORS1 and VATT 1.8m imaging, so we present CTIO 1.5m H $\alpha$  imaging from Oct 2001 (Kennicutt et al. 2003) in Fig. A22. The closest nebular emission to SN 2002ap is an extended, Orion-like, H II region 10'' (0.4 kpc) to the SSE. Additional sources lie 17'' (0.75 kpc) and 22'' (1 kpc) to the SE, the latter with a H $\alpha$ + [N II] flux of  $4 \times 10^{-15}$  erg s $^{-1}$  cm $^{-2}$  (4'' radius aperture).

Crockett et al. (2007) present deep, 3.6m CFHT broad-band imaging from Oct 1999, together with post-SN HST ACS/HRC imaging from Jan 2003–Aug 2004 from which the progenitor star could not be identified. We have also inspected CFHT/CFH12K H $\alpha$  images of the site of SN2002ap from Jun 1999 (PI J.-C. Cuillandre) which confirm the CTIO results, while nebular emission is not detected in shallow HST ACS/HRC F658N images from Jan 2003 (GO 9144, PI R.P. Kirschner).

#### A25 SN 2002hh in NGC 6946

This type II-P supernova was discovered in Oct 2002, 2.2' (0.4  $R_{25}$ ) SW of the nucleus of NGC 6946 (Li 2002), corresponding to 4.5 kpc for the adopted distance of 7 Mpc to NGC 6946 (3'' approximates to 100 pc). Fig. A23 presents our Oct 2009 Gemini GMOS H $\alpha$  imaging. SN 2002hh occurred close to the periphery of an extended giant H II region 1''.5–3''.5 (50–120 pc) to its NW, whose

radius is  $\sim 4''$ . In addition, a faint knot of nebular emission is observed at the position of SN 2002hh, likely arising from the SNR, with a  $H\alpha + [N II]$  flux of  $4 \times 10^{-16} \text{ erg s}^{-1} \text{ cm}^{-2}$  ( $1''$  radius aperture), corresponding to a luminosity several times lower than Orion. As discussed by e.g. Otsuka et al. (2012), SN 2002hh is detected in F606W filter observations with HST ACS/HRC from Sep 2005 (GO 10607, PI B.Sugerman) and WFPC2/PC images from July 2007 (GO 11229, PI M. Meixner). In addition, the extended nebular emission to the NW is spatially resolved in ACS/HRC F658N imaging from Sep 2005, with the brightest knot  $2''.3$  (80 pc) NW of SN 2002hh.

#### A26 SN 2003B in NGC 1097

SN 2003B (II-P) was discovered by R. Evans in Jan 2003,  $3'$  NW of the nucleus of NGC 1097 (Evans & Quirk 2003), equivalent to a galactocentric distance of  $4.9'$  ( $1.04 R_{25}$ ) or 20 kpc for the 14.2 Mpc distance to NGC 1097. Fig. A24 presents CTIO 1.5m  $H\alpha$  imaging from Oct 2001 (Kennicutt et al. 2003). SN 2003B lies at the periphery of a spatially extended H II region, cited in early spectroscopy of SN 2003B by Kirshner & Silverman (2003). The luminosity of this giant H II region is comparable to N66 in the SMC.

#### A27 SN 2003gd in M 74

This type II-P supernova was also discovered by R. Evans in Jun 2003,  $2.7'$  ( $0.51 R_{25}$ ) SSE of the nucleus of M 74 (Evans & McNaught 2003). As for SN 2002ap, deprojection effects are negligible owing to the low inclination of M 74 (Kamphuis & Briggs 1992), so the galactocentric distance is 7.0 kpc based on our 9 Mpc distance. The location of the SN is intermediate between three large, star forming complexes to the SW, NE and NW (Hodge 1976). Fig. A25 presents the Oct 2007 VLT/FORS1 imaging, for which the precise SN location is identified from differential astrometry using post-explosion HST ACS/HRC F555W observations from Aug 2003 (GO 9733, PI S.J. Smartt). Diffuse nebosity is observed several arcsec to the NE of SN 2003gd, whose integrated  $H\alpha + [N II]$  flux of  $4 \times 10^{-16} \text{ erg s}^{-1} \text{ cm}^{-2}$  ( $1''.5$  radius aperture) implies a luminosity significantly inferior to the Orion nebula.

The closest H II regions to SN 2003gd are compact sources to the N and SW, each  $7''$  (0.3 kpc) away, catalogued as #641 and #640 from Hodge (1976), respectively. Each has a luminosity comparable to the Orion nebula. The main complex of the SW nebosity (#639 from Hodge 1976) peaks  $12''$  (0.5 kpc) from SN 2003gd, and has a  $H\alpha + [N II]$  flux an order of magnitude larger. The luminosity of another complex, #636 and #637 from Hodge (1976), which peaks  $18''$  (0.8 kpc) to the NW of the SN, is comparable to N66 in the SMC, while the complex  $15''$  to the NE (#649–651 from Hodge 1976) has an intermediate luminosity. Hendry et al. (2005) refer to the NW complex in their study of SN 2003gd via #72–73 from Belley & Roy (1992).

HST ACS/HRC F625W imaging (GO 10272, PI A.V. Filippenko) also reveals very faint nebosity several arcsec W of the SN position, while no cluster is seen at the site of the SN. Pre-SN HST WFPC2 and Gemini GMOS imaging from May–Aug 2002 enabled Smartt et al. (2004) to identify a red supergiant as the progenitor of SN 2003gd (see also Maund & Smartt 2009).

#### A28 SN 2003jg in NGC 2997

This type Ib/c supernova was discovered by R. Martin in Oct 2003,  $13''$  NW of the nucleus of NGC 2997 (Martin & Biggs 2003), which deprojects to  $18''$  ( $0.07 R_{25}$ ) or a galactocentric distance of 1.0 kpc using a 11.7 Mpc distance to NGC 2997. This galaxy is undergoing an intense, ring-like star formation episode in its nucleus, with a luminosity comparable to 30 Doradus in the LMC. Fig. A26 presents Danish 1.5m  $H\alpha$  images (Larsen & Richtler 1999), revealing that SN 2003jg lies  $2''$  (140 pc) W of a modest, Orion-like H II region, apparently associated with this intense activity. It is unclear whether this region is extended from the Danish 1.5m imaging, so we have examined high quality VLT/FORS1 R-band imaging from Mar 1999 (60.A-9203), which indicate that the source is spatially extended NS. No source is coincident with the SN progenitor based on HST WFPC2 imaging from Aug 2001 using the F450W filter (GO 9042, PI S.J. Smartt).

#### A29 SN 2004dj in NGC 2403

SN 2004dj (II-P) was discovered by K. Itagaki in July 2004,  $2.7'$  east of the nucleus of NGC 2403 (Nakano et al. 2004). Based on the inclination and PA of the major axis of NGC 2403 from HyperLeda, this corresponds to a deprojected distance of  $3.7'$  ( $0.34 R_{25}$ ) or 3.4 kpc for a 3.16 Mpc distance to NGC 2403, the second closest ccSNe in our sample. Figure. A27 shows KPNO 2.1m  $H\alpha$  observations of NGC 2403 from Nov 2001 (Kennicutt et al. 2003), while we have also inspected higher spatial resolution  $H\alpha$  observations of the central region of NGC 2403 from NOT/ALFOSC (Larsen & Richtler 1999).

Maíz-Apellániz et al. (2004) identified SN 2004dj with a young, compact star cluster, #96 from Sandage (1984). From Fig. A27, this is not a source of  $H\alpha$  emission, with the faint, diffuse emission  $\sim 8''$  to the SE, a deprojected distance of 170 pc away. The nearest prominent star forming regions each lie  $21''$  (450 pc) NW and SE. The former H II region is spatially extended, albeit relatively compact, with a luminosity similar to the Rosette nebula, while the latter contains multiple knots, separated by several arcsec and has an integrated luminosity comparable to N66.

Vinkó et al. (2006, 2009) have studied Sandage 96, from which both ‘young’ (10–16 Myr,  $15\text{--}20 M_{\odot}$ ) and ‘old’ (30–100 Myr,  $< 10 M_{\odot}$ ) solutions were obtained. From post-explosion 2.3m Bok  $H\alpha$  imaging, they also note that Sandage 96 lacks extended  $H\alpha$  emission and attribute the bulk of the compact  $H\alpha$  emission that they detected to SN 2004dj itself. Diffuse emission is not detected in HST ACS/HRC F658N imaging from Aug 2005 (GO 10607, PI B.E. Sugerman), while the compact nature of the NW source is confirmed from HST WFPC2 F606W imaging from Apr 2008 (GO 11229, PI M. Meixner).

#### A30 SN 2004et in NGC 6946

This type II-P supernova was discovered by S. Moretti in Sep 2004,  $4.5'$  ( $0.8 R_{25}$ ) SE of the nucleus of NGC 6946 (Zwitter et al. 2004) corresponding to a galactocentric distance of 9.6 kpc based on a 7.0 Mpc distance to NGC 6946. This region, far from any large star forming regions, falls beyond the field-of-view of the Gemini GMOS imaging, so Fig. A28 shows KPNO 2.1m  $H\alpha$  imaging from Mar 2001 (Kennicutt et al. 2003). The closest nebular emission lies  $9''$  (300 pc) N of the position of SN 2004et, extends NE–SW over several arcsec, and has an integrated luminosity comparable to the Orion nebula. Crockett et al. (2011) discuss constraints upon

the progenitor of SN 2004et from various facilities, including pre-SN CFHT/CFH12K R-band imaging and post-SN HST WFPC2/PC (GO 11229, P.I. M. Meixner) F606W imaging from Jan 2008, with a second (point) source detected  $0''.25$  E of the SN position. The extended nebular emission N of SN 2004et is apparent in both datasets.

### A31 SN 2005at in NGC 6744

This type Ic supernova was jointly discovered by R. Martin and L. Monard in Mar 2005,  $2'.3$  NNE of the nucleus of NGC 6744 (Martin et al. 2005), corresponding to a galactocentric distance of  $3'.0$  ( $0.30 R_{25}$ ) or  $10.0$  kpc for a  $11.6$  Mpc distance to NGC 6744. In Fig. A29 we present our VLT/FORS1 continuum-subtracted  $H\alpha$  imaging from Jun 2008. The SN occurred within an extended  $H\text{II}$  region whose luminosity is comparable to the Rosette nebula. This nebula is also detected in pre-SN Danish  $1.5\text{m}$  imaging from Feb 1998 (Larsen & Richtler 1999). The faint continuum source at the position of SN 2005at in Fig. A29 is likely due to the SNR itself. A bright continuum source lies  $8''.5$  S of SN 2005at, at a deprojected distance of  $0.6$  kpc, which is poorly subtracted in the VLT/FORS1 net  $H\alpha$  image. The SN has also been imaged with HST WFPC2/PC using the F555W filter (GO 10877, PI W. Li) in Apr 2007.

### A32 SN 2005cs in M 51a

This type II-P supernova was discovered by W. Kloehr in June 2005, within a complex star forming region,  $1.1'$  ( $0.2 R_{25}$ ) SSW of the nucleus of M 51a (Kloehr et al. 2005), with negligible projection effects, such that the galactocentric distance is  $2.7$  kpc for a  $8.39$  Mpc distance to M 51a. Fig. A30 presents KPNO  $2.1\text{m}$  imaging from Mar 2001 (Kennicutt et al. 2003), revealing that SN 2005cs coincides with a region of nebular emission extending N-S. Orion-like  $H\text{II}$  regions are located  $1''$  ( $40$  pc) E,  $2''.7$  ( $110$  pc) N and  $4''.3$  ( $175$  pc) E, while brighter star forming knots are located  $>9''$  ( $>0.35$  kpc) to the N, NE and E, the brightest of which is spatially extended N-S, lies  $13''$  ( $0.55$  kpc) E of the SN and has a luminosity comparable to the Rosette nebula. These sources are poorly resolved in ground-based R-band imaging, except that by far the brightest continuum source is that  $9''$  NE of the SN.

We have inspected HST ACS/WFC (GO 10452, PI S. Beckwith) images obtained with the F555W and F658N ( $H\alpha$ + $[N\text{II}]$ ) filters in Jan 2005. As shown in Fig. 2, SN 2005cs is not associated with nebular emission, although compact  $H\alpha$  sources lie  $1''$  ( $40$  pc) to the SE and NE, plus there is a compact star cluster  $\sim 0''.2$  ( $8$  pc) to the SW (see Li et al. 2006).

### A33 SN 2005kl in NGC 4369

SN 2005kl was discovered by M. Migliardi in Nov 2005,  $10''$  ( $0.17 R_{25}$ ) NW of the centre of NGC 4369 (Migliardi et al. 2005). In view of the low inclination of this galaxy ( $18.9^\circ$ ), there are negligible projection effects, so the galactocentric distance is  $0.6$  kpc for a  $11.2$  Mpc distance to NGC4369. Although we do not have access to calibrated  $H\alpha$  imaging of NGC 4369, Fig. A31 presents Liverpool Telescope RATCam  $H\alpha$  and (Sloan)  $r'$ -band imaging of NGC 4369 from Feb 2007 (Anderson & James 2008). This type Ic supernova occurred at the periphery of a bright, spatially extended  $H\text{II}$  region, the peak of which lies  $1''.5$  ( $80$  pc) to the SE of the supernova, with the main (continuum) body of the galaxy further to the E. Anderson

& James (2008) quote a normalized cumulative rank (NCR) pixel value of  $0.570$  from their RATCam imaging.

### A34 SN 2007gr in NGC 1058

This type Ic supernova was discovered by W. Li in Aug 2007,  $0.5'$  NW of the nucleus of NGC 1058 (Li et al. 2007), corresponding to a deprojected offset of  $0.7'$  ( $0.45 R_{25}$ ) for the HyperLeda inclination and major axis PA, i.e. a  $2.0$  kpc galactocentric distance for the  $9.86$  Mpc distance to NGC 1058. This SN occurred within a large star forming complex (Crockett et al. 2008). Fig. A32 shows  $2.3\text{m}$  Bok imaging obtained in Nov 2003 (Kennicutt et al. 2008), in which the primary source of  $H\alpha$  emission within this complex is a giant  $H\text{II}$  region, comparable in luminosity to the SMC's N66. This lies  $\sim 2''$  W of SN 2007gr, corresponding to a deprojected distance of  $130$  pc, and itself is spatially extended. Diffuse nebular emission is found at the location SN 2007gr, while another bright component is observed  $1''.5$  to the NW, with a luminosity similar to the Rosette nebula. Anderson et al. (2012) quote a NCR pixel value of  $0.157$  for SN 2007gr based on JKT imaging. Crockett et al. (2008) have studied pre- and post-SN images of NGC 1058 including archival INT imaging. INT/WFC  $H\alpha$  and  $r'$ -band imaging from Jan 2005 reveal bright, spatially extended emission  $2''.7$  ( $170$  pc) W of the SN location, plus faint nebulosity  $1''$  to the S, and to the E. More recent HST WFPC2/F675W imaging from Nov 2008 (GO 10877, PI W. Li) and WFC3/F625W imaging from Jan 2010 (GO 11675, PI J. Maund) indicate fainter nebulosity at the SN position.

### A35 SN 2008bk in NGC 7793

This type II-P supernova was discovered in Mar 2008, offset  $2.1'$  NNE of the nucleus of NGC 7793 (Monard 2008a). This corresponds to a deprojected radial offset of  $3.5'$  ( $0.75 R_{25}$ ) for the adopted inclination and PA (Carignan & Puche 1990), equivalent to  $3.7$  kpc for a  $3.61$  Mpc distance to NGC 7793. Since this position lays beyond the field-of-view of our VLT/FORS1  $H\alpha$  images, so Fig. A33 presents continuum subtracted CTIO  $1.5\text{m}$   $H\alpha$  images from Oct 2001 (Kennicutt et al. 2003). SN 2008bk is neither spatially coincident with nebular emission nor a bright continuum source. A  $H\alpha$  arc extends to the N and W of the SN position,  $\sim 6''$  away, corresponding to a deprojected distance of  $175$  pc, and connects to a spatially extended  $H\text{II}$  region,  $7''$  ( $200$  pc) to the SW. In addition to this source, which is somewhat more luminous than the Orion nebula, other fainter star formation knots lie  $11$ – $12''$  to the S and SE of SN 2008bk. Mattila et al. (2008) and van Dyk et al. (2012) confirm a red supergiant progenitor for SN 2008bk from, respectively, pre-explosion VLT/FORS1 and Gemini/GMOS imaging. Archival VLT/FORS1  $H\alpha$  and R-band imaging from Sep 2001 (067.D-0006(A)), the former uncalibrated, confirm the nebular morphology of CTIO  $1.5\text{m}$  imaging. Post-SN F814W imaging has also been obtained with HST WFC3 from Apr 2011 (GO 12262, PI J.R. Maund).

### A36 SN 2008eh in NGC 2997

This probable type Ib/c supernova (Horiuchi et al. 2011) was discovered in July 2008,  $2.1'$  ENE of the nucleus of NGC 2997 (Monard 2008b), close to its major axis, such that the deprojected radial distance is  $2'.2$  ( $0.5 R_{25}$ ) or  $7.4$  kpc for a  $11.3$  Mpc distance to NGC 2997. Fig. A34 shows the site of SN 2008eh at the periphery of a giant  $H\text{II}$  region,  $2''$  ( $110$  pc) to the SW, based on  $1.5\text{m}$

Danish H $\alpha$  imaging of Larsen & Richtler (1999). A brighter, N66-like, giant H II region 4".5 (250 pc) lies to the S. Both sources are prominent in R-band images.

#### A37 SN 2009N in NGC 4487

This type II-P supernova was discovered by K. Itagaki in Jan 2009, 1.3' ENE of the nucleus of NGC 4487 (Nakano et al. 2009), which corresponds to a deprojected radial distance of 1.6' (0.77  $R_{25}$ ) or 5.1 kpc for a 11 Mpc distance to NGC 4487. Figure A35 shows continuum-subtracted JKT H $\alpha$  imaging (Knapen et al. 2004), from which we identify a compact H II region 3" to the NW, a deproject distance of 200 pc away, with a luminosity comparable to the Orion nebula. In addition, a more extended H II region lies 3" (200 pc) to the NE, closer in luminosity to the Rosette nebula. SN 2009N is not associated with either of these star forming regions.

#### A38 SN 2009ib in NGC 1559

SN 2009bi (II-P) was discovered in Aug 2009, 37" NE of the centre of NGC 1559 (Pignata et al. 2009). This corresponds to a radial distance of 70" (0.67  $R_{25}$ ) or galactocentric distance of 4.2 kpc for a 12.6 Mpc distance to NGC 1559. Fig. A36 shows pre-SN VLT/FORS1 continuum subtracted H $\alpha$  imaging from Aug 2005. Faint nebulosity is observed at the site of the SN, with an extended H II region 1".5 to the SE, a deprojected distance of 170 pc away. Extended, giant H II regions lie to the W of SN 2009bi, including a source 6" (0.7 kpc) SW of the SN comparable in luminosity to N66, plus a supergiant H II region 13" (1.5 kpc) to the ESE with a H $\alpha$ + [N II] flux of  $1.5 \times 10^{-13}$  erg s $^{-1}$  cm $^{-2}$  (2".5 aperture radius). Pre-SN HST imaging with WFPC2 using the F606W filter (GO 9042, PI S.J. Smartt) reveals a potential host cluster within the error circle of the SN location, plus diffuse nebular emission.

#### A39 SN 2011dh in M 51a

This type IIb supernova was discovered in late May 2011, 2.6' SE of the nucleus of M 51a (Griga et al. 2011), corresponding to a radial distance of 2'.8 (0.5  $R_{25}$ ) or 6.8 kpc for a 8.39 Mpc distance to M 51a. Fig. A37 shows that the SN position is close to the centre of a ring of star forming regions, based on KNPO 2.1m H $\alpha$  imaging (Kennicutt et al. 2003). Of these, the closest to the site of the SN lies 8" (0.35 kpc) SE and has a similar luminosity to the Rosette nebula. Other, spatially extended, giant H II region complexes lie 11–13" to the NE, NW and SW. Anderson et al. (2012) report a NCR pixel value of 0.00 for SN 2011dh from INT imaging, while inspection of archival HST ACS/WFC images confirms the absence of nebular emission at the position of SN 2011dh. The (point source) SN progenitor is detected in ACS/WFC F555W and F658N images (e.g. van Dyk et al. 2011; Maund et al. 2011), which also resolve the star forming region to the SE into two main components, separated by 1".0 (45 pc). H II regions to the NE and NE are largely dominated by one main component, while that to the SW is highly complex, comprising multiple compact sources.

#### A40 SN 2012A in NGC 3239

This type II-P supernova was discovered in Jan 2012, is 50" SE of the nucleus of NGC 3239 (Moore et al. 2012). Based on the HyperLeda inclination of NGC 3239, this corresponds to a radial distance of 64" (0.42  $R_{25}$ ) for this galaxy, corresponding to 3.1 kpc

at 10 Mpc. Fig. A38 presents continuum-subtracted H $\alpha$  and R-band imaging from VATT 1.8m (Kennicutt et al. 2008). SN 2012A is located close to a very bright star forming complex, although it is neither spatially coincident with nebular emission nor a continuum source. An extended nebula with a luminosity comparable to the Rosette nebula lies 2" (120 pc) to the S, with the main complex extending over several hundred pc due E of the SN. Within this region, the closest knot of star formation lies 7" (0.4 kpc) to the E of the SN and has an integrated H $\alpha$ + [N II] flux of  $2 \times 10^{-14}$  erg s $^{-1}$  cm $^{-2}$  (2" aperture radius), comparable to N66 in the SMC. Supergiant H II regions are found 10" (0.6 kpc) to the NE and 12" (0.75 kpc) to the SE, each similar to NGC 604 in luminosity.

#### A41 SN 2012aw in M 95

This type II-P supernova was discovered in Mar 2012, 2'.1 SW of the nucleus of M 95 (NGC 3351). This corresponds to a radial distance of 2'.3 (0.62  $R_{25}$ ) using an inclination and PA of its major axis from HyperLeda, i.e. a galactocentric distance of 6.7 kpc at 10 Mpc. Continuum-subtracted H $\alpha$  imaging from KPNO 2.1m (Kennicutt et al. 2003) is presented in Fig. A39. Nebular emission is not observed at the site of the SN, with a H II region 5" (260 pc) to the NNE, somewhat less luminous than the Orion nebula. A further pair of faint H II regions are located 7" (370 pc) to the W, plus an extended H II region 10" (525 pc) to the SW that is comparable to the Orion nebula. The closest giant H II regions lie 19" (1.0 kpc) SSE and 22" (1.2 kpc) ENE, with the integrated H $\alpha$ + [N II] flux of the former  $4 \times 10^{-14}$  erg s $^{-1}$  cm $^{-2}$  (4" aperture radius), implying a luminosity comparable to N66 (SMC). HST WFPC2 imaging of the site of SN 2012aw was obtained in Nov 1994 using the F555W filter (GO 5397, PI J. Mould).

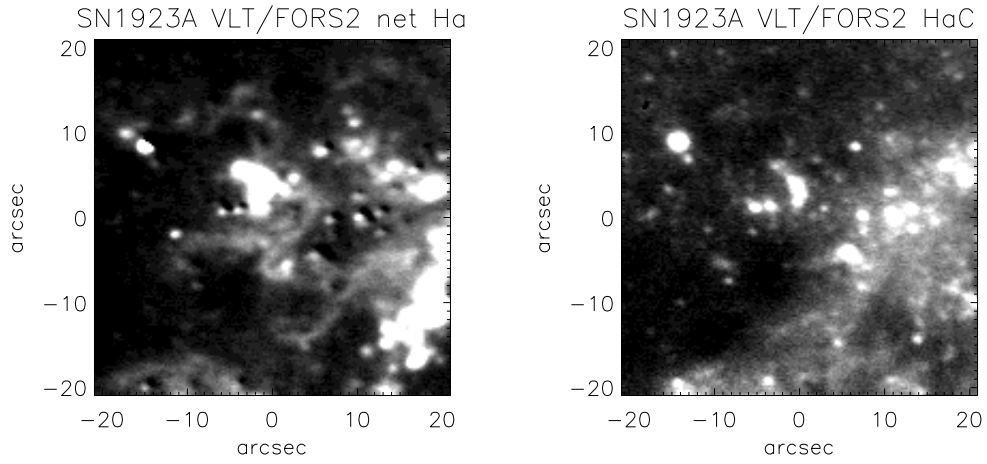


**Figure A1.** (left) VLT/FORS2 net  $H\alpha$  image (from Hadfield et al. 2005) showing the nebular environment of SN 1923A (at centre of image, Class 5). The  $42\times 42$  arcsec<sup>2</sup> field of view projects to  $1\times 1$  kpc<sup>2</sup> at the 4.9 Mpc distance of M 83; (right) Continuum image ( $\lambda_c = 6665\text{\AA}$ ). North is up and east is to the left for these and all subsequent images.

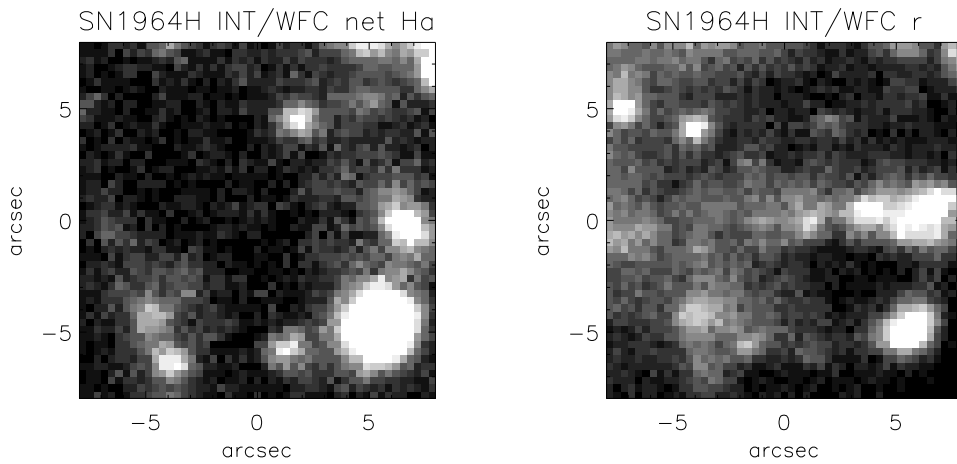


**Figure A2.** (left) INT/WFC net  $H\alpha$  image showing the nebular environment of SN 1964H (at centre of image, Class 2). The  $16\times 16$  arcsec<sup>2</sup> field of view projects to  $1\times 1$  kpc<sup>2</sup> at the 12.9 Mpc distance of NGC 7292; (right) r-band image.

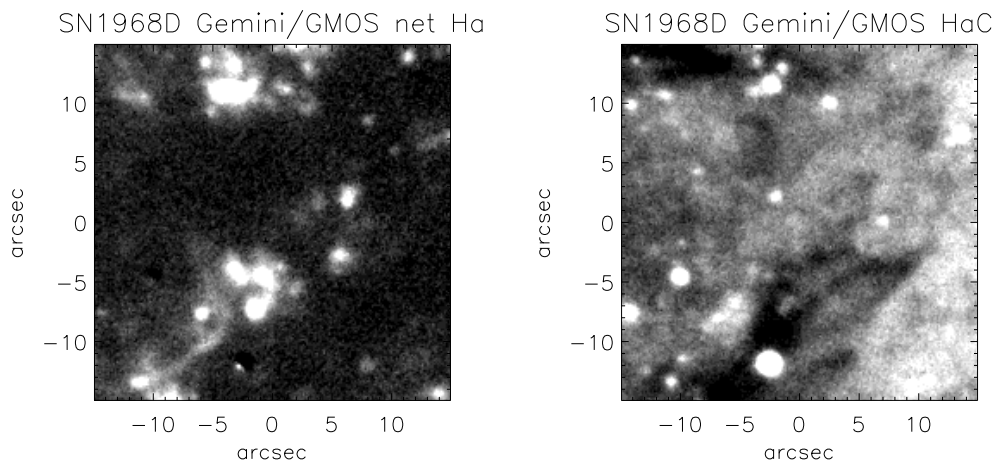


**Figure A3.** (left) Gemini/GMOS net  $H\alpha$  image (from GN-2009B-Q-4) showing the nebular environment of SN 1968D (at centre of image, Class 2). The  $30\times 30$  arcsec<sup>2</sup> field of view projects to  $1\times 1$  kpc<sup>2</sup> at the 7.0 Mpc distance of NGC 6946; (right) Continuum image ( $\lambda_c = 6620\text{\AA}$ ).



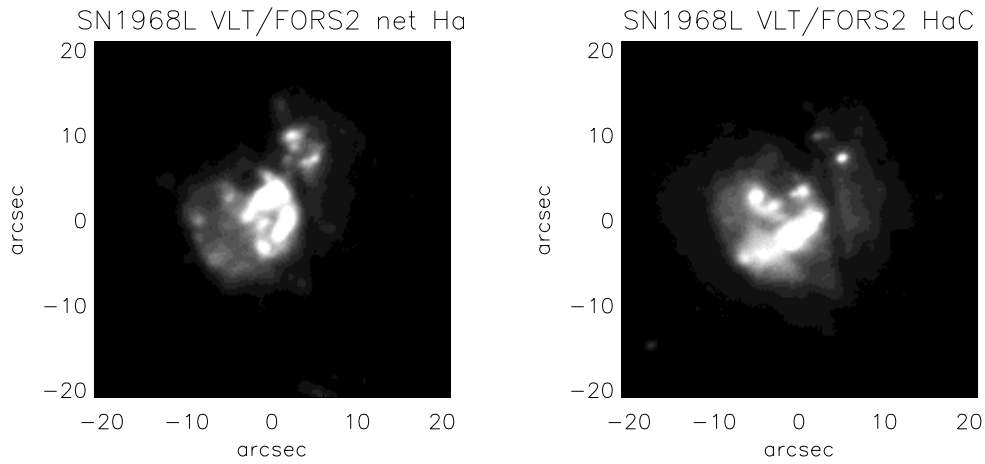


**Figure A4.** (left) VLT/FORS2 net H $\alpha$  image (from Hadfield et al. 2005) showing the nebular environment of SN 1968L (at centre of image, Class 5). 42 $\times$ 42 arcsec<sup>2</sup> field of view projects to 1 $\times$ 1 kpc<sup>2</sup> at the 4.9 Mpc distance of M 83; (right) Continuum image ( $\lambda_c = 6665\text{\AA}$ ).

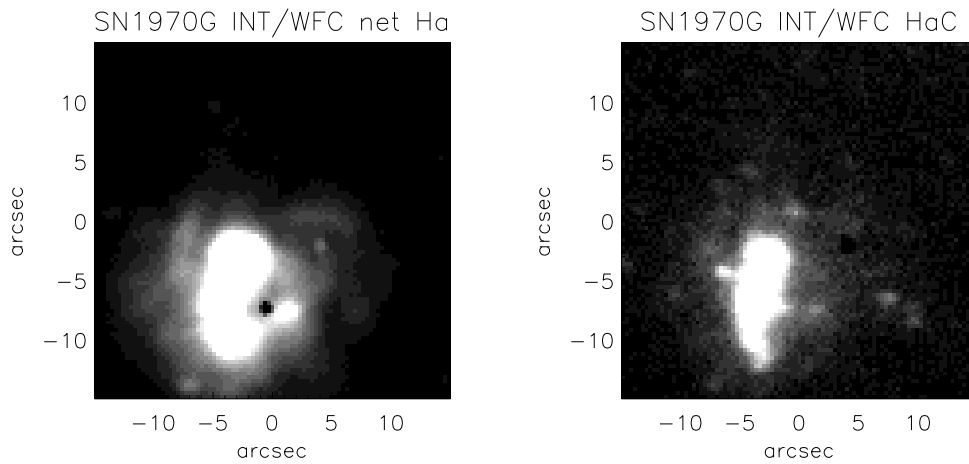


**Figure A5.** (left) INT/WFC net H $\alpha$  image showing the nebular environment of SN 1970G (at centre of image, Class 5). The 30 $\times$ 30 arcsec<sup>2</sup> field of view projects to 1 $\times$ 1 kpc<sup>2</sup> at the 6.96 Mpc distance of M 101; (right) Continuum image ( $\lambda_c = 6657\text{\AA}$ ).

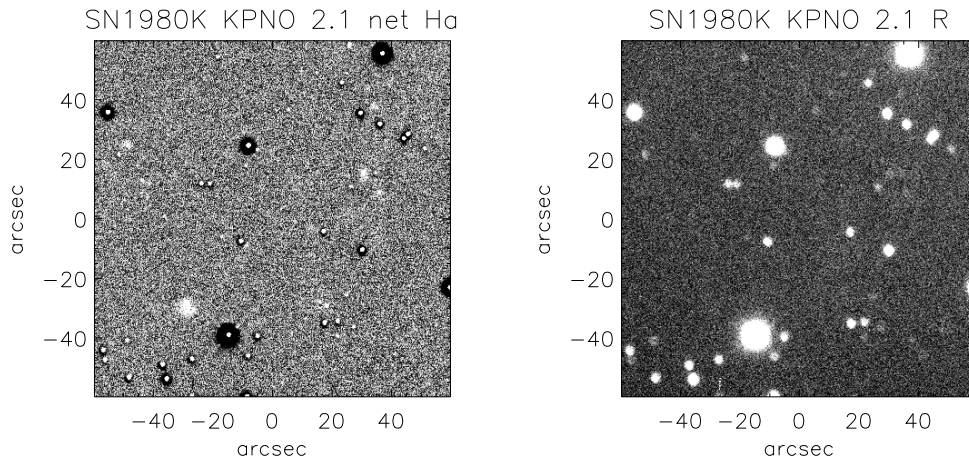


**Figure A6.** (left) KPNO 2.1m net H $\alpha$  image (from Kennicutt et al. 2003) showing the nebular environment of SN 1980K (at centre of image, Class 2). Bright field stars are poorly subtracted. The 120 $\times$ 120 arcsec<sup>2</sup> field of view projects to 4 $\times$ 4 kpc<sup>2</sup> at the 7 Mpc distance of NGC 6946; (right) R-band image.

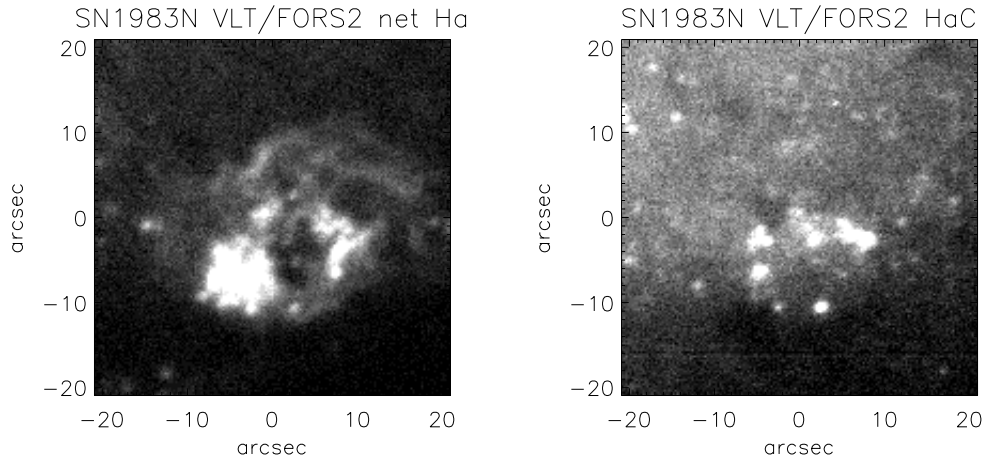


**Figure A7.** (left) VLT/FORS2 net  $H\alpha$  image (from Hadfield et al. 2005) showing the nebular environment of SN 1983N (at centre of image, Class 4). The  $42\times 42$  arcsec<sup>2</sup> field of view projects to  $1\times 1$  kpc<sup>2</sup> at the 4.9 Mpc distance of M 83; (right) Continuum image ( $\lambda_c = 6665\text{\AA}$ ).

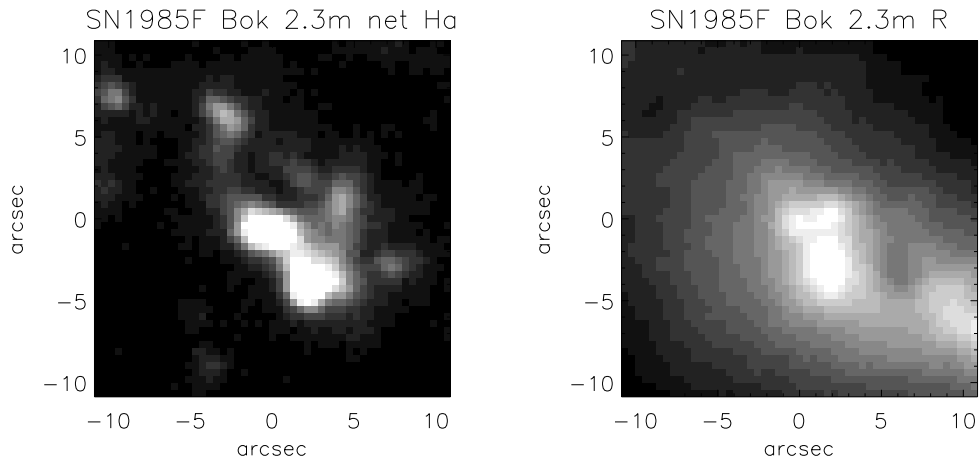


**Figure A8.** (left) Bok 2.3m net  $H\alpha$  image (from Kennicutt et al. 2008) showing the nebular environment of SN 1985F (at centre of image, Class 5). The  $22\times 22$  arcsec<sup>2</sup> field of view projects to  $1\times 1$  kpc<sup>2</sup> at the 9.2 Mpc distance of NGC 4618; (right) R-band image.

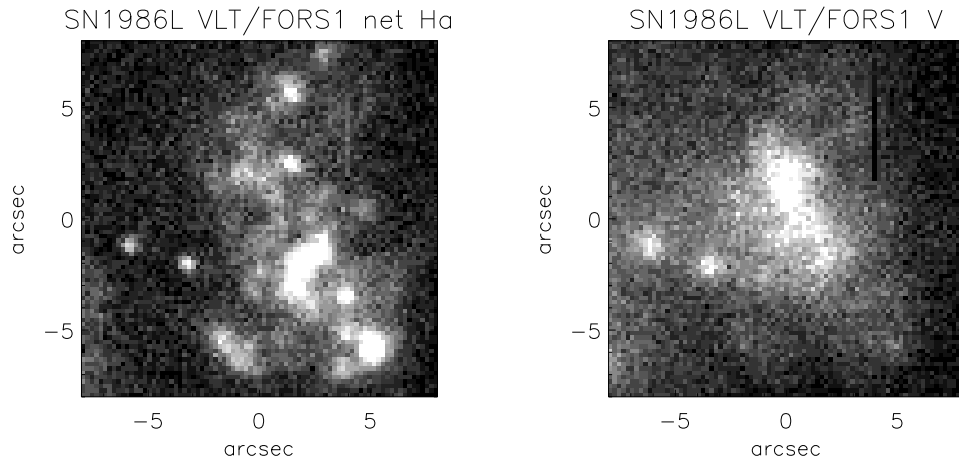


**Figure A9.** (left) VLT/FORS1 net  $H\alpha$  image (from 075.D-0213(A)) showing the nebular environment of SN 1986L (at centre of image, Class 3). The  $16\times 16$  arcsec<sup>2</sup> field of view projects to  $1\times 1$  kpc<sup>2</sup> at the 12.6 Mpc distance of NGC 1559; (right) V-band image.

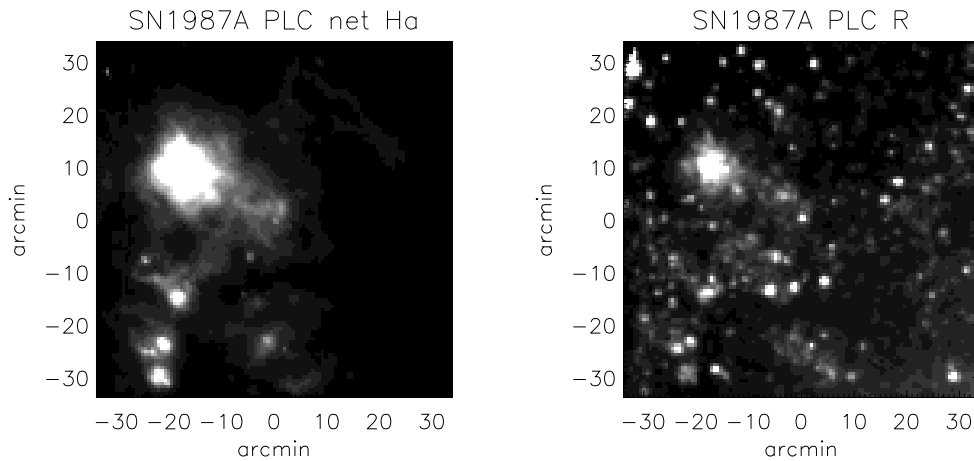


**Figure A10.** (left) Parking Lot Camera net  $H\alpha$  image (from Kennicutt et al. 1995) showing the nebular environment of SN 1987A (at centre of image, Class 4). The  $68\times 68$  arcmin<sup>2</sup> field of view projects to  $1\times 1$  kpc<sup>2</sup> at the 50 kpc distance of the LMC; (right) R-band image (from Bothun & Thompson 1988).

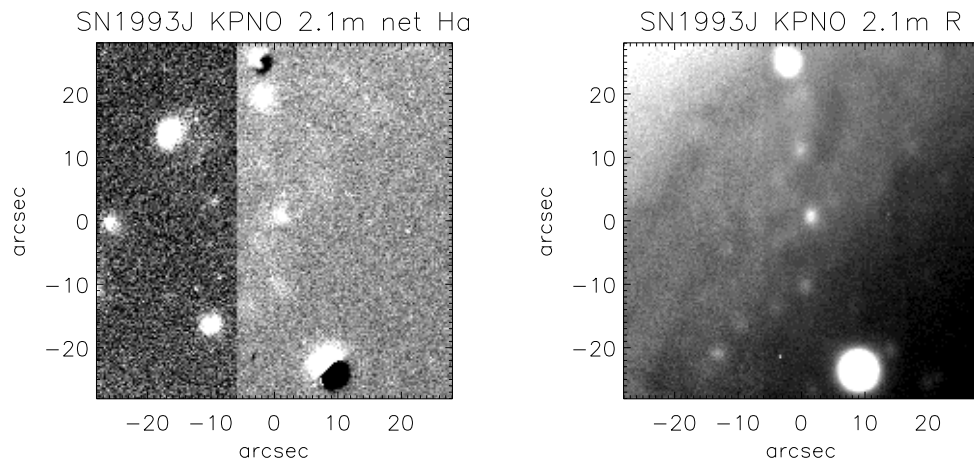


**Figure A11.** (left) KPNO 2.1m net  $H\alpha$  image (from Kennicutt et al. 2003) showing nebular emission close to the position of SN 1993J (at centre of image, Class 2). The  $56\times 56$  arcsec<sup>2</sup> field of view projects to  $1\times 1$  kpc<sup>2</sup> at the 3.6 Mpc distance of M 81. The apparent change in sky background arises from the mosaicing of several pointings of M 81; (right) R-band image.

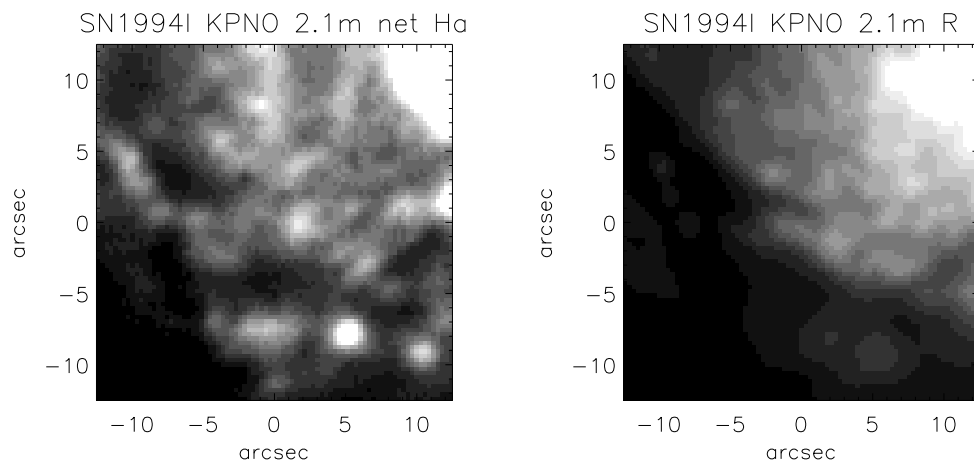


**Figure A12.** (left) KPNO 2.1m net  $H\alpha$  image (from Kennicutt et al. 2003) showing nebular emission close to the position of SN 1994I (at centre of image, Class 5). The  $25\times 25$  arcsec<sup>2</sup> field of view projects to  $1\times 1$  kpc<sup>2</sup> at the 8.4 Mpc distance of M 51a; (right) R-band image.

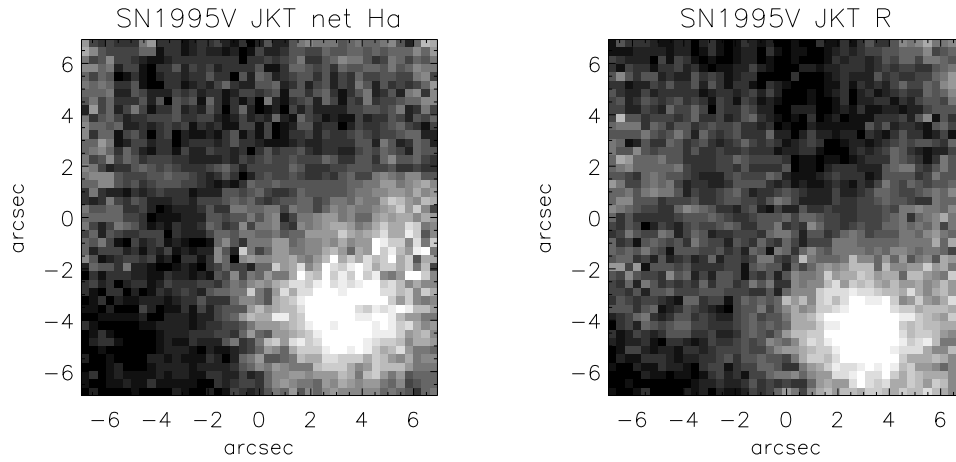


**Figure A13.** (left) JKT net  $H\alpha$  image (from James et al. 2004) showing the nebular environment of SN 1995V (at centre of image, Class 2). The  $14\times 14$  arcsec<sup>2</sup> field of view projects to  $1\times 1$  kpc<sup>2</sup> at the 14.4 Mpc distance of NGC 1087; (right) R-band image.

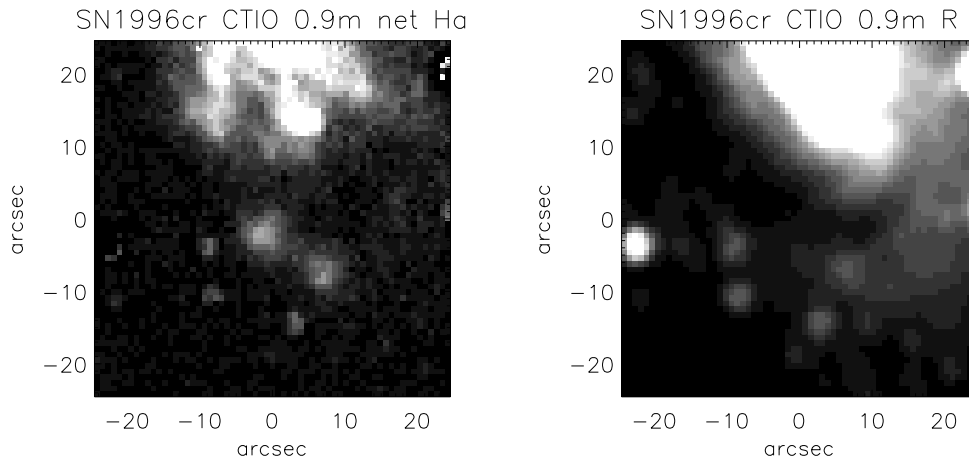


**Figure A14.** (left) CTIO 0.9m net  $H\alpha$  image (from Kennicutt et al. 2008) showing the nebular environment of SN 1996cr (at centre of image, Class 5). The  $50\times 50$  arcsec<sup>2</sup> field of view projects to  $1\times 1$  kpc<sup>2</sup> at the 4.21 Mpc distance of Circinus; (right) R-band image.

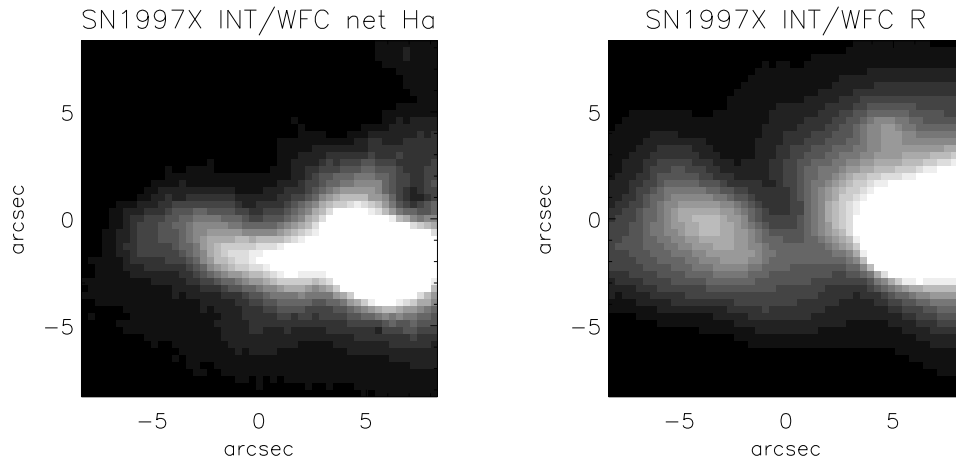


**Figure A15.** (left) INT/WFC net  $H\alpha$  image (from Anderson & James 2008) showing the nebular environment of SN 1997X (at centre of image, Class 3). The  $17\times 17$  arcsec<sup>2</sup> field of view projects to  $1\times 1$  kpc<sup>2</sup> at the 12 Mpc distance of NGC 4691; (right) R-band image.

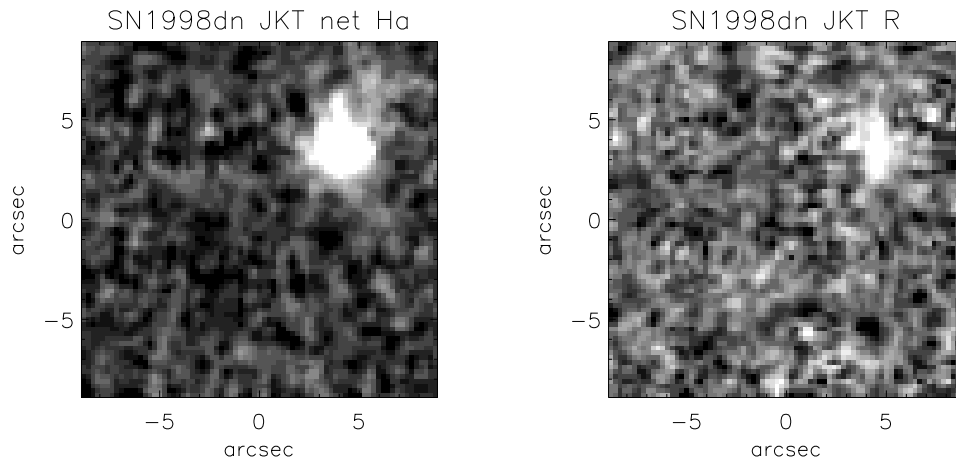


**Figure A16.** (left) JKT net  $H\alpha$  image (from Knapen et al. 2004) showing the nebular environment of SN 1998dn (at centre of image, Class 2). The  $18\times 18$  arcsec<sup>2</sup> field of view projects to  $1\times 1$  kpc<sup>2</sup> at the 12 Mpc distance of NGC 337A; (right) R-band image.

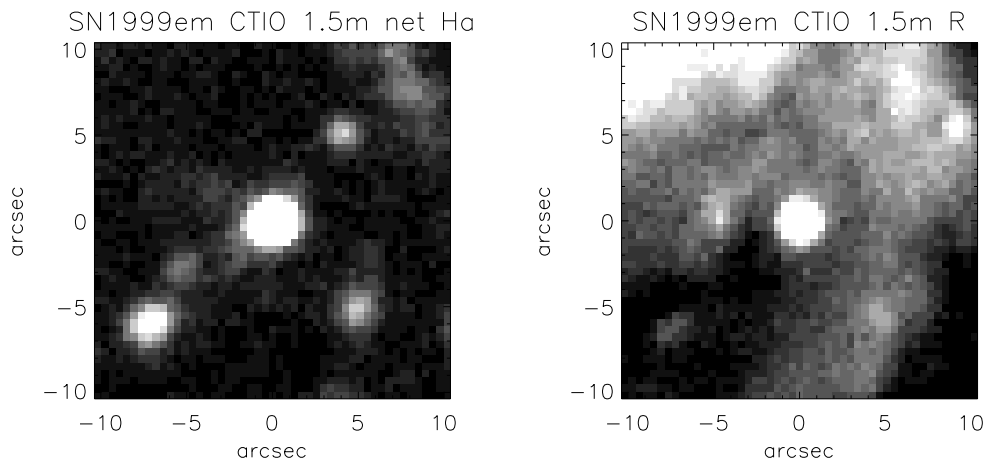


**Figure A17.** (left) CTIO 1.5m net  $H\alpha$  image from 26 Oct 2000 (Meurer et al. 2006) showing the nebular environment of SN 1999em (bright source at centre of image, Class 2). The  $21\times 21$  arcsec<sup>2</sup> field of view projects to  $1\times 1$  kpc<sup>2</sup> at the 9.77 Mpc distance of NGC 1637; (right) R-band image.

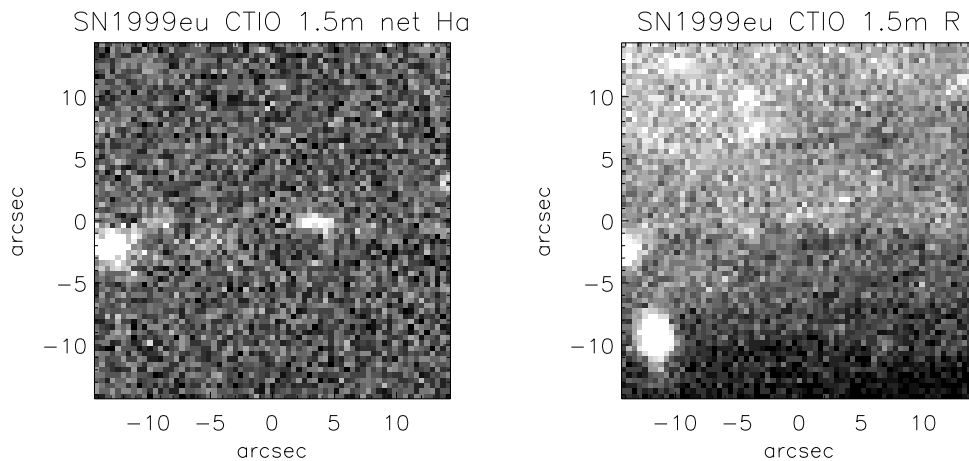


**Figure A18.** (left) CTIO 1.5m net  $H\alpha$  image (Kennicutt et al. 2003) showing the nebular environment of SN 1999eu (at centre of image, Class 2). The  $29\times 29$  arcsec<sup>2</sup> field of view projects to  $2\times 2$  kpc<sup>2</sup> at the 14.2 Mpc distance of NGC 1097; (right) R-band image.

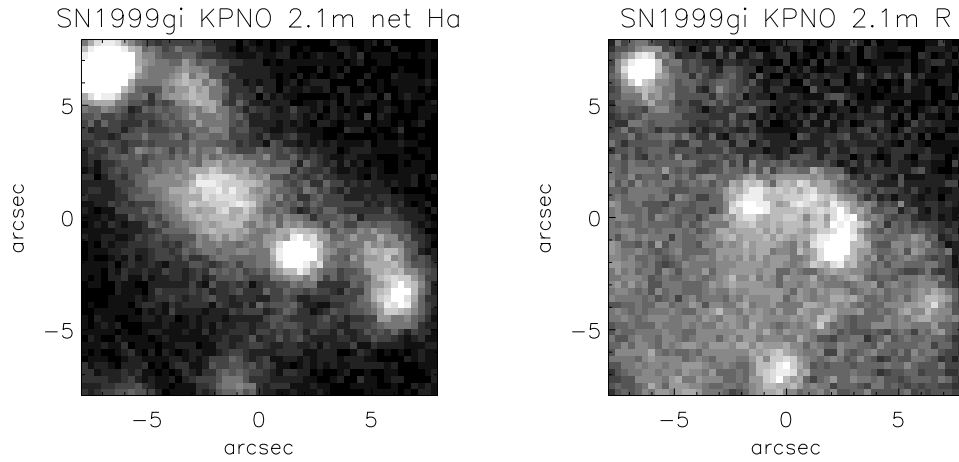


**Figure A19.** (left) KPNO 2.1m net  $H\alpha$  image (Kennicutt et al. 2003) showing the nebular environment of SN 1999gi (at centre of image, Class 5). The  $16\times 16$  arcsec<sup>2</sup> field of view projects to  $1\times 1$  kpc<sup>2</sup> at the 13 Mpc distance of NGC 3184; (right) R-band image.

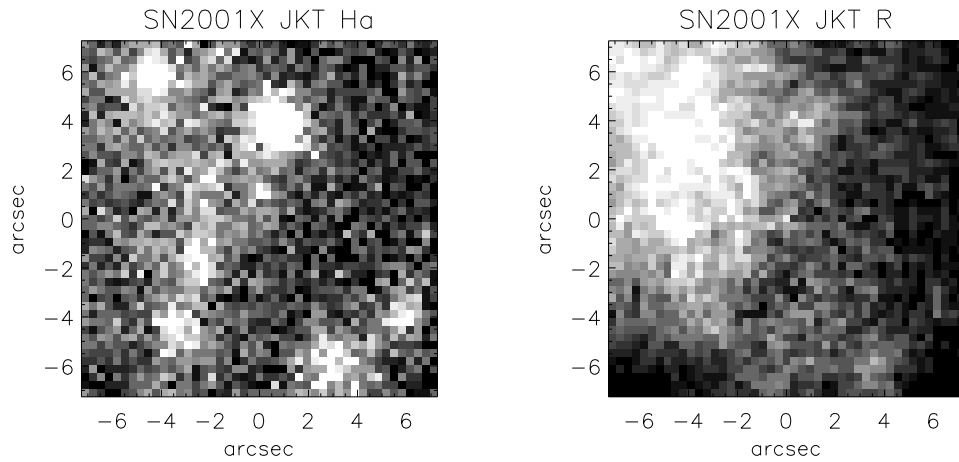


**Figure A20.** (left) JKT  $H\alpha$  image from Mar 1999 showing the nebular environment of SN 2001X (source at centre of image, Class 3). The  $14.7\times 14.7$  arcsec<sup>2</sup> field of view projects to  $1\times 1$  kpc<sup>2</sup> at the 14 Mpc distance of NGC 5921; (right) R-band image from Mar 2003.

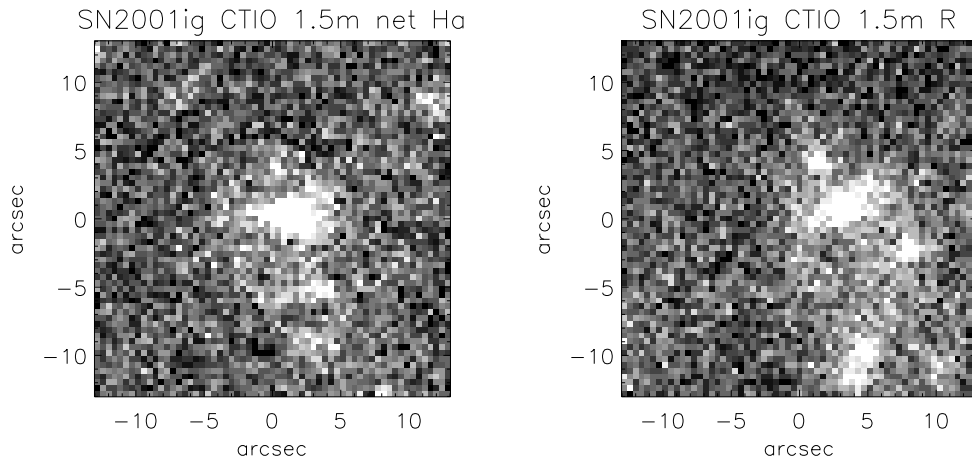


**Figure A21.** (left) CTIO 1.5m  $H\alpha$  imaging (Meurer et al. 2006) showing the nebular environment of SN 2001ig (source at centre of image, Class 4). The  $16\times 16$  arcsec<sup>2</sup> field of view projects to  $1\times 1$  kpc<sup>2</sup> at the 7.94 Mpc distance of NGC 7424; (right) R-band imaging.

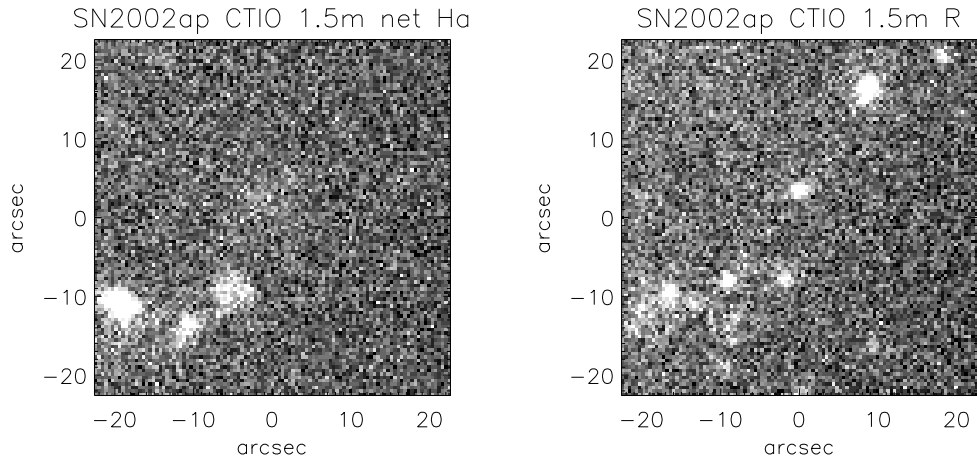


**Figure A22.** (left) CTIO 1.5m  $H\alpha$  imaging (Kennicutt et al. 2003) showing the nebular environment of SN 2002ap (source at centre of image, Class 2). The  $46\times 46$  arcsec<sup>2</sup> field of view projects to  $2\times 2$  kpc<sup>2</sup> at the 9 Mpc distance of M 74; (right) R-band imaging.

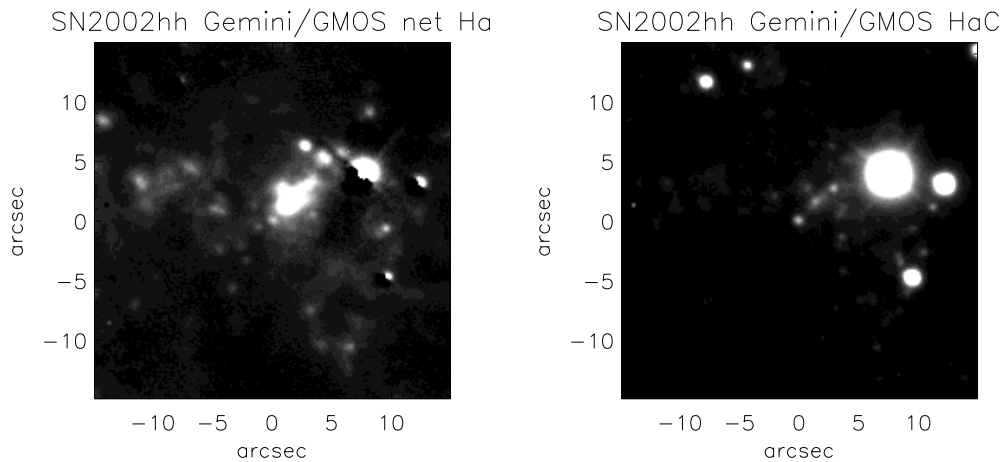


**Figure A23.** (left) Gemini/GMOS net  $H\alpha$  image (from GN-2009B-Q-4) showing nebular emission close to the position of SN 2002hh (at centre of image, Class 5). The  $30\times 30$  arcsec<sup>2</sup> field of view projects to  $1\times 1$  kpc<sup>2</sup> at the 7.0 Mpc distance of NGC 6946; (right) Continuum image ( $\lambda_c = 6620\text{\AA}$ ).

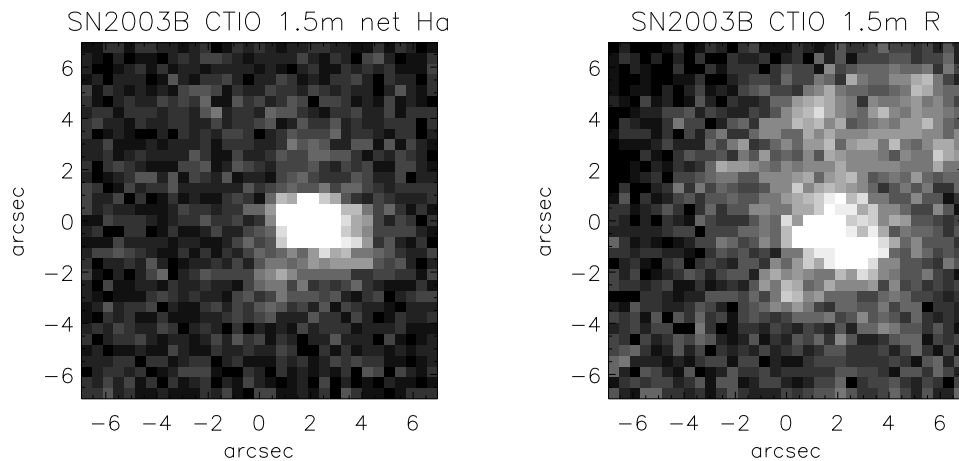


**Figure A24.** (left) CTIO 1.5m net  $H\alpha$  image (Kennicutt et al. 2003) showing the nebular environment of SN 2003B (at centre of image, Class 5). The  $14.5\times 14.5$  arcsec<sup>2</sup> field of view projects to  $1\times 1$  kpc<sup>2</sup> at the 14.2 Mpc distance of NGC 1097; (right) R-band image.

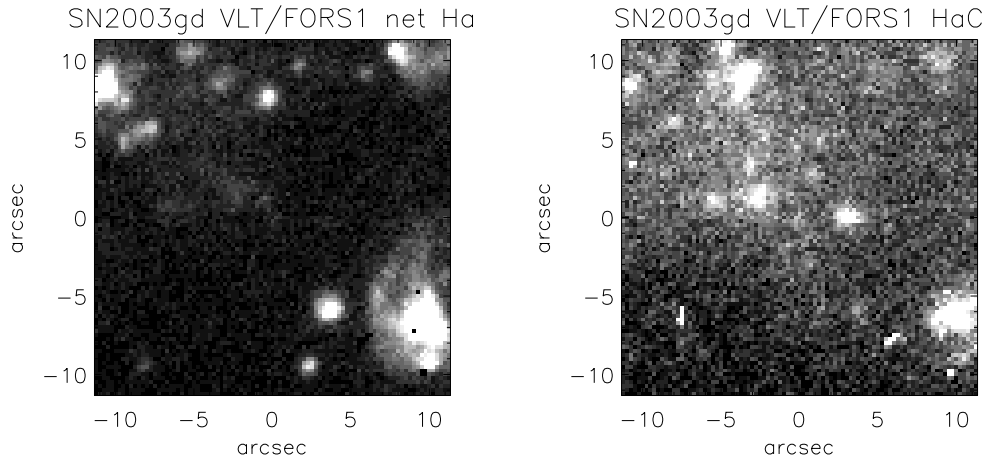


**Figure A25.** (left) VLT/FORS1 net  $H\alpha$  image showing the nebular environment of SN 2003gd (at centre of image, Class 2). The  $23\times 23$  arcsec<sup>2</sup> field of view projects to  $1\times 1$  kpc<sup>2</sup> at the 9.0 Mpc distance of M 74; (right) -band image.

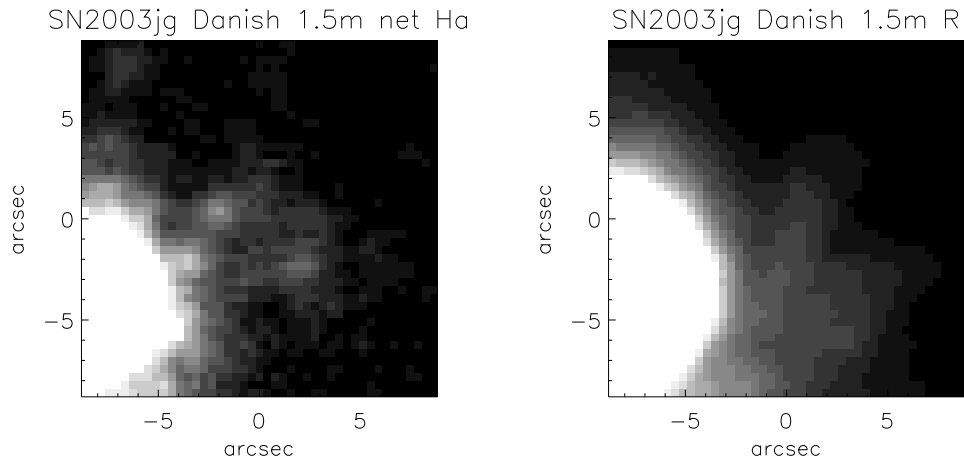


**Figure A26.** (left) Danish 1.5m net  $H\alpha$  image (from Larsen & Richtler 1999) showing the nebular environment of SN 2003jg (at centre of image, Class 2). The  $18\times 18$  arcsec<sup>2</sup> field of view projects to  $1\times 1$  kpc<sup>2</sup> at the 11.7 Mpc distance of NGC 2997; (right) R-band image.

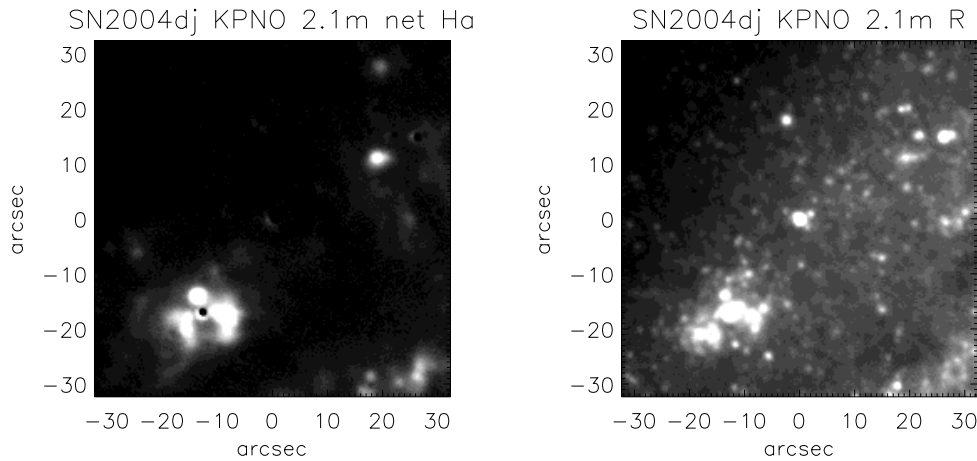


**Figure A27.** (left) 2.1m KPNO  $H\alpha$  image (from Kennicutt et al. 2003) showing the nebular environment of SN 2004dj (at centre of image, Class 1). The  $65\times 65$  arcsec<sup>2</sup> field of view projects to  $1\times 1$  kpc<sup>2</sup> at the 3.16 Mpc distance of NGC 2403; (right) R-band image.



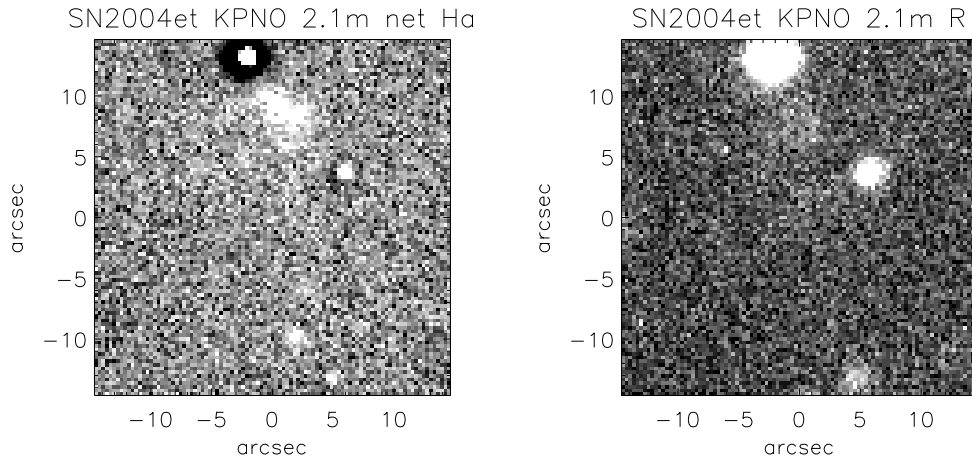


**Figure A28.** (left) 2.1m KPNO H $\alpha$  image (from Kennicutt et al. 2003) showing the nebular environment of SN 2004et (at centre of image, Class 2). The 30 $\times$ 30 arcsec<sup>2</sup> field of view projects to 1 $\times$ 1 kpc<sup>2</sup> at the 7.0 Mpc distance of NGC 6946; (right) R-band image.

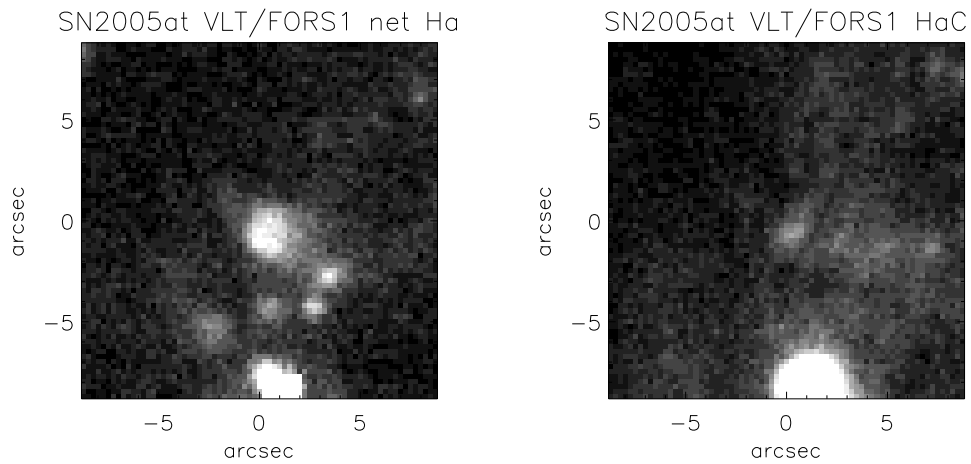


**Figure A29.** (left) VLT/FORS1 H $\alpha$  image (081.B-0289(C), PI P.A. Crowther) showing the nebular environment of SN 2005at (at centre of image, Class 4). The 18 $\times$ 18 arcsec<sup>2</sup> field of view projects to 1 $\times$ 1 kpc<sup>2</sup> at the 11.6 Mpc distance of NGC 6744; (right) Continuum ( $\lambda_c = 6665\text{\AA}$ ) image.

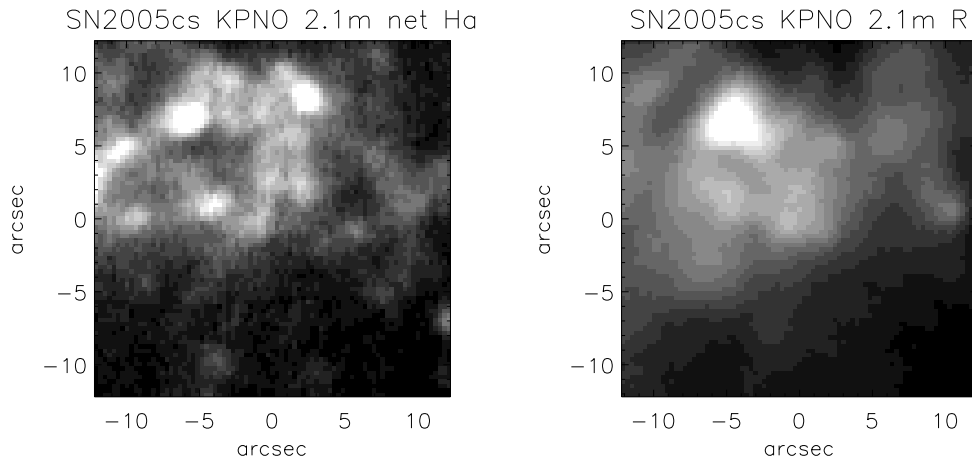


**Figure A30.** (left) KPNO 2.1m net H $\alpha$  image (from Kennicutt et al. 2003) showing the nebular environment of SN 2005cs (at centre of image, Class 4). The 25 $\times$ 25 arcsec<sup>2</sup> field of view projects to 1 $\times$ 1 kpc<sup>2</sup> at the 8.4 Mpc distance of M 51a; (right) R-band image.

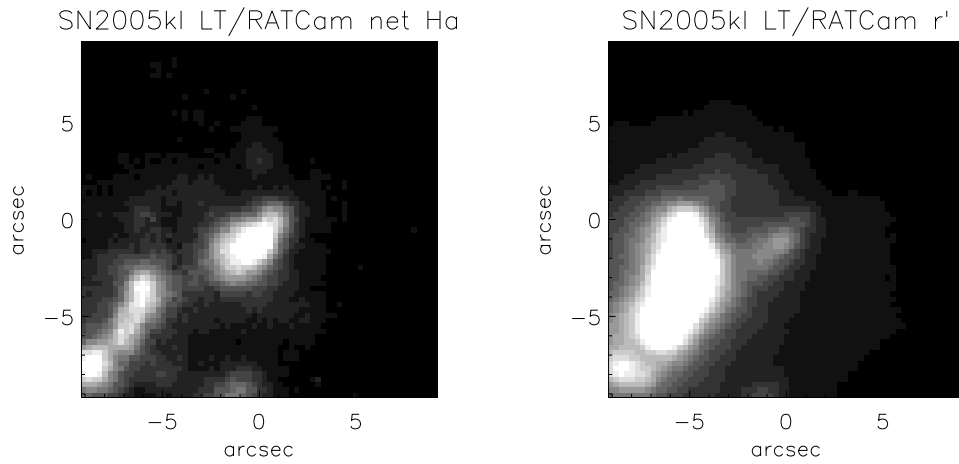


**Figure A31.** left) Liverpool Telescope RATCam net  $H\alpha$  image (from Anderson & James 2008) showing the nebular environment of SN 2005kl (at centre of image, Class 5). The  $18\times 18$  arcsec<sup>2</sup> field of view projects to  $1\times 1$  kpc<sup>2</sup> at the 11.2 Mpc distance of NGC 4369; (right) Sloan  $r'$ -band image.

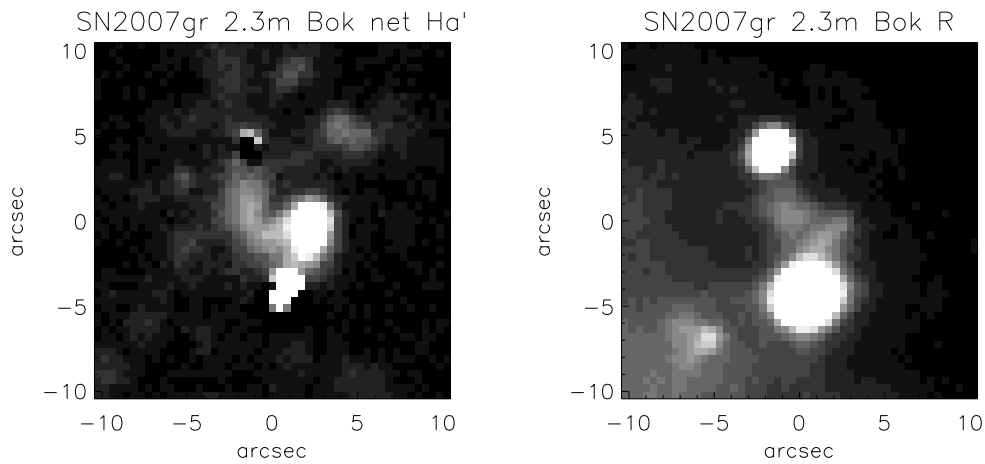


**Figure A32.** left) Bok 2.3m net  $H\alpha$  image (from Kennicutt et al. 2008) showing the nebular environment of SN 2007gr (at centre of image, Class 5). The  $21\times 21$  arcsec<sup>2</sup> field of view projects to  $1\times 1$  kpc<sup>2</sup> at the 9.86 Mpc distance of NGC 1058; (right) R-band image.

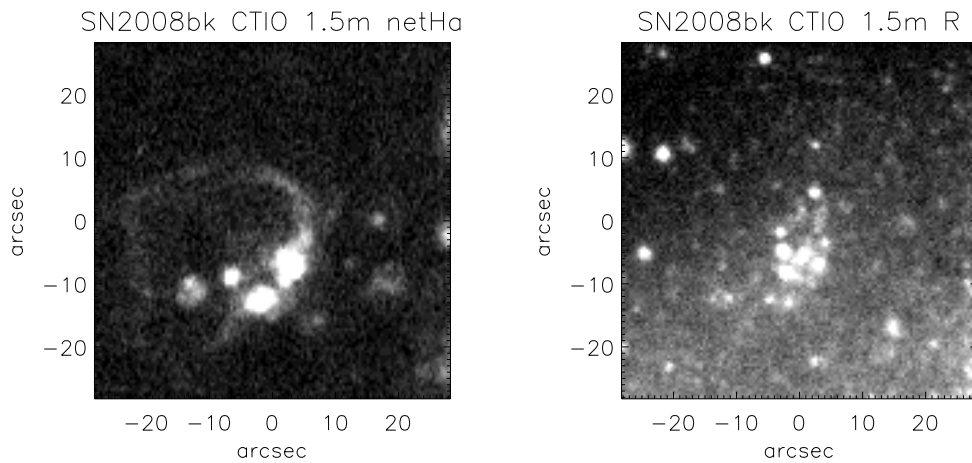


**Figure A33.** left) CTIO 1.5m net  $H\alpha$  image (from Kennicutt et al. 2003) showing the nebular environment of SN 2008bk (at centre of image, Class 2). The  $57\times 57$  arcsec<sup>2</sup> field of view projects to  $1\times 1$  kpc<sup>2</sup> at the 3.61 Mpc distance of NGC 7793; (right) R-band image.

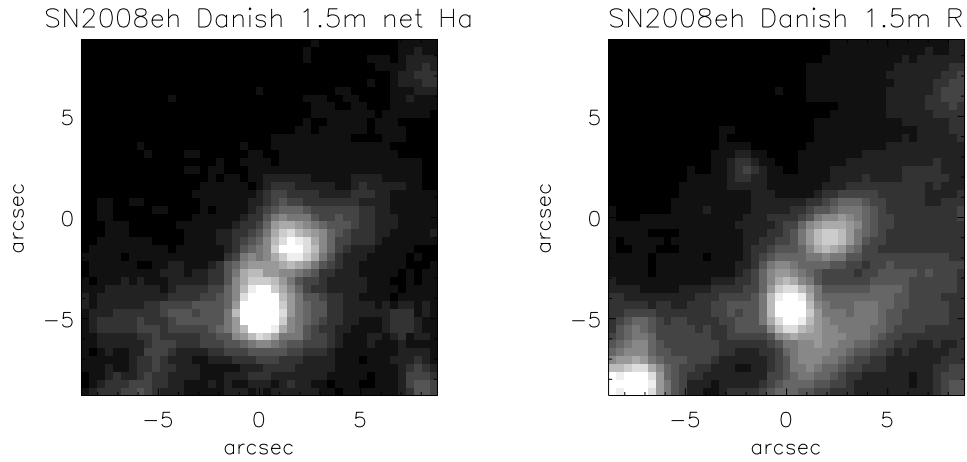


**Figure A34.** (left) Danish 1.5m net  $H\alpha$  image (from Larsen & Richtler 1999) showing the nebular environment of SN 2008eh (at centre of image, Class 5). The  $18\times 18$  arcsec<sup>2</sup> field of view projects to  $1\times 1$  kpc<sup>2</sup> at the 11.7 Mpc distance of NGC 2997; (right) R-band image.

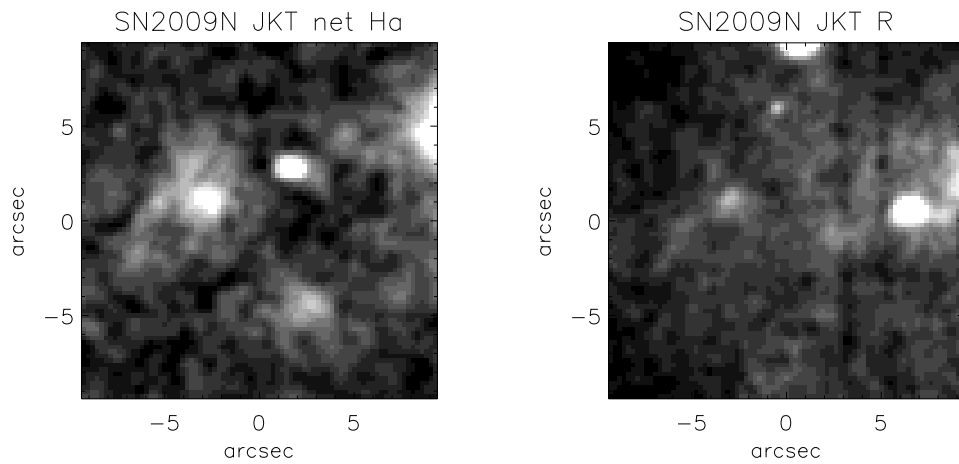


**Figure A35.** (left) JKT net  $H\alpha$  image (from Knapen et al. 2004) showing the nebular environment of SN 2009N (at centre of image, Class 2). The  $19\times 19$  arcsec<sup>2</sup> field of view projects to  $1\times 1$  kpc<sup>2</sup> at the 11.0 Mpc distance of NGC 4487; (right) R-band image.

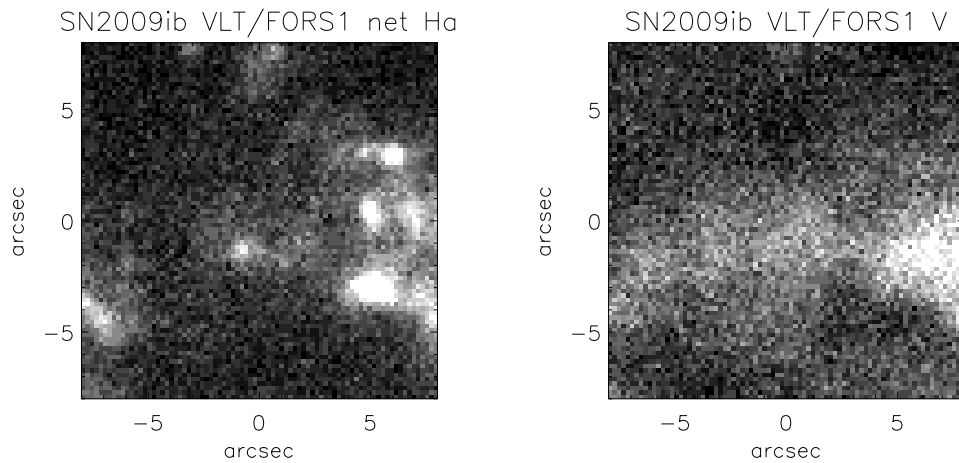


**Figure A36.** (left) VLT/FORS1 net  $H\alpha$  image (from 075.D-0213(A)) showing the nebular environment of SN 2009ib (at centre of image, Class 2). The  $16\times 16$  arcsec<sup>2</sup> field of view projects to  $1\times 1$  kpc<sup>2</sup> at the 12.6 Mpc distance of NGC 1559; (right) V-band image.

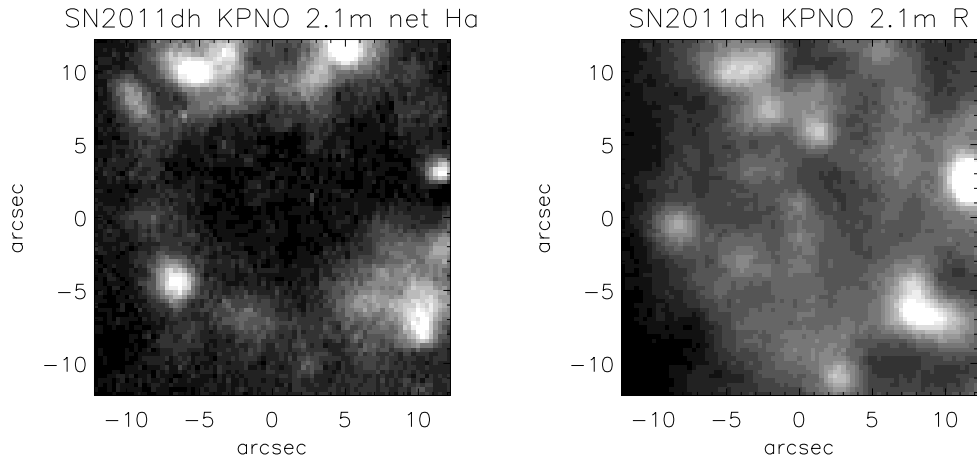


**Figure A37.** (left) KPNO 2.1m net  $H\alpha$  image (from Kennicutt et al. 2003) showing the nebular environment of SN 2011dh (at centre of image, Class 2). The  $25\times 25$  arcsec<sup>2</sup> field of view projects to  $1\times 1$  kpc<sup>2</sup> at the 8.39 Mpc distance of M 51a; (right) R-band image.

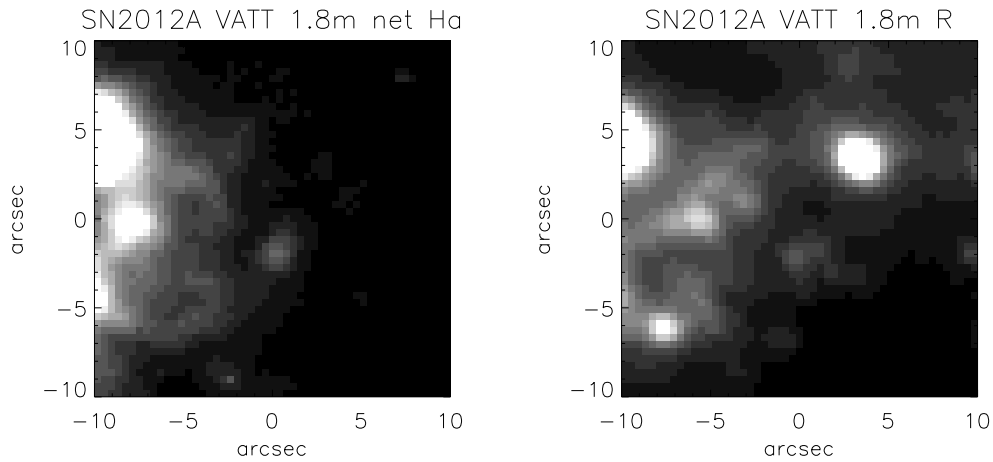


**Figure A38.** (left) VATT 1.8m net  $H\alpha$  image (from Kennicutt et al. 2008) showing the nebular environment of SN 2012A (at centre of image, Class 4). The  $20\times 20$  arcsec<sup>2</sup> field of view projects to  $1\times 1$  kpc<sup>2</sup> at the 10.0 Mpc distance of NGC 3239; (right) R-band image.

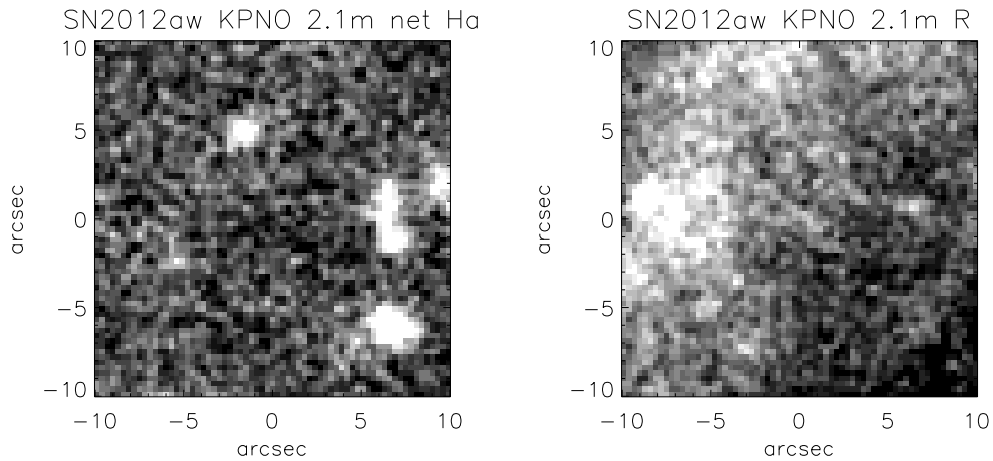


**Figure A39.** (left) KPNO 2.1m net  $H\alpha$  image (from Kennicutt et al. 2003) showing the nebular environment of SN 2012aw (at centre of image, Class 2). The  $20\times 20$  arcsec<sup>2</sup> field of view projects to  $1\times 1$  kpc<sup>2</sup> at the 10.0 Mpc distance of M 95; (right) R-band image.

## APPENDIX B: CORE-COLLAPSE SNE LOCATED AT DISTANCES OF 15–20 MPC

Basic properties of ccSNe host galaxies located at distances of 15–20 Mpc (from Tully et al. 2009). Separate Tables are presented for low inclination ( $\leq 65^\circ$ ) hosts for which accurate ccSNe positions are known (Table B1) and high inclination hosts and ccSNe whose coordinates are imprecisely known (Table B2, online-only).

## REFERENCES

- Allen, R.J., Goss, W.M., Ekers, R.D., de Bruyn, A.G. 1976, *A&A* 48, 253  
 Anderson, J.P., James, P.A. 2008, *MNRAS*, 390, 1527  
 Anderson, J.P., Haberman, S.M., James, P.A., Hamuy, M., 2012, *MNRAS* 424, 1372  
 Balam, D. 1995, *IAU Circ* 6203  
 Bauer, F. 2007, *CBET*, 879  
 Belley, J., Roy, J.-R., 1992, *ApJS* 78, 61  
 Cao, L. 1998, *IAU Circ*. 6994  
 Carignan, C., Puche, D. 1990, *AJ* 100, 394  
 Chandar, R., Whitmore, B.C., Calzetti, D., Di Nino, D., Kennicutt, R.C., Regan, M., Schinnerer, E. 2011, *ApJ* 727, 88  
 Clocchiatti, A., Wheeler, J.C., Benetti, S., Frueh, M. 1996, *ApJ* 459, 547  
 Cowan, J.J., Goss, W.M., Sramek, R.A. 1991, *ApJ* 379, L49  
 Crockett, R.M. et al. 2007, *MNRAS* 381, 835  
 Crockett, R.M. et al. 2008, *ApJ* 672, L99  
 Crockett, R.M., Smartt, S.J., Pastorello, A., Eldridge, J.J., Stephens, A.W., Maund, J.R., Mattila, S. 2011, *MNRAS* 410, 2767  
 Evans, R.O., McNaught, H. 2003, *IAU Circ* 8150, 2  
 Evans, R.O., Phillips, M.M. 1992, *IAU Circ* 5625, 2  
 Evans, R.O., Quirk, S. 2003, *IAU Circ* 8042, 1  
 Evans, R.O., McNaught, R., Cragg, T., Thompson, G. 1986, *IAU Circ* 4260  
 Evans, R.O., Jarman, J., Cragg, T. et al. 1995, *IAU Circ* 6197  
 Evans, R.O., White, B., Bembrick, C. 2002, *IAU Circ* 7772  
 Filippenko, A.V., Sargent, W.L.W. 1985, *IAU Circ* 4042  
 Filippenko, A.V., Sargent, W.L.W. 1986, *AJ* 91, 691  
 Griga, T. et al. 2011, *CBET* 2736, 1  
 Hadfield, L.J., Crowther, P.A., Schild, H., Schmutz, W. 2005, *A&A* 439, 265  
 Harris, J., Calzetti, D., Gallagher, J.S., Conselice, C.J., Smith, D.A. 2001, *AJ* 122, 3046  
 Hendry, M.A. et al., 2005 *MNRAS* 359, 906  
 Hendry, M.A., 2006, PhD thesis, University of Cambridge  
 Hodge, P.W., 1976, *ApJ* 205, 728  
 Hodge, P.W., Gurwell, M., Goldader, J.D., Kennicutt, R.C. Jr, 1990, *ApJS* 73, 661  
 Hoopes, C.G., Walterbos, R.A.M., Bothun, G.D. 2001, *ApJ*, 559, 878  
 Horiuchi, S., Beacom, J.F., Kochanek, C.S., Prieto, J.L., Stanek, K.Z., Thompson, T.A. 2011, *ApJ* 738, 154  
 James, P.A. et al. 2004, *A&A*, 414, 23  
 Jha, S., Challis, P., Garnavich, P., Kirshner, R., Calkins, M., Stanek, K. 1999, *IAU Circ* 7296  
 Kamphuis, J., Briggs, F. 1992, *A&A* 253, 335  
 Kennicutt, R.C. Bresolin, F., Bomans, D.J., Bothun, G.D., Thompson, I., B. 1995, *AJ*, 109, 594  
 Kennicutt, R.C. et al. 2003, *PASP*, 115, 928  
 Kennicutt R.C., Lee, J.C., Funes, S.J., José, G., Sakai, S., Akiyama, S. 2008, *ApJS* 178, 247  
 Kirshner R., Silverman, J. 2003, *IAU Circ* 8042 2  
 Kloehr, W., Muendlein, R., Li, W., Yamaoka, H., Itagaki, K. 2005, *IAU Circ* 8553, 1  
 Knapen, J.H. et al. 2004 *A&A* 426, 1135  
 Larsen, S.S., Richtler T. 1999, *A&A*, 345, 59  
 Leonard, D.C. et al. 2002, *AJ* 124, 2490  
 Li, W.D. 1999, *IAU Circ* 7294  
 Li, W.D. 2002, *IAU Circ* 8005  
 Li, W., Fan, Y., Qiu, Y.L., Hu, J.Y. 2001, *IAU Circ* 7591  
 Li, W., van Dyk, S.D., Filippenko, A.V., Cuillandre, J.-C., Jha, S., Bloom, J.S., Riess, A.G., Livio, M. 2006, *ApJ* 641, 1060  
 Li, W.D., Chen, T.-W., Klotz, A., Itagaki, K., Monard, L.A.G., Sehga, A., Newton, J., Orff, T. 2007, *IAU Circ* 8864, 1  
 Maíz-Apellániz, J., Bond, H.E., Siegel, M.H. 2004, *ApJ* 615, L113  
 Marconi, A., Moorwood, A.F.M., Origlia, L., Oliva, E. 1994, *ESO Messenger*, 78, 20  
 Martin, R., Biggs, J. 2003, *IAU Circ* 8235, 1  
 Martin, R., Yamaoka, H., Monard, L.A.G. 2005, *IAU Circ* 8496, 1  
 Mattila, S., Smartt, S.J., Eldridge, J.J., Maund, J.R., Crockett, R.M., Danziger, I.J. 2008, *ApJ* 688, L91  
 Maund, J.R., Smartt, S.J. 2009, *Sci*, 324, 486  
 Maund, J.R., Smartt, S.J., Kudritzki, R.-P., Podsiadlowski, P. 2004, *Nat* 427, 129  
 Maund, J.R. et al. 2011, *ApJ* 739, L37  
 McNaught, R.H., Waldron, D. 1986, *IAU Circ* 4261  
 Meurer, G.R. et al. 2006, *ApJS* 165, 307  
 Migliardi, M., Dimai, A., Burket, J., Li, W., Frieman, J. 2005, *IAU Circ* 8634, 2  
 Monard, L.A.G. 2008a, *CBET* 1315, 1  
 Monard, L.A.G. 2008b, *CBET* 1445,  
 Moore, B., Newton, J., Puckett, T., 2012 *CBET* 2974, 1  
 Mueller, J., Griffith, D., Gizis, J., Filippenko, A.V., Leonard, D.C. 1995, *IAUC* 6211  
 Munari, U., Barbon, R., Piemonte, A., Tomasella, L., Rejkuba, M. 1998, *A&A* 333, 159  
 Nakano, S. et al. 1997, *IAU Circ* 6552, 1  
 Nakano, S., Aoki, M. 1999a, *IAU Circ* 7304, 1  
 Nakano, S., Kushida, R., 1999b, *IAU Circ* 7329, 1  
 Nakano, S., Hirose, Y., Kushida, R., Li, W., 2002, *IAU Circ* 7810  
 Nakano, S., Itagaki, K., Bouma, R.J., Lehky, M., Hornoch, K. 2004, *IAU Circ* 8377, 1  
 Nakano, S., Kadota, K., Buzzzi, L. 2009, *CBET* 1670, 1  
 Otsuka, M. et al. 2012, *ApJ* 744, 26  
 Panagia, N., Romaniello, M., Scuderi, S., Kirschner, R.P. 2000, *ApJ* 539, 197  
 Pennington, R.L., Talbot, R.J.Jr, Dufour, R.J. 1982, *AJ* 87, 1538  
 Pignata, G. et al. 2009, *CBET* 1902  
 Porter, A.C. 1993, *PASP* 105, 1250  
 Puckett, T. et al. 1994, *IAU Circ* 5961, 1  
 Ripero, J. et al. 1993, *IAU Circ* 5731, 1  
 Rumstay, K.S., Kaufman, M., 1983, *ApJ*, 274, 611  
 Rupen, M.P., Sramek, R.A., van Dyk, S.D., Weiler, K.W., Panagia, N., Richmond, M.W., Filippenko, A.V., Treffers, R.R. 1994, *IAU Circ* 5963, 1  
 Ryder, S.D., Dopita, M.A. 1993, *ApJS* 88, 415  
 Ryder, S.D., Murrowood, C.E., Stathakis, R.A. 2006, *MNRAS* 369, L32  
 Sandage, A. 1984, *AJ* 89, 630  
 Schmidt, B.P., Kirschner, R.P., Eastman, R.G., Phillips, M.M., Suntzeff, N.B., Hamuy, M., Maza, J., Aviles, R. 1994, *ApJ* 432, 42  
 Sicoli, P., Cavagna, M., Manca, F. 1995, *IAUC* 6212  
 Smartt, S.J., Gilmore, G.F., Trentham, N., Tout, C.A., Frayn, C.M., 2001, *ApJ* 556, L29  
 Smartt, S.J., Gilmore, G.F., Tout, C.A., Hodgkin, S.T., 2002, *ApJ* 565, 1089  
 Smartt, S.J., Maund, J.R., Hendry, M.A., Hendry, M.A., Tout, C.A., Gilmore, G.F., Mattila, S., Benn, C.R., 2004, *ApJ* 499, 503  
 Smartt, S.J., Eldridge, J.J., Crockett, R.M., Maund, J.R., 2009, *MNRAS*, 395, 1409  
 Smith, M.C., Leiton, R., Pizarro, S. 2000 in: D. Allion, K. Olsen & G. Galaz (eds.), *Stars, Gas and Dust in Galaxies: Exploring the Links* (San Francisco: ASP), ASP Conf. Ser 221, p. 83  
 Solanes, J.M., Sanchis, T., Salvador-Solé, E., Giovanelli, R., Haynes, M.P. 2002, *AJ* 124, 2440  
 Sramek, R.A., Panagia, N., Weiler, K.W. 1984, *ApJ* 285, L59  
 Sugerman, B. et al. 2012, *ApJ* 749, 170  
 Tully, R.B., Rizzi, L., Shaya, E.J., Courtois, H.M., Makarov, D.I., Jacobs, B.A. 2009, *AJ* 138, 323  
 van Dyk, S., Hyman, S.D., Sramek, R.A., Weiler, K.W. 1994, *IAU Circ* 6045  
 van Dyk, S., Hamuy, M., Filippenko, A.V. 1996, *AJ* 111, 2017

**Table B1.** Basic properties of host galaxies of ccSNe, drawn from RC3 or HyperLeda, for which EDD distances lie in the range 15–20 Mpc, restricted to low inclination ( $\leq 65^\circ$ ) hosts for which accurate ccSNe positions are known. SN imposter hosts are also omitted (e.g. SN 2003gm in NGC 5334, Smartt et al. 2009)

PGC	M	NGC	UGC	Type	$cz$ (km s $^{-1}$ )	$i$	$d$ (Mpc)	Ref	ccSNe
02081		157		SAB(rs)bc	1652	61.8	20.0	1	2009em
03572		337		SB(s)d	1648	50.6	19.5 $\pm$ 1.6	1	2011dq
06826		701		SB(rs)c	1831	62.4	19.3 $\pm$ 3.8	1	2004fc
09236		918	01888	SAB(rs)c?	1507	57.6	16.1 $\pm$ 3.2	1	2009js
09846		991		SAB(rc)s	1532	28.1	17.3 $\pm$ 1.1	1	1984L
10464		1084		SA(s)c	1407	49.9	17.3 $\pm$ 1.1	1	1996an, 1998dl, 2009H
11479		1187		SB(r)c	1390	44.3	18.9 $\pm$ 2.6	1	1982R, 2007Y
13179		1365		SB(s)b	1636	62.7	18.0 $\pm$ 1.8	1	1983V, 2001du
14617		– ESO G420-G009 –		SB(s)c	1367	41.7	17.7 $\pm$ 1.2	2	2003bg
14620		1536		SB(s)c pec?	1217	44.8	18.0 $\pm$ 1.0	1	1997D
15850		1640		SB(r)b	1604	17.2	16.8 $\pm$ 3.5	1	1990aj
29469			05460	SB(rs)d	1093	39.7	20.0	1	2011ht
31650		3310	05786	SAB(r)bc pec	993	16.1	20.0	1	1991N
32529		3423	05962	SA(s)cd	1011	32.1	17.0 $\pm$ 2.5	1	2009ls
34767		3631	06360	SA(s)c	1156	34.7	18.0	1	1964A, 1965L, 1996bu
36243		3810	06644	SA(rs)c	992	48.2	16.3 $\pm$ 1.7	1	1997dq, 2000ew
37229		3938	06856	SA(s)c	809	14.1	17.1 $\pm$ 0.8	1	1961U, 1964L, 2005ay
37290		3949	06869	SA(s)bc?	800	56.5	17.1 $\pm$ 0.8	1	2000db
37306		3953	06870	SB(r)bc	1052	62.1	17.1 $\pm$ 0.8	1	2006bp
37735			06983	SB(rs)cd	1082	37.4	17.1 $\pm$ 0.8	1	1994P
37845		4030	06993	SA(s)bc	1465	47.1	19.5 $\pm$ 1.5	1	2007aa
38068		4051	07030	SAB(rs)bc	700	30.2	17.1 $\pm$ 0.8	1	1983I, 2003ie, 2010br
39578	99	4254	07345	SA(s)c	2407	20.1	1.8 $\pm$ 0.8	1	1967H, 1972Q, 1986I
40001	61	4303	07420	SAB(rs)bc	1566	18.1	17.6 $\pm$ 0.9	1	1926A, 1961I, 1964F, 1999gn, 2006ov, 2008in
40153	100	4321	07450	SAB(s)bc	1571	23.4	15.2 $\pm$ 1.5	1	1979C
40745		4411B	07546	SAB(s)cd	1272	26.6	16.8 $\pm$ 0.8	1	1992ad
41050		4451	07600	Sbc?	864	53.6	16.8 $\pm$ 0.8	1	1985G
41746		4523	07713	SAB(s)m	262	25.1	16.8 $\pm$ 0.8	1	1999gq
42833		4651	07901	SA(rs)c	788	49.5	16.8 $\pm$ 0.8	1	1987K, 2006my
43321		4699		SAB(rs)b	1394	42.6	15.3 $\pm$ 1.0	1	1983K
43972		4790		SB(rs)c?	1344	58.8	15.3 $\pm$ 1.0	1	2012au
44797		4900	08116	SB(rs)c	960	19.0	15.6 $\pm$ 1.0	1	1999br
45948		5033	08307	SA(s)c	875	64.6	18.5 $\pm$ 1.1	1	1985L, 2001gd
52935		– Arp 261 –		IB(s)m pec	1856	58.8	20	1	1995N
58827		6207	10521	SA(s)c	852	64.7	18.1 $\pm$ 2.1	1	2004A
59175		6221		SB(s)c	1499	50.9	15.6 $\pm$ 1.7	1	1990W
70094		– IC 5267 –		SA0/a(s)	1712	48.4	18.7 $\pm$ 1.6	1	2011hs

1: Tully et al. (2009), 2: NED (Virgo + GA + Shapley)

van Dyk, S.D. et al. 2011, *ApJ* 741, L28van Dyk, S.D. et al. 2012, *AJ* 143, 19Vinkó, J. et al. 2006, *MNRAS* 369, 1780Vinkó, J. et al. 2009, *ApJ* 695, 619Wamsteker, W. 1993, *IAU Circ* 3838, 1Weiler, K.W., van Dyk, S.D., Panagia, N., Sramek, R.A. 1992, *ApJ* 398, 248Wilson, A.S., Shopbell, P.L., Simpson, C., Storchi-Bergmann, T., Barbosa, F.K.B., Ward, M.J. 2000, *AJ* 120, 1325Yoon, S.-C., Gräfenor, G., Vink, J.S., Kozyreva, A., Izzard, R.G. 2012, *A&A*, 544, L11

**Table B2.** Basic properties of host galaxies of ccSNe, drawn from RC3 or HyperLeda, for which EDD distances lie in the range 15–20 Mpc, restricted to high inclination ( $\geq 65^\circ$ ) hosts and ccSNe whose coordinates are imprecisely known (in italics). SN imposters are omitted.

PGC	M	NGC	UGC	Type	$cz$ (km s $^{-1}$ )	$i$	d (Mpc)	Ref	ccSNe
09057		908		SA(s)c	1509	<b>65.1</b>	19.0 $\pm$ 1.6	1	1994ai
09354	—	Mk 1039	—	Sc?	2111	<b>75.6</b>	19.2 $\pm$ 4.0	1	<i>1985S</i>
10065		1035		SA(s)c?	1241	<b>74.5</b>	17.3 $\pm$ 1.1	1	<i>1990E</i>
12007		1255		SAB(rs)bc	1686	58.8	20.0 $\pm$ 1.2	1	<i>1980O</i>
13586		1433		(R)SB(r)ab	1075	<b>67.4</b>	16.8 $\pm$ 1.0	1	1985P
13633			02813	Im?	1392	<b>76.6</b>	16.1 $\pm$ 1.5	1	2008fb
13727		1448		SAcd?	1168	<b>86.1</b>	16.8 $\pm$ 1.0	1	<i>1983S</i> , 2003hn
13985	–	ESO G302-G014	–	IB(s)m	872	<b>73.6</b>	16.8 $\pm$ 1.0	1	2008jb
14123			02890	Sdm pec?	1155	<b>90</b>	16.1 $\pm$ 1.5	1	2009bw
19531		2280		SA(s)cd	1899	<b>66.2</b>	20.0 $\pm$ 1.4	1	2001fz
19579		2273B	03530	SB(rs)cd:	2101	<b>67.9</b>	17.9 $\pm$ 2.2	1	2011fd
36699		3877	06745	SA(s)c?	895	<b>83.2</b>	17.1 $\pm$ 0.8	1	1998S
37912	IC 755	4019	07001	SBb?	1524	<b>90</b>	16.8 $\pm$ 0.8	1	1999an
38302		4088	07081	SAB(rs)bc	757	<b>71.2</b>	17.1 $\pm$ 0.8	1	1991G, 2009dd
38580		4129		SB(s)ab?	1177	<b>90</b>	18.0 $\pm$ 3.8	1	2002E
38618		4136	07134	SAB(r)c	609	22	16.3 $\pm$ 0.9	1	<i>1941C</i>
38795		4157	07183	SAB(s)b?	774	<b>90</b>	17.1 $\pm$ 0.8	1	<i>1937A</i> , 2003J
39724		4274	07377	(R)SB(r)ab	930	<b>68</b>	16.3 $\pm$ 0.9	1	1999ev
39974		4302	07418	Sc?	1149	<b>90</b>	16.8 $\pm$ 0.8	1	1986E
40530	–	IC 3311	–	Sdm?	–122	<b>90</b>	20.0 $\pm$ 1.0	2	2004gk
41608	–	IC 3476	–	IB(s)m?	–169	51.2	16.8 $\pm$ 0.8	1	<i>1970A</i>
41789		4527	07721	SAB(s)bc	1736	<b>81.2</b>	17.6 $\pm$ 0.9	1	2004gn
42069		4568	07776	SA(rs)bc	2255	<b>67.5</b>	16.8 $\pm$ 0.8	1	1990B, 2004cc
42975		4666	07926	SABc:	1529	<b>69.6</b>	15.7 $\pm$ 2.9	1	<i>1965H</i>
43189		4688	07961	SB(s)cd	986	23.7	15.6 $\pm$ 1.0	1	<i>1966B</i>
43969		4809	08034	Im pec	915	<b>90</b>	15.6 $\pm$ 1.0	1	2011jm
53247		5775	09579	SBc?	1681	<b>83.2</b>	19.8 $\pm$ 1.0	1	1996ae
54117		5879	09753	SA(rs)bc?	772	<b>72.7</b>	15.5 $\pm$ 0.9	1	<i>1954C</i>
54470		5907	09801	SA(s)c?	667	<b>90</b>	17.2 $\pm$ 0.9	1	<i>1940A</i>

1: Tully et al. (2009), 2: Solanes et al. (2002)